Danger Signaling Pathways in Aortic Disease

Dissertation

zur

Erlangung des Doktorgrades (Dr. rer. nat.)

der

Mathematisch-Naturwissenschaftlichen Fakultät

der

Rheinischen Friedrich-Wilhelms-Universität Bonn

Nicola Willemsen

aus Kevelaer, Deutschland

Bonn, 20.07.2023

Angefertigt mit Genehmigung der Mathematisch-Naturwissenschaftlichen Fakultät
der Rheinischen Friedrich-Wilhelms-Universität Bonn

1. Gutachter: Prof. Dr. Sebastian Zimmer

2. Gutachter: Prof. Dr. Günter Mayer

Tag der Promotion: 20.10.2023
Erscheinungsjahr: 2024

Table of content

Abstract

The aorta connects the heart to the peripheral circulation and organs. It is necessary for the regulation of hemodynamics and therefore, aortic disease affects all organs and the survival of the individual. In aortic valve stenosis, the thin and smooth cusps that make up the aortic valve become thickened, fibrous, and calcified, leading to valve stiffness and reduced cusp compliance. Aortic valve stenosis is associated with significant morbidity and mortality. Nevertheless, there is still a lack of a reliable marker to predict disease progression. Current treatments for aortic valve stenosis are surgical and invasive, therefore, there is a need for earlier indicators. The development and progression of aortic valve stenosis is caused by certain factors, for instance chronic inflammation and the accumulation of cholesterol. This study specifically focuses on investigating these two factors and shedding light on their pivotal role in the development of aortic valve stenosis, to gain a deeper understanding and potential avenues for intervention in the management of this condition. The first project addressing chronic inflammation is about cellular and biochemical pathways activated by the innate immune system. Essential components of the innate immune system are pattern recognition receptors, which recognize microbial molecular patterns as well as altered or mislocalized self-molecules. Pattern recognition receptors include a variety of receptors, such as the Toll-like receptor family. One part of this thesis provides an insight into the role of Toll-like receptor 3 in valve cells and mice. Activation of this receptor caused calcification and inflammation in cells and in the living organism, which could be blunted after Toll-like receptor 3 inhibition or knockdown. Thus, the findings not only support the endogenous role of Toll-like receptor 3 in the development of aortic valve stenosis, but also suggest that specific Toll-like receptor 3 inhibition may be beneficial for the treatment or prevention of aortic valve stenosis. The second part of this study moves on to describe the role of cholesterol crystals in the pathogenesis of aortic valve stenosis. Cholesterol crystal infiltration has been recognized as a contributing factor in the formation of atherosclerotic plaques and the initiation of inflammatory processes. Furthermore, it has been implicated in the onset of calcification. By investigating the role of cholesterol crystals, this study aims to shed light on their involvement in the underlying mechanisms of aortic valve stenosis, providing insights into the progression of the disease and potentially uncovering novel therapeutic strategies targeting cholesterol crystal-related pathways. This work could demonstrate the ability to solubilize these crystals with cyclodextrin. In this way, *in vitro* experiments could further demonstrate a higher calcification pattern after the addition of cholesterol crystals, which in turn could be reduced by solubilizing the crystals with cyclodextrin.

List of abbreviation

AAA	Abdominal aortic aneurysm
ABCA1	ATP-Binding Cassette Transporter
ABCG1	ATP Binding Cassette Subfamily G Member 1
ACAT1	Acetyl-CoA Acetyltransferase
ACTA2	Smooth Muscle alpha-2 Actin
AR	Aortic Regurgitation
AS	Aortic valve stenosis
ATP	Adenosine Triphosphate
BM	Basal Medium
BMP	Bone Morphogenetic Protein 2
CAVD	Calcific Aortic Valve Disease
CC	Cholesterol Crystals
CCDR	Cholesterol Crystal Dissolution Rate
CD	Cyclodextrin
CD68	Cluster of Differentiation 68
CDNA	Complementary DNA
CETP	Cholesteryl Ester Transfer Protein
cGAS	Cyclic GMP-AMP Synthase
CLR	C-type Lectin Receptors
CVD	Cardiovascular Disease
Cyp27A1	Cytochrome P450 Family 27 Subfamily A Member 1
C4a	Compound 4a
DAMP	Damage-Associated Molecular Patterns
DDX58	DEAD (Asp-Glu-Ala-Asp) Box Polypeptide 58
DNA	Deoxyribonucleic Acid
dsRNA	Double-stranded RNA
EC	Endothelial Cell
ECG	Electrocardiographic
EMT	Epithelial to Mesenchymal Transition
EndMT	Endothelial to Mesenchymal Transition
eNOS	Nitric Oxide Synthase 3
FBS	Fetal Bovine Serum

FDA	Food and Drug Administration
g	Gravity
GRAS	Generally Recognized as Safe
HDL	High Density Lipoprotein
HDL-C	High Density Lipoprotein-Cholesterol
HPβCD	Hydroxypropyl-Beta-Cyclodextrin
IDL	Intermediate Density Lipoprotein
IFIH1	Interferon Induced with Helicase C Domain 1
IFN	Interferon
IL	Interleukin
IL1β	Interleukin 1 beta
IL6	Interleukin 6
IRF	Interferon Regulatory Factors
ISG	Interferon Stimulating Gene
LDL	Low Density Lipoprotein
LDL-C	Low Density Lipoprotein-Cholesterol
LXR	Liver X Receptor
MAVS	Mitochondrial Antiviral-Signaling Protein
MDA5	Melanoma Differentiation-Associated Protein 5
Mg	Milligram
Ml	Milliliter
mM	Millimolar
NLR	Nucleotide-Binding Oligomerization Domain-Like Receptors
NOS3	Nitric Oxide Synthase 3
PAMP	Pathogen-Associated Molecular Patterns
PCM	Pro-Calcifying Medium
PCR	Polymerase Chain Reaction
PECAM1	Platelet Endothelial Cell Adhesion Molecule-1
PolyIC	Polyinosinic:Polycytidylic Acid
PRR	Pattern Recognition Receptor
P/S	Penicillin/ Streptomycin
qPCR	Quantitative Real-Time Polymerase Chain Reaction
RCT	Reverse Cholesterol Transport
RIG-I	Retinoic Acid Inducible Gene I

RNA	Ribonucleic Acid
RPM	Rounds Per Minute
RUNX2	Runt-Related Transcription Factor 2
SBEβCD	Sulfobutyl Ether-Beta-Cyclodextrin
Scr	Scrambled
siRNA	Small Interfering RNA
SMC	Smooth muscle cells
SMS	Singleton-Merten Syndrome
SR-B1	Scavenger Receptor, Class B Type 1
ssRNA	Single-Stranded RNA
TAGLN	Transgelin
TAVR	Transcatheter Aortic Valve Replacement
TGFβ	Transforming Growth Factor beta
TIR	Toll/Interleukin-1 Receptor
TLR	Toll-like-Receptor
TNFα	Tumor Necrosis Factor-Alpha
TRIF	TIR-Domain-containing Adapter-inducing Interferon-β
ULDL	Ultra Low-Density Lipoproteins
VCAM1	Vascular Cell Adhesion Molecule 1
VEC	Valvular Endothelial Cell
VIC	Valvular Interstitial Cell
VLDL	Very Low-Density Lipoproteins
VWF	Von Willebrand Factor
WT	Wildtype
µg	Microgram
µl	Microliter
µm	Micrometer

1. Introduction

As part of Transregio 259 (TRR259) and its associated graduate school, this project was funded by the German Research Foundation (DFG), Collaborative Research Center (SFB): DFG, SFB TRR259/1 (397484323)

1.1 Background

1.1.1 Cardiovascular system

The cardiovascular system is responsible for circulating blood throughout the body delivering essential nutrients and oxygen to the organs. Blood flow in the cardiac system occurs through a sequence of events that involve the contraction and relaxation of the heart's 4 chambers: the right and left atria and the right and left ventricles. This sequence is known as the cardiac cycle, which is divided into 2 main phases: systole and diastole. During systole, the heart's ventricles contract and pump blood out of the heart into the arteries. During diastole, the heart's ventricles relax and fill with blood from the atria. Blood flows into the ventricles through the tricuspid and mitral valves from the right and left atria, respectively. As the ventricles fill with blood, the pressure in the heart chambers increases.

In addition to the heart, which serves as a powerful muscular pump responsible for supplying blood to the body, blood vessels play an equally important role in efficiently transporting blood and its essential components. The aorta, the largest artery in the human body, represents the gate to the whole vessel system. The aorta is divided into the ascending aorta, the aortic arch, the descending thoracic and the abdominal aorta. All components carry oxygenated blood from the heart to all body parts.

The aorta consists of 3 layers. The innermost layer, known as the tunica intima, presents a composition as it is thin and primarily consists of a single layer of endothelial cells (ECs) effectively serving as a protective barrier. Additionally, within the subendothelial region, one can find loose connective tissue alongside a small number of fibroblasts. An abundance of elastic fibers can be found within the middle layer known as the tunica media. Comprised of smooth muscle cells, collagen fibers of types I and III, as well as numerous elastic fibers, this layer exhibits a robust structural composition (Komutrattananont et al. 2019). The outer layer, the adventitia, including elastic fibers, fibroblasts, and mast cells, provides protection and the stable structure of the aorta (Komutrattananont et al. 2019). When the heart is pumping blood, it flows from the left heart ventricle into the aorta through the aortic valve. The aortic valve, one of the 4 valves of the heart, links the left ventricle and the ascending aorta. It consists of 3 cusps: the valvular cusps, that open and close with each heartbeat, allowing a one-way blood flow.

Each cusp contains layers covered in valvular endothelial cells (VECs). Wrapped in the protective embrace of these VECs, the inner layers unfold: the fibrosa, the spongiosa, and the ventricularis containing mesenchymal cells, so called valvular interstitial cells (VICs). In addition, the layers differ in their enrichments. The fibrosa contains collagen, the spongiosa glycosaminoglycans, and the ventricularis elastin fibers (Hsu et al. 2020).

1.1.2 Cardiovascular disease

The global longevity trend is increasing and life expectancy worldwide has increased by more than 6 years on average[1]. However, the most pressing question in this context is: how long will older people live in good health? On average, only 5 of these 6 additional years were spent in good health, and disability generally increases with age. The diseases that caused such disability and most deaths worldwide in 2019 were heart disease, diabetes, stroke, lung cancer, and chronic obstructive pulmonary disease. The list of the top 10 global causes of death in 2019 showed that approximately 17.9 million people died from cardiovascular diseases (CVD). This number represents 32% of all global deaths[2].

CVD are a group of diseases that affect the heart and blood vessels. CVD due to atherosclerosis includes ischemic heart disease or coronary heart disease (e.g., heart attack), cerebrovascular disease (e.g., stroke), and diseases of the aorta and arteries, including hypertension and peripheral vascular disease. Other CVDs include congenital heart disease, rheumatic heart disease, cardiomyopathies, arrhythmias, and valvular heart disease (Mendis 2011, Thiriet 2018).

1.1.3 Aortic valve stenosis

The presence of aortic valve stenosis (AS) carries a notable burden of morbidity and mortality (Aluru et al. 2022). It is currently treated with valve replacement as there is no approved drug therapy to prevent or treat AS. The process is a slowly progressing one and the disease initially remains asymptomatic in most patients. It starts with increased sclerosis of the aortic valve cusps, which is visible in echocardiography. First symptoms of a developing AS are dizziness, angina pectoris, syncope, or dyspnea in the later phases. Then, the chance of the mortality rate increase is up to 50% over 2 years (Otto and Prendergast 2014; Makkar et al. 2012). Thus, once developing an AS, the patient´s life span is less than 2 years longer without valve replacement (Clark et al. 2012; Blaser et al. 2021). 3-quarters of AS patients who develop heart failure undergo a valve replacement or pass away within the next years (Stewart et al. 1997; Blaser et al. 2021). Therefore, patients with mild or moderate AS need to be monitored regularly whereas aortic valve replacement is strongly recommended in advanced cases of severe AS in

symptomatic patients. Still, therapeutic prevention remains limited. In order to find a medical treatment for the prevention, or rather to slow the process of AS, it is important to understand the pathomechanisms of such a disease.

In recent years, the field of cardiovascular immunology has grown and is now comparable to the field of lipid metabolism in relation to cardiovascular disease. Recent studies suggest that AS is not only a consequence of mechanical stress on the valve, but rather an inflammatory process that causes endothelial damage, lipid penetration leading to fibrosis, cusp thickening, and finally calcification (Joseph et al. 2017). More specifically, activation of the innate immune system leads to endothelial dysfunction, lipid deposition, extracellular matrix remodeling, and calcification, resulting in valve stenosis. As a result, the valves are no longer able to open fully and blood flow to the body is blocked (Figure 1) (Pawade et al 2015; Dweck et al 2013; Dweck et al 2012). Accordingly, this study focused on calcific aortic valve disease (CAVD), which leads to stenosis and is referred to as AS in this thesis.

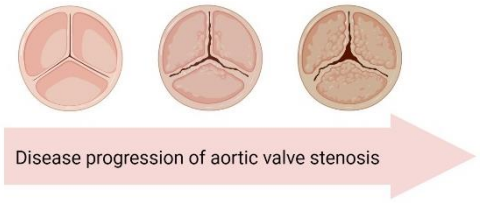

Figure 1 Progression of aortic valve stenosis

The progression of the disease is shown from left to right, with initially smooth and thin valves that function properly and allow normal blood flow. However, as AS progresses over several years, the valves undergo fibrosis and calcification, becoming thicker and less flexible. As a result, the disruption of blood flow impairs the valves' ability to open and close accurately. This places an increased workload on the heart, leading to cardiac hypertrophy. The first symptoms are dizziness, angina, or dyspnea, and the only treatment in the later stages of the disease is the replacement of the aortic valves, either through open-heart surgery or transcatheter aortic valve replacement. Figure created with Biorender.com

AS= Aortic valve stenosis

1.1.4 Calcific aortic valve disease

CAVD mostly occurs in the population aged over 60 years (Zhou et al. 2021; Osnabrugge et al. 2013) and causes the highest morbidity as well as mortality at that age.

In 1663, Lazare Rivière described a patient's necropsy in 1646 who died due to symptoms of heart problems like palpitations and progressive dyspnea. During the necropsy, he found an enlarged left ventricle and large “caruncle-like” masses obstructing the outflow to the aorta (Vaslef and Roberts 1993). This case and subsequent necropsy of patients showing ossified

deposits on the aortic valves were attributed to endocarditis. Hasse refuted this theory in 1846 and described the phenomenon as degenerative ossification. Several theories have been put forward and the calcific AS was associated, among others, with rheumatic causes. Following the discovery of X-rays by Roentgen in 1895, Simmonds in 1908, and Cutler together with Sosman in 1924, were able to demonstrate these valvular calcific deposits after the patient's death with X-rays. In 1931, calcification in the aortic valve could be observed for the first time in a living patient (Vaslef and Roberts 1993). Since the discovery of CAVD and the many theories that have been put forward but not properly explained with evidence, there has been increasing interest in advancing the early hypotheses and understanding the molecular mechanisms that cause calcification of the aortic valve. Surgical developments, such as the implantation of prostheses or the heart-lung machine, have followed. However, CAVD still has a high prevalence and is associated with high morbidity and mortality.

What is known so far, CAVD describes the formation of nodules of calcific minerals in valve tissue that resemble the hydroxyapatite of bone. Most commonly, CAVD begins in the fibrosa with bone formation within the calcific deposits. VICs play an important role in this process, as these cells can exhibit an osteoblast-like phenotype and express extracellular bone matrix proteins (Merryman and Schoen 2013). Yip and colleagues discuss various mechanisms leading to aortic valve calcification, such as apoptosis-induced calcification leading to myofibrotic activation of VICs. Another idea discussed in this manuscript is calcium deposition associated with necrotic cells and bone formation by resident VICs as well as bone marrow-derived cells, or finally calcification due to extracellular matrix stiffness (Yip et al. 2009). However, the cellular mechanisms in VICs that contribute to calcification are still unknown and need to be investigated.

1.1.5 Endothelial to mesenchymal transition

VICs are crucial in the development of AS, but ECs also play an important role. In general, the endothelium separates the vascular lumen from the surrounding tissue and is a thin monolayer of ECs that allow the transport of molecules, nutrients, etc. to and from the tissue (Aman et al. 2016). ECs also recruit other cell types such as pericytes and smooth muscle cells to build and stabilize tissues such as blood vessels. In addition, ECs can change their morphology and phenotype through a phenomenon called endothelial to mesenchymal transition (EndMT) (Figure 2). It is a dynamic process in response to chemical and mechanical signals that is essential for embryonic development and wound healing. Interestingly, EndMT has been shown to play a role in cardiac diseases such as atherosclerosis, pulmonary hypertension, valvular heart

disease as well as in fibroelastosis, tissue fibrosis and cancer (Ma et al. 2020; Kovacic et al. 2019; Jiao et al. 2020). During the process of EndMT, physical changes occur: ECs undergo a phenotypic change towards a mesenchymal cell, such as a myofibroblast, or a smooth muscle cell. The cells start to reorganize their cytoskeleton, lose their cell-cell adhesion and cellular polarity. In this way, ECs become fibroblast-like cells. Furthermore, different markers can be detected during the process of EndMT: the gene expression of endothelial markers such as *PECAM1* (Platelet Endothelial Cell Adhesion Molecule-1, CD31), *CDH5* (VE-cadherin) and *VWF* (von Willebrand factor) decreases, while mesenchymal markers such as *Vimentin, ACTA2* (smooth muscle alpha-2 actin), *MMPs* (matrix metalloproteinases) and *FSP*-1 (fibroblast-specific protein 1) increase (Kovacic et al. 2019; Ma et al. 2020). A known inducer of EndMT is TGFβ, which upregulates the expression of transcription factors (TFs): *SNAI1* (snail), *SNAI2* (slug), and *Zeb1* (zinc finger transcription factor), which in turn upregulate the expression of mesenchymal genes *ACTA2*, *TAGLN* (transgelin), *CNN* (calponin), *Vimentin*, *COL1A* (type I collagen), *FN1* (fibronectin), *FSP*-1 (fibroblast specific protein 1), *CDH2* (N-Cad), *MMP2*, *MMP9* (matrix metalloproteinases 2/9) (Cho et al. 2018). Other experiments investigating the overexpression or inhibition of TGFβ have demonstrated its role in renal fibrosis leading to chronic kidney disease (Meng et al. 2016; (Xavier et al. 2015). TGFβ activates myofibroblasts via various signaling pathways, thereby disrupting extracellular matrix homeostasis.

The pro-inflammatory cytokine IL1β was also shown to be involved as an inducer in the process of EndMT (Maleszewska et al. 2015). In addition, Cho and colleagues have shown that TNFα also induces EndMT and that combinations of cytokines such as TGFβ1, IL1β, and TNFα are more potent than a single cytokine (Cho et al. 2018). Similar findings have been reported for epithelial-mesenchymal transition (EMT), confirming that TNFα and IL1β enhance TGFβ1-induced EMT (Kawata et al. 2012). Another important driver of EMT in tumor progression is inflammation (Kawata et al. 2012). Therefore, other extracellular signals, including those originating from the immune system, are capable of inducing EMT (Moustakas and Heldin 2007; Kawata et al. 2012). This led us to investigate the innate immune system in relation to the process of EndMT.

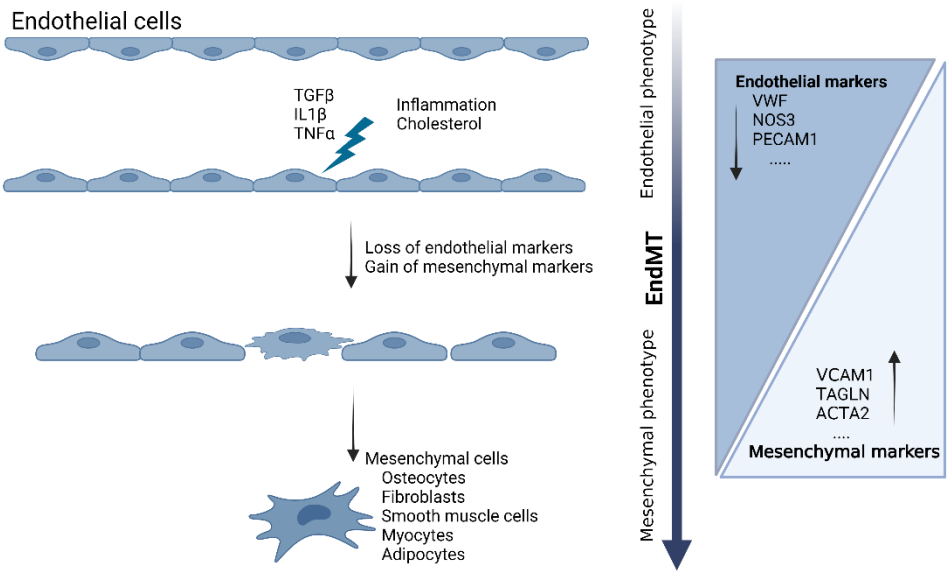

Figure 2 Illustration of the process of endothelial to mesenchymal transition

This study aimed to investigate the role of the innate immune system as well as cholesterol crystals in the process of EndMT. Herein, endothelial cells undergo a transition into mesenchymal-like cells. It is a dynamic process in response to chemical and mechanical signals. Figure created with Biorender.com

TLR3= Toll-like receptor 3; EndMT= Endothelial to mesenchymal transition

1.1.6 Valve replacement

Transcatheter aortic valve replacement (TAVR), a minimally invasive approach, has become the common treatment for AS, offering patients a valve replacement procedure that avoids the need for open-heart surgery and provides a quicker recovery. Until 1960, it was not possible at all to treat patients with valve replacements. The first mitral prosthesis was implanted in dogs in 1958. At first, the treatment seemed successful, however, within 2 or 3 days of implantation, the dogs died of pulmonary edema caused by a thrombus closing the valve (Starr et al. 2002; Starr and Edwards 1961). Following, other types of valves, such as a shielded valve that allowed a long-term survival in experimental animals without a thrombus, were tested (Starr et al. 2002). Donald Ross developed the homograft in 1962 (Ross 1962; Starr et al. 2002), which still is a crucial instrument with its advantages as well as disadvantages in today's surgical medicine. On the positive side, there are less anticoagulation and systemic embolization to be found, on the negative side, the tissues themselves are degrading over the years after implantation. After various modifications, in 1965 the final model "6120 silastic mitral valve and the model 1260 aortic ball valve" could be provided and the mortality rapidly decreased (Starr et al. 2002; Starr et al. 1967).

Within the next years, new techniques and new types of mechanical valve implants as well as porcine tissue were tested. The valves became more durable and the surgical technique could be improved. As a result, only a small incision was required for mitral valve replacement, and aortic valve replacements could be performed through a hemi-sternotomy (Starr et al. 2002).
Subsequently, the valve replacements could be revolutionized and TAVR was developed. 2002, the first valve was implanted by TAVR. In this case, the patient was inoperable and had severe AS, hence, this was the only treatment option (Kourkoveli et al. 2018; Spears et al. 2020). Since the first TAVR, the technique has been further developed in procedural techniques and biomedical engineering. It is now an essential therapeutic option to treat patients with high surgical risk (Kourkoveli et al. 2018). Particularly, since the emergence of TAVR, the risk for surgical valve replacement could be lowered among the elderly (Osnabrugge et al. 2013). Nevertheless, we have to understand the disease, its origin, and the different pathways belonging to it to find a treatment for preventing a surgical intervention. Previous publications demonstrated the role of the innate immune system with regard to CVD. The following chapters will provide an overview of key players within the innate immune system and the factors that drive AS.

1.2 The role of the innate immune system and its pattern recognition receptors in the development of aortic valve stenosis

We are all exposed to different organisms, pathogens, or self-damaged tissues. It is depending on the pathogenicity of the organism and whether it causes diseases, but furthermore, it is depending on the host's defense mechanism: the immune system. It is a highly sophisticated interactive network of organs, cells, and signaling molecules that fight invading pathogens. Most of the time one does not recognize the hard-working system in the body unless it does not function properly anymore by underactivity or overactivity. In the case of underactivity, infections are developing, and tumors can be formed. In the case of overactivity, on the contrary, autoimmune diseases and allergies can develop. The whole immune system is divided into 2 parts: the innate and the adaptive immune system. The innate immune system is the first line of defense and comprises physical and chemical barriers, humoral and cell-mediated components, which become active immediately after a pathogen invasion and which exhibit a first response (Riera Romo et al. 2016). It reacts quickly but not specifically, so it can cause damage to healthy tissue. On the other hand, the adaptive immune system is precise and its response is antigen-specific through T- and B- lymphocytes. However, the adaptive immune system needs days, or weeks to develop specific response (Parkin and Cohen 2001; Medzhitov 2008).

The first protection in all living vertebrates includes physical components such as the skin. The skin contains epithelial layers with tight junctions and proteins that provides mechanical protection against invading pathogens. Further, the skin consists of external secretion that is enriched in molecules with antimicrobial activity, for instance, lysozyme (Riera Romo et al. 2016). The cellular innate immune defense is mainly organized by myeloid phagocytic cells for instance monocytes, macrophages, neutrophils, etc. These cells can be categorized into the group of leukocytes and are able to destroy pathogens, secrete cytokines and release important soluble mediators, such as reactive oxygen species (Riera Romo et al. 2016). Leukocytes, as well as complement, cytokines, and acute phase proteins of the innate immune system, but also non-immune cells, such as tissue cells, recognize pathogens and amplify a first immune response by recruiting other immune cells. Via specific signals, not only innate immune cells are recruited, but also cells of the adaptive immune system are activated and start producing antigen specific antibody producing lymphocytes (Kaur and Secord 2019; Bonilla and Oettgen 2010). Taken together, the earlier mentioned myeloid phagocytic cells as well as other non-immune cells like epithelial cells, endothelial cells, etc. contribute to the innate immune response. In this way, they exhibit so called pattern recognition receptors (PRR) that detect pathogens by pathogen-associated molecular patterns (PAMPs) or damaged- associated molecular patterns (DAMPS) that represent damaged tissue due to inflammation and infection (Kaur and Secord 2019). PRRs can be localized extracellular at the cell membrane or intracellular in the cytoplasm or endosomes (Janeway and Medzhitov 2002; Kim et al. 2016; Takeuchi and Akira 2010). The PRRs are classified into 5 receptor families depending on their structure, protein domains, and specific targets: Toll-like receptors (TLRs), localized at the cell surface and on endosomes, c-type lectin receptors (CLRs) at the cell surface, cytoplasmic proteins such as the retinoic acid-inducible gene (RIG)-I-like receptors (RLRs), nucleotide-binding oligomerization domain (NOD)-like receptors (NLRs) at the endosomal membrane as well as in the cytoplasm, and absent in melanoma 2 (AIM2)-like receptors (ALRs) in the cytoplasm and nucleus (Takeuchi and Akira 2010; Schneider et al. 2014; Brubaker et al. 2015). Within these receptors, our research focused on TLRs and RLRs. In figure 3, an example of TLR and RLR signaling is illustrated. Transcription factors are activated and bind to specific promotors triggering the expression of pro-inflammatory cytokines, interferons (IFNs), and subsets of interferon stimulated genes (ISGs). Pro-inflammatory cytokines as well as IFNs activate the Janus-Kinase/ signal transducers and activators of transcription (JAK-STAT) pathway resulting in an expression of further cytokines and ISG´s that in turn recruit other cells, activate phagocytosis, cytokine expression, and cell death (Jin et al. 2013; Schneider et al. 2014; Deretic 2021).

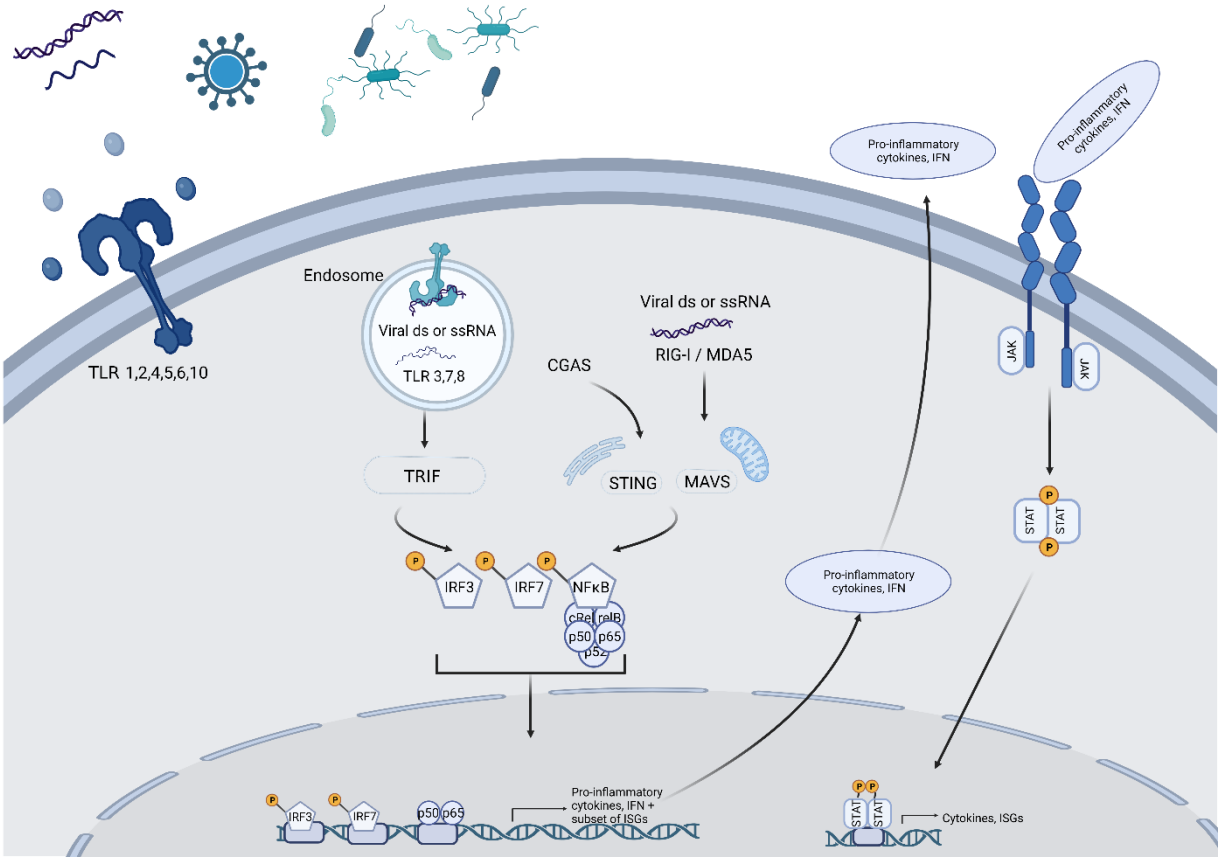

Figure 3 Schematic figure of the innate immune system

Extracellular PRRs at the cell membrane as well as intracellular receptors recognize specific PAMPs and DAMPs. Intracellular receptors in endosome and cytosolic PRRs recognize viral double-stranded or single stranded DNA or RNA. Activation of TLR3 leads to phosphorylation of IRF3/7 and NF-κB through TRIF. On the other hand, RIG-I, MDA5, and cGAS transduce PRR signaling to transcription factor activity by activating STING and MAVS which leads to phosphorylation of IRF3/7 and NF-κB. Phosphorylated dimers of IRF3/7 or NF-κB translocate to the nucleus and bind to specific promotors resulting in transcription of IFN and subsets of ISG. Pro-inflammatory cytokines and IFN activates the JAK-STAT pathway and leads to an expression of further cytokines as well as ISGs, that acts as negative or positive regulators of further signaling.

cGAS= Cyclic GMP-AMP synthase; DAMP= Damaged-associated molecular pattern; PAMP= Pattern-associated molecular pattern; PRR= Pattern recognition receptors; ssRNA= Single-stranded RNA; TLR3= Toll-like receptor 3; IRF3/7= Interferon response factors 3 and 7; NF-κB= Nuclear factor 'kappa-light-chain-enhancer' of activated B-cells; TRIF= TIR-domain-containing adapter-inducing Interferon-β; IFN= Interferon; STING= Stimulator of interferon gene; MAVS= Mitochondrial antiviral-signaling protein; ISG= Interferon stimulated gene; JAK-STAT= Janus-kinase/ signal transducers and activators of transcription

Figure created with Biorender.com

1.2.1 Toll-like receptor 3

There are thirteen members within the mammalian TLR family. In the human system, the TLR family consists of 10 members (Takeda and Akira 2015). As transmembrane signaling receptors, TLRs contain an extracellular domain with a repetitive structure rich in leucine residues (leucine rich repeat motif) for ligand recognition at the N-terminus and an intracellular Toll/Interleukin-1 (IL1) receptor (TIR) domain at the C-terminus for intracellular signaling (Takeuchi and Akira 2010; Akira and Takeda 2004; Kaisho and Akira 2006). The effect and immune response depend on the activated TLR as every receptor has its specific function and localization: TLR1, TLR2, TLR4, TLR5, TLR6, and TLR10 are localized on the cell membrane and TLR3, TLR7, TLR8, and TLR9 are located in the endosomal compartment. TLR ligands can be molecular components derived from microorganisms, such as lipids, proteins, and nucleic acids (Kaisho and Akira 2006) (Figure 3). Within these TLRs, this study focused on TLR3, which is expressed in immune cells such as macrophages and myeloid dendritic cells but it could also be found in certain other cells like fibroblasts, neurons, endothelial, and epithelial cells (Bugge et al. 2017, Liu et al. 2018). It recognizes double-stranded RNA (dsRNA), thus viral-derived molecules and host nucleic acids (García-Rodríguez et al. 2018; Takeda and Akira 2015). After binding to the receptor, TLR3 starts to dimerize and recruits the adaptor molecule TIR domain-containing adapter-inducing interferon (TRIF) and thereby activates the transcription factors nuclear factor-kappa B (NF-κB), mitogen-activated protein kinases (MAPKs), and interferon regulatory factor 3 (IRF3). This cascade leads to the production of pro-inflammatory cytokines and IFN (Zhan et al. 2017; García-Rodríguez et al. 2018; Bugge et al. 2017). Compared to other PRRs, it is speculated, that RIG-I rather detects viral genomes in the aortic wall, whereas TLR3 is activated by a non-viral mechanism, precisely, by self-RNA from damaged or necrotic tissue (Jabłońska et al. 2018; Kaiser et al. 2013; Karikó et al. 2004; Cavassani et al. 2008).

A synthetic analog of dsRNA termed polyriboinosinic:polyribocytidylic acid (PolyIC) is able to activate the TLR3-TRIF-NF-κB pathway and thereby upregulates inflammatory mediators in human VICs (Zhan et al. 2017; Zhan et al. 2015). These mediators include MCP1, IL8, IL6, and ICAM1. MCP1, IL8, and ICAM1 are able to mediate leukocyte recruitment. IL6 upregulation can lead to an osteogenic response in vascular and valvular cells (Zhan et al. 2017; Zhan et al. 2015). Zhan and colleagues confirmed this finding with upregulated gene expression of calcification markers *BMP2*, *TGFβ1*, and *ALP* and verified calcium deposit formation in human VICs. Thus, PolyIC led to such a strong pro-osteogenic effect by activating TLR3 mediated NF-κB and ERK1/2 pathways (Zhan et al. 2017; Zhan et al. 2015).

It is not only possible to pharmacologically activate TLR3 with PolyIC, but furthermore to inhibit the receptor and thereby repressing any downstream signaling, since Cheng and colleagues found the TLR3 antagonist TLR3/dsRNA Complex Inhibitor Compound 4a (C4a). It is a small molecule, that competitively inhibits the dsRNA binding to TLR3 by disrupting the TLR3/dsRNA complex. It is highly specific and directly binds to TLR3 without affecting other PRRs (Cheng et al. 2011).

1.2.2 Melanoma differentiation-associated gene 5 (MDA5)

Besides the TLR family, the RLRs are a crucial initiator and regulator of the innate immune system. RLRs are cytosolic nucleic acid sensors and belong to the DExD box RNA helicase family (Jabłońska et al. 2018). 3 members of the RLR family are known: RIG-I (encoded by DEAD (Asp-Glu-Ala-Asp) Box Polypeptide 58 (*DDX58*)), MDA5 (melanoma differentiation-associated gene 5, encoded by Interferon Induced with Helicase C Domain 1 (*IFIH1)*), and LGP2 (laboratory of genetics and physiology 2, encoded by *DHX58*) (Yoneyama et al. 2004; Loo and Gale 2011). Within the members, RIG-I and MDA5 recognize viral single stranded RNA (ssRNA) and dsRNA. Once activated, RIG-I and MDA5 trigger their adaptor protein mitochondrial antiviral signaling protein (MAVS) that recruits TNF receptor-associated factor (TRAF) to assemble a signaling complex. Thereby, IRF3, IRF7, Activator Protein1 (AP1), and NF-κB are phosphorylated leading them to transfer into the nucleus for inducing the expression of IFNs, pro-inflammatory cytokines, ISG, etc. to amplify a first immune response. Previous studies have shown MDA5 and RIG-I to be mutated in various diseases such as systemic lupus erythematosus (SLE), Aicardi–Goutières syndrome (AGS), and Single-Merten Syndrome (SMS) (Lu and MacDougall 2017; Soda et al. 2019). The background and further information still remain to be investigated. Nonetheless, it is thought to be a gain of function mutation leading MDA5 and RIG-I to be activated to one or more dsRNA. SMS varies in its phenotypic expression. Still, it is associated mainly with aortic and valvular calcification, dental anomalies, osteopenia, or osteoporosis (Lu and MacDougall 2017). Within the TRR259, we arranged a cooperation with Project A03 (Prof. Gunther Hartmann; Institut für Klinische Chemie und Klinische Pharmakologie, Universitätsklinikum Bonn) and experiments were performed to achieve an overview of PRRs. In this way, MDA5 emerged as a potential driver in the development of AS. These findings prompted us to start questioning the role of this receptor in AS.

1.3 The role of cholesterol in the development of aortic valve stenosis

1.3.1 Cholesterol

Among the various major factors involved in the development of aortic disease, cholesterol plays an important role and has been shown to be crucial in several types of CVD. Cholesterol is an essential lipid for our hormone system as well as the immune system providing metabolites for steroid hormones such as corticosteroids or sex hormones and for bile acids, and vitamin D that are essential for certain physiological processes. It is synthesized endogenously in the liver or ingested through the diet (Rafieian-Kopaei et al. 2014)**.**

Dietary triglycerides, phospholipids, and cholesterol are absorbed into enterocytes in the small intestine, initiating the exogenous lipoprotein pathway: Cholesterol can be released to a cholesterol acceptor, the apolipoproteins, which are important proteins with amphipathic properties that can bind and transport lipids. These proteins surround cholesterol and lipids to form a lipoprotein, which in turn is water-soluble, allowing the transport through the blood, lymph, etc. (Ramasamy 2014; Liu et al. 2003; Zimmer et al. 2016). Once absorbed, cholesterol enters the bloodstream and is carried by chylomicrons (ultra-low-density lipoproteins (ULDLs)) to the liver or tissue. Here it is metabolized by lipoprotein lipase, releasing free fatty acids which are metabolized by muscle and adipose tissue. The chylomicrons are transformed into chylomicron remnants. These chylomicron remnants are in turn taken up by the liver and the endogenous pathway begins with the formation of very low-density lipoprotein (VLDL).

Cholesterol that is carried by VLDL is metabolized in tissue by lipoprotein lipase releasing free fatty acids. This produces intermediate density lipoprotein (IDL). IDL is further metabolized, and fatty acids are cleaved off. This leads to the formation of LDL, which binds to the LDL receptor in several tissues, such as the liver. LDL also binds to scavenger receptors on peripheral cells, such as macrophages, which phagocytize cholesterol.

The reverse cholesterol transport pathway (RCT) begins with the synthesis of high-density-lipoprotein (HDL) in the liver and intestine. These HDL particles are able to take up cholesterol and phospholipids that actively efflux from cells in peripheral tissues via ABCG1 and scavenger receptor class B1 (SR-B1) or passive efflux (Figure 5). Loaded HDL transports the cholesterol back to the liver by interacting with hepatic SR-B1 or it transfers the cholesterol to VLDL or LDL via cholesteryl ester transfer protein (CETP) (Figure 4) (Feingold 2000).

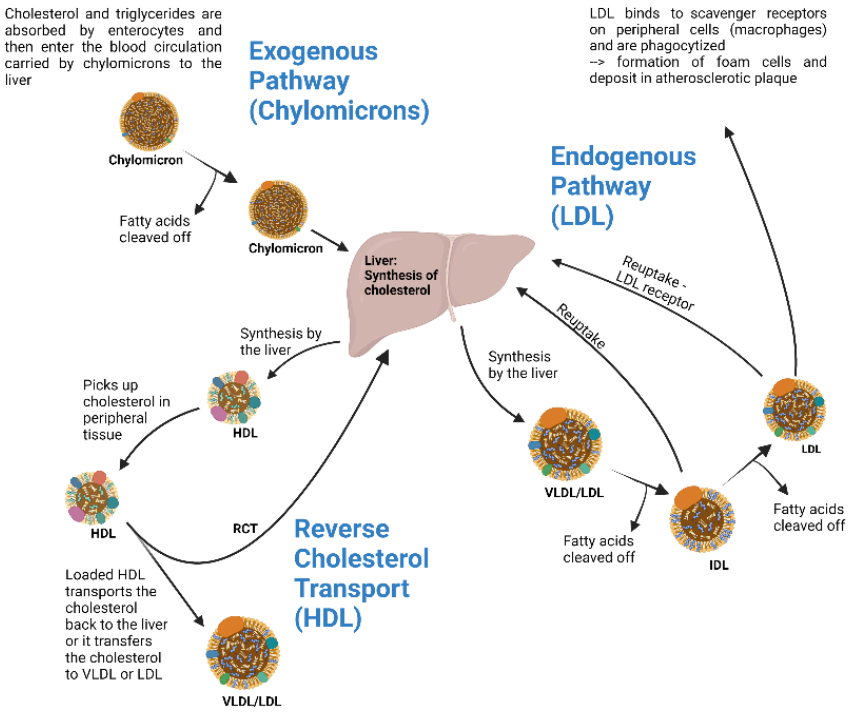

Figure 4 The lipoprotein metabolism

The lipoprotein metabolism is divided into 3 pathways exogenous pathway, endogenous pathway, and reverse cholesterol transport.

LDL= Low-density lipoprotein; HDL= High-density lipoprotein; RCT= Reverse cholesterol transport; VLDL= very low-density lipoprotein; IDL= Intermediate-density lipoprotein

Figure created with Biorender.com

In cells that phagocytose cholesterol such as macrophages, excess accumulated cholesterol is converted by Cyp27A1 into the more polar metabolite 27-hydroxycholesterol, which can passively cross the cell membrane into the aqueous medium. In addition, 27-hydroxycholesterol activates the liver X receptor (LXR), which in turn, upregulates the cholesterol efflux transporters ATP-binding cassette transporter (ABCA1) and ATP binding cassette subfamily G member 1 (ABCG1). Free cholesterol can also be stored as cholesteryl esters, which are formed by acetyl-CoA acetyltransferase (ACAT1) (Feingold 2000) (Figure 5).

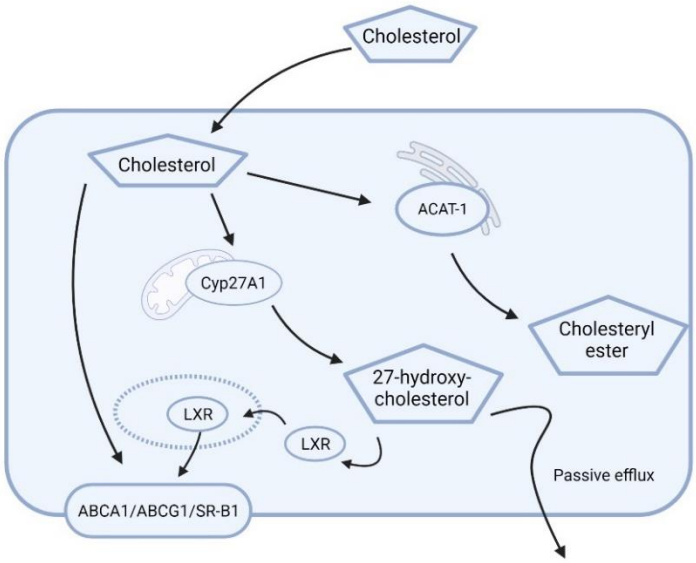

Figure 5 Cholesterol metabolism in a cell

Cholesterol metabolism and efflux capacity within a cell, e.g., a macrophage. Cholesterol can be formed into cholesteryl esters, catalyzed by ACAT1, for storage. It can also be formed into 27-hydroxycholesterol, catalyzed by Cyp27A1. 27-Hydroxycholesterol can either passively diffuse across the cell membrane or activate the TF LXR, which in turn mediates the up-regulation of the efflux transporters ABCA1, ABCG1, and SR-B1. Modified figure from (Zimmer et al. 2016). ACAT1= Acetyl-CoA acetyltransferase; ABCA1= ATP-binding cassette transporter; ABCG1= ATP binding cassette subfamily G member 1; Cyp27A1= Cytochrome P450 family 27 subfamily A Member 1; LXR= Liver x receptor; SR-B1= Scavenger receptor class B1; TF= Transcription factor

Figure created with Biorender.com

1.3.2 The role of cholesterol in cardiovascular disease

The common calorie-rich Western diet today is high in fat. We live in an affluent society with abundant food supplies and low prices for global foods throughout the year, regardless of seasonal and regional availability. In the last 20 years, the percentage of overweight adults has increased from 29.1% to 41.1%. The projection for 2040 is 46.8%[3].

In parallel, we can observe more cases of type II diabetes, cancer, obesity, and CVD in our society and there is evidence that the Western standard of diet, behavior, and lifestyle leads to more deaths from cardiovascular and other chronic diseases compared to a prudent type of diet and a healthier lifestyle (Fedacko 2012; Singh et al. 2019). However, it is important to note that CVD are not only caused by unhealthy lifestyles. Several other factors also play an important role in the development of CVD, such as family history, genetics, age, and gender.

1.3.3 Atherosclerosis

As mentioned above, CVD includes several diseases of the heart and blood vessels (Chapter 1.1.2). Atherosclerosis serves as the fundamental pathophysiological process underlying CVD and is characterized by intimal plaques found throughout the vascular system. Lipids, cholesterol crystals (CC), fibrous elements, and calcium accumulate in the inner layer of the arteries (Figure 6). As a result, immune cells infiltrate the vessel wall. These cells are able to uptake lipids and cholesterol esters and trigger an inflammation in the cell wall, causing collagen depletion and the formation of an atherosclerotic plaque (Rafieian-Kopaei et al. 2014; Duewell et al. 2010, Jebari-Benslaiman et al. 2022). On the one hand, the homeostasis of the anti-inflammatory, good cholesterol (HDL-cholesterol (HDL-C) is disturbed in the development of atherosclerosis. On the other hand, high levels of pro-inflammatory LDL-cholesterol (LDL-C) are a major risk factor (Badimon and Vilahur 2012; Elshourbagy et al. 2014). It has been shown that endothelial dysfunction can lead to the accumulation of LDL-C in the vessel wall, which in turn can be oxidized or enzymatically modified. Oxidized LDL-C can cause further damage to ECs and smooth muscle cells (SMCs), leading to their activation. Activated cells secrete pro-inflammatory cytokines to recruit monocytes into the intima, where they further differentiate into macrophages. These cells are able to take up the accumulated lipoproteins and develop into foam cells. These macrophage foam cells are retained in the subendothelial space and form the atherosclerotic plaque (Barua et al. 2003; Li et al. 2021; Moore et al. 2013). In addition, fibroblasts produce connective tissue, which, together with increased calcium and lipid deposition, leads to remodeling and thickening of the arteries. In addition, SMCs form a fibrous cap of extracellular matrix components beneath the endothelial layer, covering the accumulated lipoproteins and macrophages. In particular, this stage reflects an advanced level of atherosclerosis (Zimmer et al. 2016). Moreover, matrix degrading proteases are secreted, leading to the thinning of the fibrous cap and destabilization of the atherosclerotic plaque. The hard, ruptured, and uneven surface leads to clot formation and can cause a platelet aggregation and thrombosis as the blood flow is obstructed (Rafieian-Kopaei et al. 2014; Moore et al. 2013)**.** As a progressive chronic inflammatory disease, most cases begin asymptomatically and the discovery of plaques often occurs fortuitously during the diagnosis and treatment of other conditions like stroke or myocardial infarction. Other symptoms due to blocked arteries include chest pain, dizziness, fainting, shortness of breath, and heart palpitations. Risk factors are both behavioral, and genetic and include smoking, physical inactivity, high fat, or high cholesterol diet, alcohol, aging, gender, hyperlipidemia, and diabetes (Piper 2013).

The most common treatment is to pharmacologically inhibit cholesterol synthesis through medical drugs called statins. Other treatments include lifestyle changes to slow the process of new plaque formation. This includes a Mediterranean diet consisting of more plant foods instead of animal products, reduction of alcohol and nicotine consumption, and increased physical activity. Once atherosclerotic plaques critically occlude arteries they are usually treated with balloon angioplasty, endarterectomy, and bypass surgery to allow proper blood flow (Montalescot et al. 2013)[4].

Despite the availability of a wide range of lipid-lowering treatments, most patients still do not achieve the required LDL-C levels to prevent the development of atherosclerosis (Kavey et al. 2003; Arnett et al. 2019). In addition, the need to adjust the intensity of existing treatments for adequate CVD prevention will increase in the coming years.

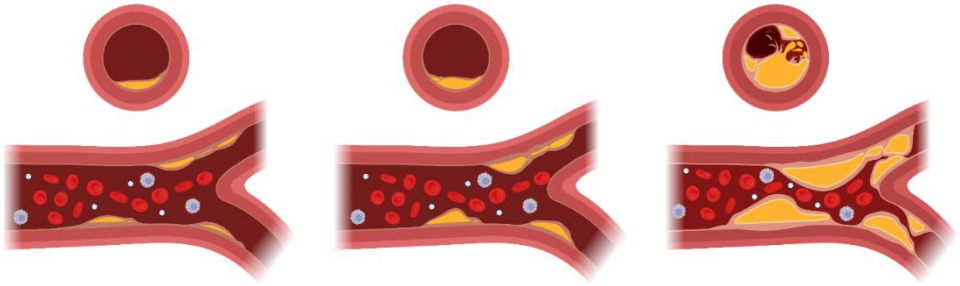

Figure 6 Development of atherosclerotic plaques in the vessels

Within the development of atherosclerotic plaques, more and more inflammatory cells, fatty deposits, calcium, and CC accumulate in the vessels forming such plaques. This leads to a narrowing of the vessel. CC= Cholesterol crystals

Figure created with Biorender.com

1.3.4 Cyclodextrin

Cyclodextrin (CD) is a cyclic oligosaccharide, in which D-glucopyranose units are linked by α-1,4 glycosidic linkages. It is of natural origin and was discovered by Antoine Villiers in 1891 (Antoine 1891, Maheriya 2017). In the following years, the subject became more and more interesting, especially in the pharmaceutical field. The Austrian microbiologist Franz Schardinger described bacterial digestion from potato starch into 2 crystalline compounds: α-dextrin and β-dextrin (Schardinger 1903, Crini 2020), which are now referred to as α-CD and β-CD. In particular, CDs are produced by the enzymatic degradation by glycosyltransferase of many starch sources, for instance potatoes, corn, etc. containing α-1.4 glycosidic linkages. The enzyme catalyzes the rearrangement of the polymer chain of starch into oligomers of 6 to 8 α-(1.4)-linked D-glucopyranose units forming a cone shape. The most common CDs are α-, β-,

and γ-CDs with 6, 7, and 8 glucopyranoside units, respectively (Figure 7) (Davis and Brewster 2004). They all contain a hydrophobic cavity with glycoside oxygen and hydrogen atoms, while the outer part is hydrophilic due to hydroxyl groups (Mahjoubin-Tehran et al. 2020; Uekama 2004; Davis and Brewster 2004). Thus, CDs are both water soluble and able to carry hydrophobic molecules in their central cavity. However, their solubility in aqueous solutions is limited and the oligomers have different aqueous solubilities: α-, β-, and γ-CD are approximately 13%, 2%, and 26% (weight by weight (w/w)) (Davis and Brewster 2004).

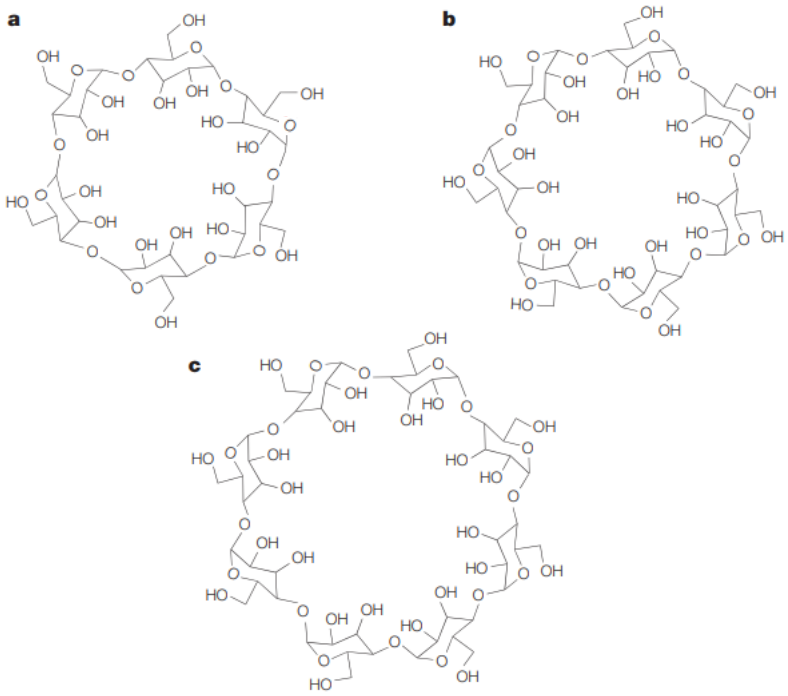

Figure 7 Chemical structures of α-, β-, and γ-cyclodextrin

*Chemical structures of α-, β-, and γ-cyclodextrin containing 6, 7, and 8 glucopyranoside units (**a, b, c**), respectively. Illustration from (Davis and Brewster 2004) with reprint permission.*

In order to increase the solubility, CDs have been chemically modified and several derivatives have been synthesized using modifications such as methylation, hydroxypropylation, and sulfobutylation. Within the modifications, all of them affect the hydroxyl groups, which are located on the outside of the ring. Therefore, the cavity diameter and the hydrophobicity are not affected, while solubility is improved (Dass 2000; Mahjoubin-Tehran et al. 2020). As a result, hydroxypropylated β-cyclodextrin (HPβCD) has a water solubility of 60% (w/w) and is still able to incorporate hydrophobic molecules into its cavity (Davis and Brewster 2004; Loftsson and Brewster 2010). This property is beneficial for taste masking and is widely used in the pharmacological field: CDs generally improve the bioavailability by entrapping poorly water-

soluble drug molecules, thereby increasing drug solubility, physical or chemical stability, absorption, etc., without affecting the drug's action. Within the CDs, β-CD is mainly used because its cavity diameter is suitable for hormones, vitamins, and also pharmaceutical compounds (Makieła et al. 2018; Mahjoubin-Tehran et al. 2020).

Another important factor that needs to be mentioned, is the resistance of CDs to stomach acids. However, α-amylases, which are found in pancreatic juice and saliva, are able to degrade CDs. The rate of hydrolysis depends on the size of the ring and the CD´s complex with other molecules. Large γ-CD is rapidly digested by α-amylases in pancreatic juice and saliva, whereas α- and β-CD are resistant to these enzymes in the gastrointestinal tract and can reach the colon after an oral administration. In the colon, α- and β-CD are degraded by fungal and bacterial enzymes whereas β-CD is more susceptible to degradation than α-CD. The bioavailability of CDs is limited and less than 4%. For instance, the oral bioavailability of HPβCD has been estimated to be between 0.5 and 3.3%. Once absorbed, after oral or intravenous administration, intact CDs mostly accumulate in the kidney and are excreted in the urine (Stella and He 2008; Stevens 1999; Loftsson and Brewster 2010).
In terms of the toxicity, parental CDs such as α-CD and β-CD have been shown to be renal toxic. Both β-CD and HPβCD have an affinity for cholesterol and can extract it from cells and form complexes. Due to the poor solubility of β-CD, these complexes are insoluble and lead to microcrystalline precipitation in the kidney resulting in renal damage. HPβCD can reduce these problems due to its higher solubility. As a result, HPβCD and sulphobutyl ether β-CD (SBEβCD) are much safer and have shown no toxic effects and no immune response in mammals. They have been accepted by the US Food and Drug Administration's (FDA) and are "generally recognized as safe" (GRAS). At high doses, only minor side effects such as diarrhea can appear (Stella and He 2008). Therefore, these CDs are already used in the pharmaceutical industry to enhance the oral bioavailability of poorly soluble drugs (Davis and Brewster 2004; M Maheriya 2017). All in all, CDs are readily available and provide a non-toxic, cost-effective, and safe delivery of important medical drugs. In this study, HPβCD was used and is referred to as CD in the following.

1.4 Aim of the project

It has recently been proposed that the innate immune system plays an important role in the process of aortic diseases. In particular, the activation of PRRs may be critical in this context. Our concept of disease development suggests that the activation of TLR3 drives the process of

EndMT, fibrosis, and calcification of the valve cusps leading to the development of AS. Therefore, we analyzed the mechanisms of calcification in VICs and EndMT in VECs. Another key research question of this project was, how does TLR3 affect the progression of AS in a living system? Therefore, mouse models that underwent an invasive intervention were established and AS was elucidated in *in vivo* experiments.

The absorption, biosynthesis, metabolism, and excretion of cholesterol must be highly regulated because excess cholesterol can be harmful. Zimmer and colleagues provided an in-depth analysis of CD showing its importance in solubilizing CC in mice developing atherosclerosis (Zimmer et al. 2016). Based on their study, this work investigated the role of CC in AS as well as CD as a treatment for AS. Therefore, human plasma from patients with AS was considered as well as *in vitro* experiments in VICs and VECs were performed. The aim was to investigate whether CC play a role in the process of calcification in VICs and EndMT in VECs and to examine the solubility of CC after the addition of CD.

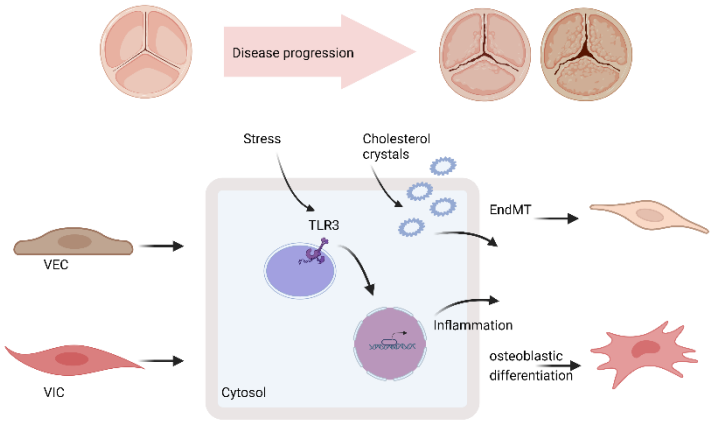

Figure 8 Aim of the study

Aim of the study was to first investigate the molecular mechanisms of PRRs in regard to the process of AS. In this way, we focused on TLR3. We analyzed TLR3 in the mechanisms of calcification in VICs and EndMT in VECs which are main drivers for the pathomechanisms of AS. Secondly, the role of CC in regard to calcification and EndMT was investigated in this study. AS= Aortic valve stenosis; CC= Cholesterol crystals; EndMT= Endothelial to mesenchymal transition; PRR= Pattern recognition receptors; TLR3= Toll-like receptor 3; VEC= Valvular endothelial cell; VIC= Valvular interstitial cell

Figure created with Biorender.com

2. Material and Methods

2.1. Reagents

Table 1 Chemicals and Kits

Equipment	Company	Catalog number
Aceton	Merck (Darmstadt, Germany)	1.00014.1011
AlamarBlue Cell Viability Reagent	Thermo Fisher Scientific (Waltham, MA, USA)	DAL1025
Alizarin Red S	Sigma Aldrich (Taufkirchen, Germany)	A5533
Anti-TLR3 Antibody	Abcam (Waltham, MA, USA)	ab62566
BCA Kit	Thermo Fisher Scientific (Waltham, MA, USA)	23227
BSA Fraction V	Bio&Sell (Nürnberg, Germany)	BSA.FV.0050
Bromphenol blue	Merck (Darmstadt, Germany)	0061159
Caspase-Glo® 3/7 Assay	Promega (Mannheim, Germany)	G8091
Cavitron	Ashland (Covington, Kentucky, USA)	826764
Cell Scrapers	Sarstedt (Nümbrecht, Germany)	83.1830
Cholesterol	Merck (Darmstadt, Germany)	C8667
Chloroform	Carl Roth (Karlsruhe, Germany)	6340.1
Cryo-SFM	PromoCell (Heidelberg, Germany)	C-29912
Dako Pen (Delimiting Pen)	Dako (Hamburg, Germany)	S2002
DAPI Vectashield®	Vector Laboratories (Stuttgart, Germany)	H-1200
Direct Red 80 (Sirius Red)	Sigma Aldrich (Taufkirchen, Germany)	365548
Dulbecco's Modified Eagle's Medium (DMEM), Glucose GlutaMAX Supplement	Thermo Fisher Scientific (Waltham, MA, USA)	31966047
Dulbecco´s Phosphate- Buffered Saline (DPBS)	Gibco Life Technologies (Carlsbad, CA, USA)	14190-094
EBM-2 (Endothelial Cell Growth Basal Medium)	Lonza (Basel, Switzerland)	CC-3156
EGMTM -2 MV Microvascular Endothelial Cell Growth	Lonza (Basel, Switzerland)	CC-4147
Entellan	Millipore Sigma (Billerica, MA, USA)	1079600500

Eosin	Carl Roth (Karlsruhe, Germany)	X883.2
Ethanol ROTIPURAN® ≥99,8 %, p.a.	Carl Roth (Karlsruhe, Germany)	9065.4
Fetal Bovine Serum (FBS)	Gibco Life Technologies (Carlsbad, CA, USA)	A3160802
Formaldehyde Solution 4%	Sigma Aldrich (Taufkirchen, Germany)	1.00496.5000
Glycine	Applichem (Darmstadt, Germany)	131340.0914
Hematoxylin	Carl Roth (Karlsruhe, Germany)	T864.2
High-Capacity cDNA Reverse Transcription Kit	Thermo Fisher Scientific (Waltham, MA, USA)	43-688-13
L (+)-Ascorbic Acid	Carl Roth (Karlsruhe, Germany)	3525.2
Lipofectamine 2000	Thermo Fisher Scientific (Waltham, MA, USA)	11668019
Medium-2 BulletKitTM (VECs)	Lonza (Basel, Switzerland)	CC-3202
Methanol	Applichem (Darmstadt, Germany)	131091.1212
4–15% Mini-PROTEAN	Bio-Rad (Hercules, California, USA)	4561084
Normal Goat Serum	Dianova (Holland, OH, USA)	005-000-121
Opti-MEM	Thermo Fisher Scientific (Waltham, MA, USA)	31985062
PageRuler™ Prestained Protein Ladder	Thermo Fisher Scientific (Waltham, MA, USA)	26616
PBS 10x, pH 7.4	Thermo Fisher Scientific (Waltham, MA, USA)	70011044
PBS 1x, pH 7.4	Thermo Fisher Scientific (Waltham, MA, USA)	10728775
Penicillin/Streptomycin (P/S)	Millipore Sigma (Billerica, MA, USA)	516106
Picric Acid- Solution 1.2%	Applichem (Darmstadt, Germany)	A2520
Polyinosinic-Polycytidylic Acid Sodium Salt	Sigma Aldrich (Taufkirchen, Germany)	P1530
Recombinant Human IL1 Beta/IL1F2 Protein	R&D Systems (Minneapolis, Minnesota, USA)	201-LB-010
Recombinant Human TGF-Beta 1 Protein	R&D Systems (Minneapolis, Minnesota, USA)	240-B-002
Recombinant Human TNF-α	Thermo Fisher Scientific (Waltham, MA, USA)	300-01A-250
Silencer™ Select Negative Control No. 1 siRNA	Thermo Fisher Scientific (Waltham, MA, USA)	4390843

Sodium Dihydrogen Phosphate (NaH_2PO_4)	Merck (Darmstadt, Germany)	A638346
Sodiumdodecylsulfat (SDS)	Molekula Group (Darlington, UK)	15171947
TaqMan™ Gene Expression Master Mix	Thermo Fisher Scientific (Waltham, MA, USA)	4369542
TLR3/dsRNA Complex Inhibitor – Calbiochem	Millipore Sigma (Billerica, MA, USA)	614310
Trizma Base	Sigma Aldrich (Taufkirchen, Germany)	T4661
Triton™ X-100	Sigma Aldrich (Taufkirchen, Germany)	T8787
Trizol Reagent	Thermo Fisher Scientific (Waltham, MA, USA)	15596018
Tween® 20, Viscous Liquid	Sigma Aldrich (Taufkirchen, Germany)	P2287
Von Kossa Staining Kit	Abcam (Waltham, MA, USA)	ab150687
UltraPure™ DNase/RNase-Free Distilled Water	Gibco Life Technologies (Carlsbad, CA, USA)	10977049
Ultrafree-MC-DV Centrifuge Filters; Durapore-PVDF 0,65µm	Millipore Sigma (Billerica, MA, USA)	UFC30DV0S
Xylol	Applichem (Darmstadt, Germany)	251769.2714
2-Propanol, ROTIPURAN® ≥99,8 %, p.a.	Carl Roth (Karlsruhe, Germany)	6752.5
1-Propanol	Carl Roth (Karlsruhe, Germany)	9169.1

2.1.1 Taqman primer

All primers were purchased from Thermo Fisher Scientific Company (Waltham, MA, USA) with the following catalog number: 4351370.

Table 2 Taqman primer

Primer	**Description**
Bone Morphogenetic Protein 2 (*BMP2*)	Hs00154192_m1
Interleukin 6 (*IL6*)	Hs00174131_m1
Runt-Related Transcription Factor 2 (*RUNX2*)	Hs01047973_m1
Toll-Like Receptor 3 (*TLR3*)	Hs01551079_g1
Glyceraldehyde-3-Phosphate Dehydrogenase (*GAPDH*)	Hs02758991_g1
Smooth Muscle Alpha -2 Actin (*ACTA2*)	Hs00426835_g1
Von Willebrand Factor (*VWF*)	Hs01109446_m1
Platelet Endothelial Cell Adhesion Molecule (*PECAM1*)	Hs01065279_m1
Vascular Cell Adhesion Protein 1 (*VCAM1*)	Hs00365486_m1
Endothelial Nitric Oxide Synthase 3 (*NOS3*)	Hs01574665_m1
Vimentin (*VIM*)	Hs00418522_m1
Melanoma Differentiation-Associated Protein 5 (*IFIH1*)	Hs00223420_m1
Interleukin 1 beta (*IL1β*)	Hs01555410_m1
Smooth Muscle Protein 22-Alpha (*TAGLN*)	Hs00162558_m1
Toll-Like Receptor 2 (*TLR2*)	Hs00610101_m1
Toll-Like Receptor 4 (*TLR4*)	Hs00152939_m1
Toll-Like Receptor 9 (*TLR9*)	Hs00370913_s1
Cyclic GMP-AMP Synthase (*MB21D1*)	Hs00403553_m1
Retinoic Acid-Inducible Gene I (*DDX58*)	Hs01061436_m1

2.1.2 Antibodies

Table 3 Antibodies

Antibodies from Abcam (Waltham, MA, USA), Thermo Fisher Scientific (Waltham, MA, USA), Antibodies-Online (Limerick, PA, USA), Jackson Immuno Research (Pennsylvania, USA), Sigma-Aldrich (Taufkirchen, Germany), Dianova (Holland, OH, USA), and LI-COR (Lincoln, Nebraska, USA)

Antibody	Catalog number	Host species	Dilution	Company
Anti-CD68	ABIN181836	Rat	1:100	Antibodies-Online
Anti-TLR3	ab62566	Rabbit	1:100	Abcam
Anti-eNOS	ab76198	Mouse	1:100	Abcam
Anti-CD31 (IF)	PA5-16301	Rabbit	1:50	Thermo Fisher Scientific
Anti-VCAM1	ab134047	Rabbit	1:100 (IF); 1:1000 (WB)	Abcam
Anti-BMP2	ab214821	Rabbit	1:100	Abcam
Anti-MDA5	ab79055	Rabbit	1:100	Abcam
Anti-CD31 (WB)	ab187377	Mouse	1:500	Abcam
Anti-Vimentin	ab8978	Mouse	1:100	Abcam
Anti-beta-Actin	a1978	Mouse	1:1000	Sigma-Aldrich
Anti-Histone H3	ab1791	Rabbit	1:1000	Abcam
IgG (H+L)-Cy3	111-165-144	Goat anti-Rabbit	Same as primary AB	Dianova
IgG (H+L)-Cy2	111-225-144	Goat anti-Rabbit	Same as primary AB	Dianova
IgG (H+L)-Cy3	115-165-146	Goat anti-Mouse	Same as primary AB	Dianova
IgG (H+L)-Cy2	115-225-146	Goat anti-Mouse	Same as primary AB	Dianova
IgG (H+L)-Cy3	712-165-153	Goat anti-Rat	Same as primary AB	Jackson Immuno Research
IgG (H+L)- 680RD	926-68072	Donkey anti Mouse	1:10000	LI-COR
IgG (H+L)- 800RD	926-32213	Donkey anti Rabbit	1:10000	LI-COR

IF= Immunofluorescence; WB= Western blot; AB= Antibody

2.1.3 siRNA sequences

siRNA TLR3 (Thermo Fisher Scientific (Waltham, MA, USA), Catalog number: 107055):

sense: GGUACCUGAAUUUGAAACGtt

antisense: CGUUUCAAAUUCAGGUACCtc

siRNA TLR3 (Thermo Fisher Scientific (Waltham, MA, USA), Catalog number: 107056):

sense: GGUACAUCAUGCAGUUCAAtt

antisense: UUGAACUGCAUGAUGUACCtt

2.2 Laboratory equipment

Table 4 Laboratory equipment and software

Equipment/ Software	**Company**
Centrifuge 5430	Eppendorf (Hamburg, Germany)
Centrifuge 5810 R	Eppendorf (Hamburg, Germany)
ChemiDoc Imaging Systems	Bio-Rad (Hercules, CA, USA)
Concentrator 5301	Eppendorf (Hamburg, Germany)
Cryostat 3050S	Leica (Mannheim, Germany)
FlowJo™ Software	BD Biosciences (Heidelberg, Germany)
Flow Cytometer BD FACS Calibur	BD Biosciences (Heidelberg, Germany)
Fluorescence Microscope Axiovert 200M	Zeiss (Oberkochen, Germany)
Freezing Container Mr. Frosty	Thermo Fisher Scientific (Waltham, MA, USA)
Mastercycler Pro	Eppendorf (Hamburg, Germany)
Microscope	Zeiss (Oberkochen, Germany)
Microplate Reader Infinite M Plex	TECAN (Männedorf, Switzerland)
Nanodrop 2000c Spectrophotometer	PeQLab (Erlangen, Germany)
Qubit® Protein Assay Fluorometer	Thermo Fisher Scientific (Waltham, MA, USA)
Realtime PCR Software Quant Studio 3	Applied Biosystems (Carlsbad, CA, USA)
Realtime PCR Software Quant Studio 5	Applied Biosystems (Carlsbad, CA, USA)
Thermomixer Comfort	Eppendorf (Hamburg, Germany)
ZEN Microscopy Software	Zeiss (Oberkochen, Germany)

2.3 Media and buffers

Culturing medium for valvular interstitial cells

DMEM

+10% FBS

+1% P/S

Calcification medium for valvular interstitial cells

DMEM

+5% FBS

+1% P/S

+2 mmol/l NaH_2PO_4

+50 µg/ml Ascorbic Acid

Culturing medium for valvular endothelial cells

EBM-2

+5% FBS

+0.04% Hydrocortisone

+0.4% hFGF-β (Fibroblast growth factor beta)

+0.1% VEGF (Vascular Endothelial Growth Factor)

+0.1% R3-IGF-1 (Long arginine 3- insulin-like growth factor 1)

+0.1% Ascorbic Acid

+0.1% hEGF (Human Epidermal Growth Factor)

Endothelial to mesenchymal transition induction in valvular endothelial cells

EBM-2

+5% FBS

+0.4% hFGF-B

+0.1% R3-IGF-1

+0.1% Ascorbic Acid

+0.1% hEGF

+ 30, 10 or 2 ng/ml TGFβ1

+ 1ng/ml IL1β

6x Loading buffer

+ 120mM DTT (Dithiothreitol)

+300mM Tris-HCL (pH 6,8)

+9% SDS

+48% Glycerol

+0.1% Brom phenol blue

10xTBS (Tris-Buffered Saline) pH (8.2)

+1M Tris (Tris-Base)

+1.5M NaCl

TBS-T

10xTBS diluted to 1xTBS

+0.1% Tween20

5% BSA-TBS-T (blocking buffer, antibody buffer)

TBS-T+ 5% BSA

5xTransferbuffer

+Aqua dest.

+29g/l Tris-Base

+145g/l Glycine

+5g/l SDS

1xTransferbuffer

+200ml/l 5xTransferbuffer

+200ml/l Methanol

+600ml/l Aqua dest.

2.4 Human samples

2.4.1 Collection of human aortic valve samples

Human aortic valves were obtained from the Cardiac and Thoracic Surgery Department of the University Hospital, Bonn, Germany, from patients that underwent surgical aortic valve replacement for AS or aortic regurgitation (AR). The samples were collected by our collaborators from Project B04 (research group of PD Dr. med. Felix Jansen) of the TRR259. All patients provided written informed consent. The protocol was approved by our local ethics committee under reference code AZ 078/17.

2.4.2 Immunohistochemistry and immunofluorescence of human aortic valves

Samples were deparaffinized with xylene and then the slides were slowly passed by a series of decreasing alcohol concentrations for rehydration. For antigen retrieval, slides were boiled in 10nM citrate buffer and afterwards washed again with distilled water. Slides were incubated with PBS containing 0.25% Triton X-100 to permeabilize the cells followed by 3 washing steps

with PBS. For blocking, slides were incubated in 5% BSA in PBS-T and 0.3M Glycine. Afterwards, primary antibodies diluted in 1% BSA PBS-T were added and incubated overnight at 4°C. The next day, slides were washed twice with PBS-T followed by incubation with the secondary antibody diluted in 1% BSA PBS-T. DAPI mounting medium was added and slides were covered with cover glass.

2.4.3 Collection of human blood samples

Blood samples were collected in the clinic from patients undergoing cardiac catheterization. The study was approved by the local ethics committee (Reference code from the local ethics committee, Germany: 106/14, 078/17) and written informed consent was obtained from all patients prior to blood collection. To ensure confidentiality, each sample was given a unique number and patient information was handled discreetly. Blood was collected from an arterial sheath in standard EDTA tubes. Plasma was separated from corpuscular components by centrifugation at 2000g for 15 minutes at 4°C. Samples were used for flow cytometry measurement or stored at -80°C.

2.4.4 Cholesterol crystal preparation

20mg of cholesterol was added to 1ml of 1-propanol and 2ml of endotoxin-free water. For crystallization, the mixture was incubated at room temperature for 1 hour. The precipitate was then centrifuged at 13000rpm for 2 minutes in 0.65µm filter tubes. The residue was dried overnight at 30°C in a concentrator. 2mg were resuspended in 1ml 1% BSA-PBS followed by incubation in an ultrasonic bath for 10 minutes. CC solution was stored at 4°C.

2.4.5 Measurement of cholesterol crystal dissolution rate

HPβCD was dissolved in PBS to give the following concentrations: 0.1mM, 1mM, or 10mM, which were added to samples containing plasma, and CC. Flow cytometry was performed to measure cholesterol crystal dissolution rate (CCDR) and data were analyzed using FlowJo-software (FlowJo V10.8.1). Counting beads gated in FlowJo (A in figure 9) were used to validate the crystal concentration within the samples. Initial CC suspended in PBS were validated and tested to achieve approximately 300 events per second. CC were identified using forward and side scatter characteristics. For each patient, plasma samples without CC supplementation were measured and gated to exclude background events attributed to the plasma. (B in figure 9). Plasma samples were then supplemented with CC and incubated for 0, 0.5, 2, and 4 hours before measurement.

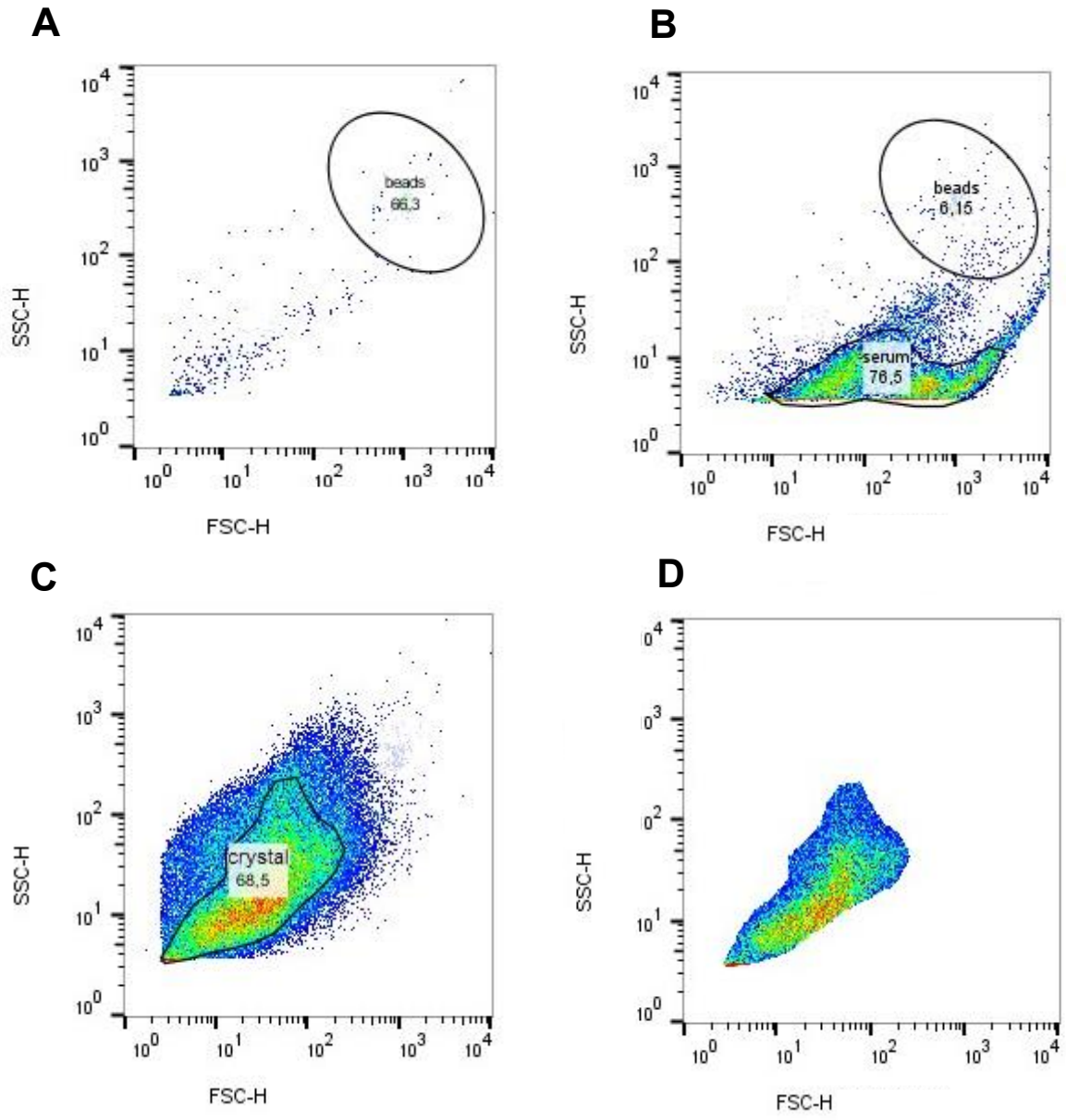

Figure 9 Gating strategy for measuring cholesterol crystal dissolution rate

A*: First, only beads were measured,* ***B****: Plasma was measured and afterwards,* ***C****: CC were measured and gated. All parameters were gated via side and forward scatter using flow cytometry method.*

FSC= Forward Scatter; SSC= Side Scatter; CC= Cholesterol crystals

2.5 Cell culture

Human VICs and VECs were purchased from Lonza. The cells were obtained from healthy donors who died of non-cardiac causes. All donors were female and the age was between 35 and 56. Cell batches from different donors showed heterogeneous results. Thus, mainly 3 biological and 2-3 technical replicates were used for each experiment.

2.5.1 Valvular interstitial cell culture

Lot: 9F4046: Female, 35 years old

Lot: 1F5026: Female, 37 years old

Lot: 0F5055: Female, 55 years old

Lot: 1F5266: Female, 49 years old

Lot: 1F5268: Female, 56 years old

VICs were cultured in flasks in a prewarmed culturing medium containing DMEM medium supplemented with 10% FBS and 1% P/S. Cells were incubated at 37°C in a humidified 5% CO_2 atmosphere. Media were changed every other day and cultured until passage 6. When confluent, cells were split using the ReagentPack from Lonza. Trypsinization was performed at 37°C for 5-10 minutes after washing with HEPES buffered saline solution and was stopped by the addition of trypsin neutralizing solution (TNS). Cells were centrifuged for 8 minutes at 800g. Cell pellets were resuspended in fresh medium and pipetted into new, sterile flasks. For long term storage, cells were cryo-conserved. For this, cell pellets were dissolved in freezing medium (Cryo-SFM) and stored in Cryo-vials (1ml/vial) in a freezing container at -80°C. After 24 hours, the cryo-vials were transferred to -150°C.

2.5.2. Valvular endothelial cell culture

Lot: 9F4047: Female, 35 years old (same donor as for VIC: 9F4046)

Lot: 1F5027: Female, 37 years old (VIC: 1F5026)

Lot: 0F5132: Female, 36 years old

Lot: 1F5269: Female, 56 years old (VIC: 1F5268)

VECs were cultured in flasks in prewarmed culturing medium containing EBM-2 basal medium supplemented with 5% FBS, 0.04% hydrocortisone, 0.4% hFGF-B, 0.1% VEGF, 0.1% R3-IGF-1, 0.1% ascorbic acid, 0,5ml GA-1000, and 0.1% hEGF until passage 6. Cells were incubated at 37°C in a humidified 5% CO_2 atmosphere and medium was changed every other day. Cells were split by changing the medium when confluency was reached. Trypsinization was performed at 37°C for 5-10 minutes after washing the cells with HEPES buffered saline solution. The trypsinization reaction was stopped by TNS and the cell suspension was centrifuged for 8 minutes at 800g. Cell pellets were resuspended in fresh medium and pipetted into new flasks. For long term storage, cells were cryo-conserved. For this, cell pellets were dissolved in freezing

medium (Cryo-SFM). Each cryo-vial was filled with 1ml of the cell suspension and stored in a freezing container at -80°C. After 24 hours, the cryo-vials were transferred to -150°C.

2.5.3 Calcification of valvular interstitial cells

Calcification was induced in conditioning medium (DMEM containing 5% FBS, 1% P/S, 2 mmol/l NaH_2PO_4, 50 µg/ml ascorbic acid), referred to as pro-calcifying medium (PCM). Cells were incubated at 37°C in a humidified 5% CO_2 atmosphere for 7 days. Every other day the medium was changed.

2.5.4 Activation of pattern recognition receptors in valvular interstitial cells

To provide an overview of the PRR expression and their putative role in AS, VICs were treated with specific stimuli to activate the underlying receptors (Table 5). Experiments were performed in cooperation with Project A03 from TRR259 (PhD student Madeleine Graef, research group of Prof. Dr. Gunther Hartmann; Institut für Klinische Chemie und Klinische Pharmakologie, Universitätsklinikum Bonn). Within these experiments, Madeleine Graef performed the treatment and was responsible for RNA isolation, as well as cDNA synthesis. I was responsible for the cell culture as well as qPCR measurements.

Table 5 Ligands and concentrations for pattern recognition receptor stimulation

Receptor	**Ligand**	**Transfection reagents**	**Amount per 1ml medium**
cGAS	dsDNA (HT-DNA)	Lipofectamine 2000	400ng/2µl Lipofectamine
MDA5	PolyIC	TransIT®-LT1 (LT1)	800ng /4.8µl LT1
RIG-I	3p-dsRNA (IVT4)	Lipofectamine 2000	400ng/2µl Lipofectamine
TLR2	Pam3CysK4	-	2µg
TLR3	PolyIC	-	10µg
TLR4	LPS	-	1µg
TLR9	CpG2006	Poly-L-Arginine	8µg/7.2µl pLArg

MDA5= Melanoma differentiation-associated protein 5; RIG-I= Retinoic Acid inducible Gene I; RUNX2= Runt-related transcription factor 2; TLR= Toll-like receptor; IVT4= 5' Triphosphate double-stranded RNA; HT-DNA= Deoxyribonucleic acid sodium salt from herring testes; PolyIC= Polyinosinic:polycytidylic acid; Pam3CysK4 =Pam3CysSerLys4; LPS= Lipopolysaccharide; CpG2006= TLR9 Ligand

Cells were incubated at 37°C in a humidified 5% CO_2 atmosphere for 72 hours after transfection. Afterwards, calcification was induced as described above (Chapter 2.5.3).

2.5.5 TLR3 knockdown in valvular interstitial cells

VICs in passage 6 were seeded on 12-well plates for gene expression, 96-well plates for cell viability tests, and 48-well plates for Alizarin Red S. When they reached approximately 80% confluence, TLR3 siRNA (concentration 10mM), PolyIC (concentration 4ng/ml), or scrambled siRNA as negative control (neg control) were transfected into cells using Lipofectamine 2000 (4µl/ml). Cells were incubated at 37°C in a humidified 5% CO_2 atmosphere for 48 hours after transfection. Subsequently, calcification was induced by incubating the cells in PCM as described in the respective chapter (Chapter 2.5.3).

2.5.6 PolyIC/ C4a treatment in valvular interstitial cells

For stimulation, cells were seeded in passage 6 on 12-well plates for gene expression, 96-well plates for cell viability tests, and 48-well plates for Alizarin Red S. When the cells reached approximately 80% confluence, they were treated with 10µg/ml PolyIC and 10µg/ml compound C4a for 72 hours. Afterwards, calcification was induced as described in the respective chapter (Chapter 2.5.3).

2.5.7 Endothelial to mesenchymal transition induction in valvular endothelial cells

Different conditions with various concentrations were tested in cooperation with Dr. Marko Bulic (Table 10, figures 55, 56, 57, in chapter 6.1). The protocol for EndMT was optimized and standardized. The following protocol was used for subsequent experiments:

Cells were incubated in EndMT medium containing EBM-2 basal medium supplemented with 5% FBS, 0.4% hFGF-B, 0.1% R3-IGF-1, 0.1% Ascorbic Acid, and 0.1% hEGF. In addition, cells were stimulated with 30ng/ml TNFα, 2ng/ml TGFβ1, and 2ng/ml TGFβ1+1ng/ml IL1β in combination. Medium was changed every other day. Cells were incubated at 37°C in a humidified 5% CO_2 atmosphere for 5-7 days.

Protein concentration was measured using the BCA Protein Assay Kit. Proteomic analysis was performed by Dr. Robert Hardt and Dr. Marc Sylvester from the core facility for mass spectrometry using the Tandem Mass Tags (TMT) method and analyzed by Dr. Farhad Shakeri and Dr. Andreas Buness from the Bioinformatics- Medical Faculty (P-459-NW PS01+02).

2.5.8 TLR3 during the process of endothelial to mesenchymal transition

VECs were first treated with PolyIC, or C4a, or both in starvation medium (without any supplements) followed by incubation of 24 hours at 37°C. Afterwards, EndMT was induced as described at the end of chapter 2.5.7.

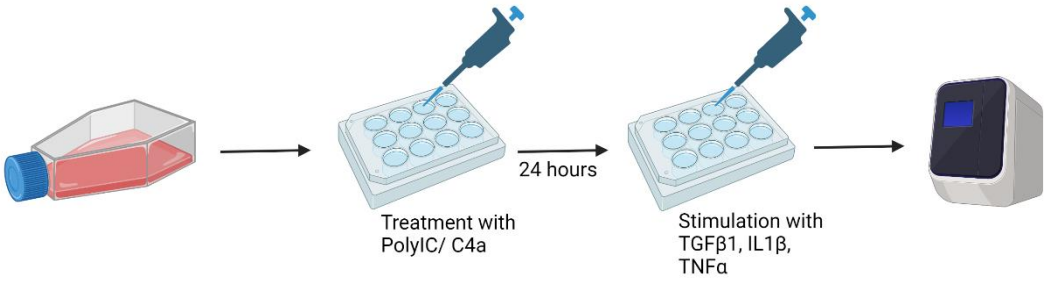

Figure 10 Schematic description of the experimental setup for endothelial to mesenchymal transition

First, VECs were treated with PolyIC/C4a or left untreated as control. After 24 hours of incubation, cells were stimulated with TGFβ1/IL1β, TNFα, for 5-7 days or left unstimulated as control.

IL1β= Interleukin 1 beta; TGFβ1= Transforming growth factor-beta 1; TNFα= Tumor necrosis factor-alpha; VEC= Valvular endothelial cells; C4a= Compound 4a; PolyIC= Polyinosinic:Polycytidylic acid

Figure created with Biorender.com

2.5.9 TLR3 knockdown in valvular endothelial cells

VECs in passage 6 were seeded on 12-well plates for gene expression. When they reached approximately 80% confluence, TLR3 siRNA, PolyIC, or scrambled siRNA as neg control were transfected into cells using Lipofectamine 2000 (2µl/ml). The transfection concentration of siRNA against TLR3 was 20nM and PolyIC concentration was 2ng/ml. Cells were incubated at 37°C in a humidified 5% CO_2 atmosphere for 24 hours after transfection.

2.5.10 Microscopic images of cholesterol crystals in valvular interstitial cells and valvular endothelial cells

To visualize CC uptake by VECs and VICs, 20µg/ml CC were added to the cell medium. Images were taken every 5 minutes for 8 hours using a microscope and its heating and culturing chamber, which allowed cells to be incubated at 37°C in a humidified 5% CO_2 atmosphere.

2.5.11 Cholesterol crystals in valvular interstitial cells

VICs were seeded in passage 6 on 12-well plates for gene expression. When the cells reached approximately 80% confluence, they were treated with 20µg/ml CC and/or 10mM CD. CD was reconstituted in DNase free water to a concentration of 1000mM and filtered through a 0.2µm syringe sterilizing filter. Cells were incubated at 37°C in a humidified 5% CO_2 atmosphere for 6 hours after treatment. Subsequently, calcification was induced by changing the medium to PCM as described in the relevant section (Chapter 2.5.3) Medium was changed every other day. In addition, 10mM CD was added to BM/PCM. After 7 days, the cells were harvested for RNA isolation.

2.5.12 Cholesterol crystals in valvular endothelial cells

VECs in passage 6 were seeded onto 12-well plates for gene expression. When the cells reached approximately 80% confluence, they were treated with 20µg/ml CC for 7 hours. Afterwards, EndMT was induced by supplementing cells with TGFβ1+IL1β or TNFα. In addition, 10mM CD was added to the respective medium. CD was reconstituted in DNase-free water to a concentration of 1000mM and sterile filtered through a 0.2µm syringe filter. Cells were incubated at 37°C in a humidified 5% CO_2 atmosphere and medium was changed every other day. RNA was isolated after 7 hours or 5 days.

2.6 RNA extraction and cDNA synthesis

For RNA isolation, cells were harvested using the already described phenol/chloroform RNA extraction (Chomczynski and Sacchi 2006; Chomczynski and Sacchi 1987). The concentration of extracted RNA was detected with Nanodrop spectrophotometer. RNA was stored at -80°C. 200ng of total RNA was reversely transcribed into complementary deoxyribonucleic acid (cDNA) using the High-Capacity cDNA Reverse Transcription Kit according to the manufacturer´s protocol.

The Kit contains all components that are needed for the quantitative conversion: a reverse transcriptase Super mix that includes 25x dNTP Mix and random hexamer primers providing coverage across a wide variety range of messenger ribonucleic acid (mRNA) templates. The reaction mix was set up to a final volume of 20µl (Table 6).

Table 6 Reaction mixture for cDNA synthesis

The reaction mix for cDNA synthesis was set up to a final volume of 20µl.

Volume	**Component**
2.0µl	2x RT Master mix
0.8µl	25x dNTP mix (100mM)
2.0µl	10x Random primers
1.0µl	Multiscribe reverse transcriptase
1.0µl	RNase inhibitor
3.2µl	Nuclease free water
10µl	RNA

The cDNA synthesis was performed with Mastercycler Pro and consists of 3 steps: In the first step, primers anneal to the mRNA template at 25°C, followed by reverse transcription at 37°C, and finally the enzyme is inactivated at 85°C (Table 7). After the cDNA has been synthesized, samples were used for qPCR or were stored at -20°C.

Table 7 Reaction protocol for cDNA synthesis

Cycles	**Time**	**Temperature**
1x	10 minutes	25°C
1x	120 minutes	37°C
1x	5 minutes	85°C
	Hold	4°C

2.7 Detection of mRNA expression using Real-Time qPCR

qPCR is generally used to quantify a gene of interest in a sample (Pfaffl 2001). The housekeeping gene *GAPDH* was used as a reference gene. Reactions were performed in 2 technical replicates using gene expression Master Mix. For gene amplification, the TaqMan™ Gene Expression Assay (FAM) was used. It contains a combination of forward and reverse primers, that match sequences of the cDNA. The qPCR reaction mix was set up to a final volume of 15µl (Table 8).

Table 8 Reaction mixture for qPCR measurement

Components	**Volume per reaction**
Gene expression master mix	10µl
Primer mix	0.75µl
Nuclease free water	1.75µl
cDNA template	5µl

During qPCR, the cDNA double strand is denatured into 2 single strands. The primers are used to bind complementary DNA sequences in opposite directions and the DNA polymerase synthesizes a complementary DNA strand. Dye molecules are detected by fluorescence. After amplification, the samples are heated to 95°C to denature double-stranded fragments before entering the reaction cycle again. qPCR was performed with the Realtime PCR Software Quant Studio 5/3. For data analysis, the relative levels of target gene expression were calculated by the Comparative Ct Method (ΔΔCt Method) for target genes as well as the housekeeping genes. Data are represented as mean ± SEM. One, or Two-way ANOVA tests, as well as Student´s t-test were performed with Prism 9 (GraphPad Software, Inc., San Diego, CA, USA) to test the statistical significance of qPCR data.

Table 9 qPCR reaction protocol

Time	Temperature	Step	
2 Minutes	50°C		Incubation stage
10 Minutes	95°C	Polymerase activation	
15 Seconds	95°C	Denature	PCR stage (50 cycles)
60 Seconds	60°C	Anneal/extend	

2.8 Alizarin Red S staining

Alizarin Red S is used to stain free calcium deposits. Cells were fixed for 15 minutes in 4% paraformaldehyde followed by a washing step with ultrapure distilled water. Afterwards, cells were incubated with 1% Alizarin Red S solution (pH 4.2) for 15-30 minutes at room temperature. The dye was removed by washing twice with ultrapure distilled water. Images of Alizarin Red S was captured by microscope.

2.9 AlamarBlue assay

AlamarBlue assay indicates metabolic active cells and therefore, was used to test cell viability. Viable cells convert resazurin into the fluorescent molecule resorufin, which is a non-toxic, cell permeable compound in blue color. The alamarBlue reagent was added to cells on a 96-well plate and incubated for 4 hours at 37°C. Afterwards, fluorescence (using 560nm excitation and 590nm emission wavelength) was detected using Tecan Microplate Reader Infinite M Plex.

2.10 Caspase 3/7 assay

To measure the Caspase 3 and 7 activities, biomarkers for apoptosis, the luminescent assay Caspase- Glo 3/7 was used. For this, cells were seeded on 96-well opaque plates. The assay reagents were mixed and added to the cells. After incubation for 3 hours at room temperature, luminescence was measured using the Tecan Microplate Reader Infinite M Plex.

2.11 Immunocytochemistry

Immunocytochemistry was used to anatomically visualize the localization of a specific protein or antigen in cells or on the cell surface. For this, the specific primary antibodies are made visible with fluorophore conjugated secondary antibodies. Cells were washed once with PBS in preparation for staining of specific proteins. Afterwards, cells were fixed with 4% formaldehyde

for 30 minutes at room temperature. After 3 more washing steps, cells were permeabilized for 10 minutes in 0.1% Triton-X-100 followed by 3 further washing steps. For blocking, cells were incubated for 30 minutes in 1% BSA, 22.52mg/ml Glycine in PBS-T (0.1% Tween20) at room temperature. Afterwards, cells were incubated with the primary antibody in 10% BSA at 4°C overnight.

On the next day, cells were washed 3 times with PBS followed by 1 hour incubation with the secondary antibody at room temperature. Afterwards, slides were mounted with DAPI and analyzed with a fluorescence microscope.

For co-staining with a second antibody, on the next day, cells were washed 3 times with PBS. Secondary antibody, diluted in 10% BSA was added and incubated for 1 hour at room temperature. After 3 washing steps, cells were blocked with 10% normal goat serum for 30 minutes in a dark area at room temperature. Afterwards, cells were incubated overnight at 4°C with the second primary antibody in 1% normal goat serum. After another 3 washing steps on the next day, cells were incubated with the secondary antibody at room temperature for 1 hour followed by washing with PBS. Finally, cells were mounted with DAPI and analyzed with a fluorescence microscope.

2.12 Western blot

Western blot was used to confirm protein expression in VECs and VICs. This method is based on the separation of proteins by gel electrophoresis and their immunodetection of a specific antigen using antibodies after transferring them to a membrane. Before quantifying the protein expression, cells were treated respectively. For protein quantification, samples were lysed adding RIPA buffer with protease inhibitors on ice. After centrifugation and ultrasound bath, the supernatant was kept and stored at -80°C. The protein concentration was determined by Qubit™ protein assay and normalized to 30µg in 6x loading buffer. Samples were heated to 95°C for 10 minutes in a heat block.

Proteins were separated through denatured SDS- polyacrylamide gel electrophoresis. Samples were loaded onto the 4–15% Mini-PROTEAN gel and ran in 1x SDS Electrophoresis buffer. For identification, the PageRuler Prestained Protein Ladder was additionally loaded onto the gel. The gel was run for 60 minutes at 80V until the blue dye front migrated to the bottom of the gel. Afterwards, the gel was transferred to a PVDF membrane. The sandwich, containing sponges, the filter papers, the gel, and the membrane was placed into the transfer puffer between a tank cassette into the transfer tank. The whole gel transfer took 1 hour at 350mA.

The membrane was transferred after the electrophoresis into a blocking buffer, shaking at room temperature for 1 hour. Then, the primary antibody was added to the membrane and incubated overnight shaking at 4°C. After incubation, the membrane was washed 3 times at room temperature. Subsequently, the secondary antibody was added to the membrane in a blocking buffer for 1 hour, shaking at room temperature. 3 washing steps were performed followed by visualizing the blot via immunofluorescence using ChemiDoc Imaging Systems.

2.13 *In vivo* experiments

Animal models, such as mice, rats, rabbits, dogs, and pigs, have advanced the understanding of important research areas including CVD. Within these models, the utilization of murine organisms as a common model in the study of CVD is widely practiced. Due to their mammalian nature, mice share numerous genetic similarities with humans. Moreover, the shorter lifespan of mice, their amenability to genetic manipulation, and the availability of genotypically similar samples make them an attractive model for investigating the underlying pathomechanisms of several diseases, including heart diseases and tumors over extended periods and during the aging process. Mice are relatively easy to handle and the associated housing costs are minimal, further enhancing their appeal as a research model for this study. All *in vivo* experiments were performed in collaboration with Dr. Sven Niepmann (Medical Clinic and Polyclinic II, University Hospital, Bonn). For these experiments, 10-12-week-old male C57/BL6-J (wildtype, WT) mice were used and purchased from Janvier Lab (France). TLR3 knockout ($TLR3^{-/-}$) mice on a C57/BL6-J background were obtained through the breeding program within the group. All animals were maintained in a room at 22°C, with a 12 hours light/dark cycle, and received chow and drinking water ad libitum. All animal experiments were performed in accordance with the institutional guidelines and the German animal protection law and were approved by the LANUV (Landesamt für Natur, Umwelt und Verbraucherschutz Nordrhein-Westfalen) (81-02.04. 2018.A250).

Regardless of treatment or mouse type, the experimental setups were consistent, starting with a baseline ultrasound, followed by wire injury and further ultrasound every 2 weeks. Mice were euthanized by cervical dislocation 6 weeks after injury (Figures 11, 12, 13, 14). For staining and further analysis, hearts were isolated, cleaned with 0.9% sodium chloride solution, and embedded in tissue-freezing medium.

The first model included WT mice with C57/BL6-J background that were treated with PolyIC. After surgery, mice were injected daily intraperitoneally with PolyIC (100µg dissolved in 0.9%

sodium chloride (NaCl)) to activate TLR3. After 6 weeks, animals were euthanized by cervical dislocation.

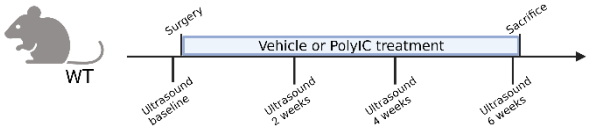

Figure 11 Schematic description of in vivo experiments including WT mice injected with PolyIC

The experiment was performed using WT mice that were treated daily with PolyIC, starting with baseline ultrasound, followed by wire injury and further ultrasound every 2 weeks. Mice were euthanized 6 weeks after injury via cervical dislocation. Figure created with Biorender.com

For the second model, $TLR3^{-/-}$ mice were used to investigate the role of endogenous TLR3 activation. No treatment was required for this experiment.

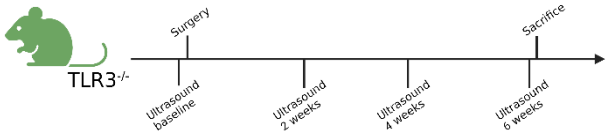

Figure 12 Schematic experimental setup for in vivo experiments with $TLR3^{-/-}$ mice

The experiment was performed using TLR3 knockout mice without treatment, starting with baseline ultrasound, followed by wire injury and further ultrasound every 2 weeks. Mice were euthanized 6 weeks after injury via cervical dislocation. Figure created with Biorender.com

WT mice were used again in a third approach and the TLR3/dsRNA-complex inhibitor Compound 4a was injected to inhibit TLR3 (27.5µg dissolved in 200µl PBS). The animals underwent subcutaneous injections every other day following wire injury and they were subsequently sacrificed after a period of 6 weeks.

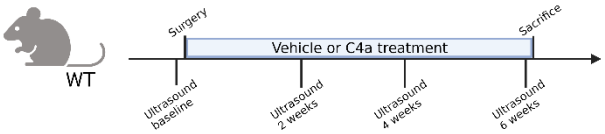

Figure 13 Schematic description of in vivo experiments including WT mice injected with C4a

The experiment was performed using WT mice that were treated every other day with C4a, starting with baseline ultrasound, followed by wire injury and further ultrasound every 2 weeks. Mice were euthanized 6 weeks after injury via cervical dislocation. Figure created with Biorender.com

In another experiment, MDA5$^{-/-}$ mice were used to elucidate the endogenous role of MDA5. Genotype was confirmed via PCR of tail tips. Here, no medical treatment was needed and WT served as control. 6 weeks after surgery, mice were sacrificed.

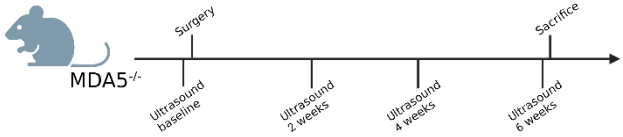

Figure 14 Schematic experimental setup for in vivo experiments with MDA5$^{-/-}$ mice

The experiment was performed using MDA5 knockout mice without treatment, starting with baseline ultrasound, followed by wire injury and further ultrasound every 2 weeks. Mice were euthanized 6 weeks after injury via cervical dislocation. Figure created with Biorender.com

2.13.1 Echocardiography

All experiments regarding echocardiography were performed by Dr. Sven Niepmann using the Fujifilm VisualSonics Vevo 2100 or 3100 Ultra High Frequency Imaging Platform. After anesthesia with 1.5% isoflurane, mice were depilated with hair removal cream on the chest to guarantee image quality. Animals were monitored with an electrocardiogram, respiratory rate, and body temperature. Using a pulse-wave Doppler with angle correction between 40° and 50°, the aortic valve peak velocity was measured in the suprasternal view. Left ventricular (LV) function, ejection fraction, fractional shortening, and ventricular volumes were measured in the parasternal long-axis and short-axis views using the Vevo LV-Trace function. Wall thickness was measured in parasternal long-axis and short-axis views, respectively, in M-mode images. The AR was measured by using the color-Doppler mode in the parasternal long-axis and suprasternal views. All analyses were performed using Fujifilm VisualSonics VevoLab software (Niepmann et al. 2019, Niepmann et al. 2023).

2.13.2 Aortic wire injury

The protocol for the wire injury was established by Dr. Sven Niepmann (Niepmann et al. 2019), based on the publication of Honda and colleagues in 2014 (Honda et al. 2014). Surgeries were performed in 2018 and 2019

First, mice were anesthetized using 150mg/kg ketamine and 16mg/kg xylazine, injected intraperitoneally. After exposing the right carotid artery by blunt dissection, a guide wire with a 15° angled tip (ASAHI INTECC MIRACLEbros 6) was introduced into the left ventricle. The guide wire passed over the aortic valve and advanced into the left ventricular apex and pulled back into the left ventricular outlet, below the aortic valve level. The wire was pushed in and

out of the apex 10 times, followed by 200 rotations. Finally, the wire was removed and the carotid artery was ligated. The proceedings were monitored by echocardiography. For control, sham surgery was performed in the same way except for advancing into the left ventricle across the aortic valve. Instead, the wire was only inserted into the right carotid artery (Niepmann et al. 2019).

2.13.3 Histological analysis of murine samples

6 weeks after the wire injury, mice were euthanized via cervical dislocation. The hearts were isolated and rinsed with a 0.9% sodium chloride solution through the LV followed by embedding in a tissue-freezing medium. The hearts were sectioned with cryostat in 8µm thickness and stored at -80°C. The sections were stained using different methods as described in the following chapters.

2.13.4 CD68 staining

Cluster of Differentiation 68 (CD68) staining was used to show macrophage infiltration in the aortic valve area. For staining, samples were fixed with acetone for 20 minutes at room temperature followed by 3 washing steps with PBS. A circle was drawn with a Dako pen around the staining reagent on the slide to provide a hydrophobic barrier that prevents the mixing of reagents. Samples were blocked using 2% BSA for 30 minutes at room temperature. CD68 primary antibody was added in 2% BSA and incubated overnight at 4°C in a wet chamber. The next day, the slides were washed 3 times with PBS. Secondary antibody, diluted 1:500 in 2% BSA was added and incubated for 1 hour at room temperature. After the following washing steps, slides were mounted with DAPI and analyzed with a fluorescence microscope. CD68 staining was quantified using Zeiss ZEN Imaging Software.

2.13.5 Sirius Red staining

Pico Sirius Red Staining was used to show collagen fibers. Sections were slowly rehydrated by dipping them into decreasing concentrations of ethanol followed by washing steps. Afterwards, sections were incubated in hematoxylin for 20 seconds and then washed under running water for 10-15 minutes. Sirius Red staining was accomplished after 15-30 minutes of incubation with Sirius Red at room temperature. The slides were passed slowly through increasing concentrations of alcohol finishing the steps with incubation in xylene. Sections were then covered with Entellan and images were obtained with a light/polarization microscope. Collagen deposits were quantified using Zeiss ZEN Imaging Software.

2.13.6 Von Kossa staining

Von Kossa staining was used to show tissue calcification in the aortic valve area. For the staining, samples were fixed with acetone for 5-10 minutes at room temperature followed by 30-60 minutes incubation in silver nitrate solution (5%) at room temperature while exposed to 100 watts incandescent. Afterwards, sections were rinsed in several changes of distilled water and incubated in sodium thiosulfate solution (5%) for 2-3 minutes. Another rinse for 2 minutes in running tap water and 2 changes of distilled water were performed followed by incubation in nuclear fast red solution for 5 minutes at room temperature. Slides were rinsed again for 2 minutes in running tap water and water was changed again 2 times. Subsequently, samples underwent rapid dehydration by progressively increasing ethanol concentrations (70%, 80%, 100%). Sections were then covered with Entellan and images were taken by light microscopy. Calcium deposits were quantified with Zeiss ZEN Imaging Software.

2.13.7 Hematoxylin/Eosin staining

Hematoxylin/Eosin (HE) staining was used to measure the aortic valve area and to get an overview of the general structure. Hematoxylin stains the nuclei blue-purple and eosin stains the cytoplasm and extracellular components pink. Sections were slowly rehydrated by dipping them into decreasing concentrations of ethanol (100%, 90%, 70%) followed by 2 quick incubations in distilled water. Sections were incubated in hematoxylin for 30 seconds, washed under running water, and then 30 seconds incubated with 0.5% Eosin staining. After further washing steps, the slides were passed slowly through increasing concentrations of ethanol (70%, 90%, 100%), finishing the steps with incubation in xylene. Sections were then covered with Entellan and images were taken with a microscope. Aortic valve thickness was measured using ZEN Imaging Software.

3. Results

The role of the innate immune system and its pattern recognition receptors in the development of aortic valve stenosis

Part of this chapter was published in the manuscript “Toll-like receptor-3 contributes to the development of aortic valve stenosis”- Sven Thomas Niepmann*, Nicola Willemsen*, Ann Sophie Boucher, Marta Stei, Philip Goody, Andreas Zietzer, Marko Bulic, Hannah Billig, Alexandru Odainic, Christina Katharina Weisheit, Christine Quast, Matti Adam, Susanne V.

Schmidt, Farhad Bakhtiary, Felix Jansen, Georg Nickenig, Eike Latz & Sebastian Zimmer- https://doi.org/10.1007/s00395-023-00980-9 (Niepmann et al. 2023)
* Sven Thomas Niepmann and Nicola Willemsen have contributed equally to this work

AS is the most common heart valve disease requiring therapeutic intervention. However, the molecular mechanisms contributing to AS development are poorly understood. Currently, no preventative or medical therapies have demonstrated efficacy in AS and therefore surgical or interventional valve replacement is the only available treatment approach. It is believed that the development of calcification in the valve cusps is driven by chronic inflammation. This localized inflammatory response plays a crucial role in the pathological processes leading to valve dysfunction. Emerging evidence suggested that the activation of PRRs may be a critical factor in this context. PRRs are responsible for recognizing specific patterns or structures associated with pathogens and damaged tissues and activating immune responses, and promoting inflammation. Thus, the study aimed to shed light on their potential contributions to the development and progression of AS. Herein, TLR3 and MDA5 expression in human aortic valves could be confirmed. Furthermore, the role of TLR3 was analyzed in *in vitro* approaches during calcification in VICs and the process of EndMT in VECs. Additionally, the involvement of TLR3 was translated and investigated in *in vivo* studies.

3.1 TLR3 and MDA5 were expressed in human aortic valve tissue

Aortic valve samples were obtained from patients suffering from aortic disease and consequently underwent a valve replacement. *TLR3* and *IFIH1* (MDA5) expression of explanted human aortic valve tissue from patients was measured via qPCR analysis, which demonstrated slightly elevated *TLR3* and *IFIH1* mRNA expression in AS compared to AR samples (Figure 15). Measurements and analysis were performed by Dr. Sven Niepmann (Niepmann et al. 2023). Cross-section of stenotic aortic valves were stained with HE to visualize the structure of the aortic valve tissue and cells and thereby to achieve an overview of the valve (Figure 15). Additionally, TLR3 and MDA5 expression could be detected via immunohistochemistry and immunofluorescence (Figure 15). In conclusion, TLR3 as well as MDA5 expression could be shown to be expressed in all layers within the aortic valve.

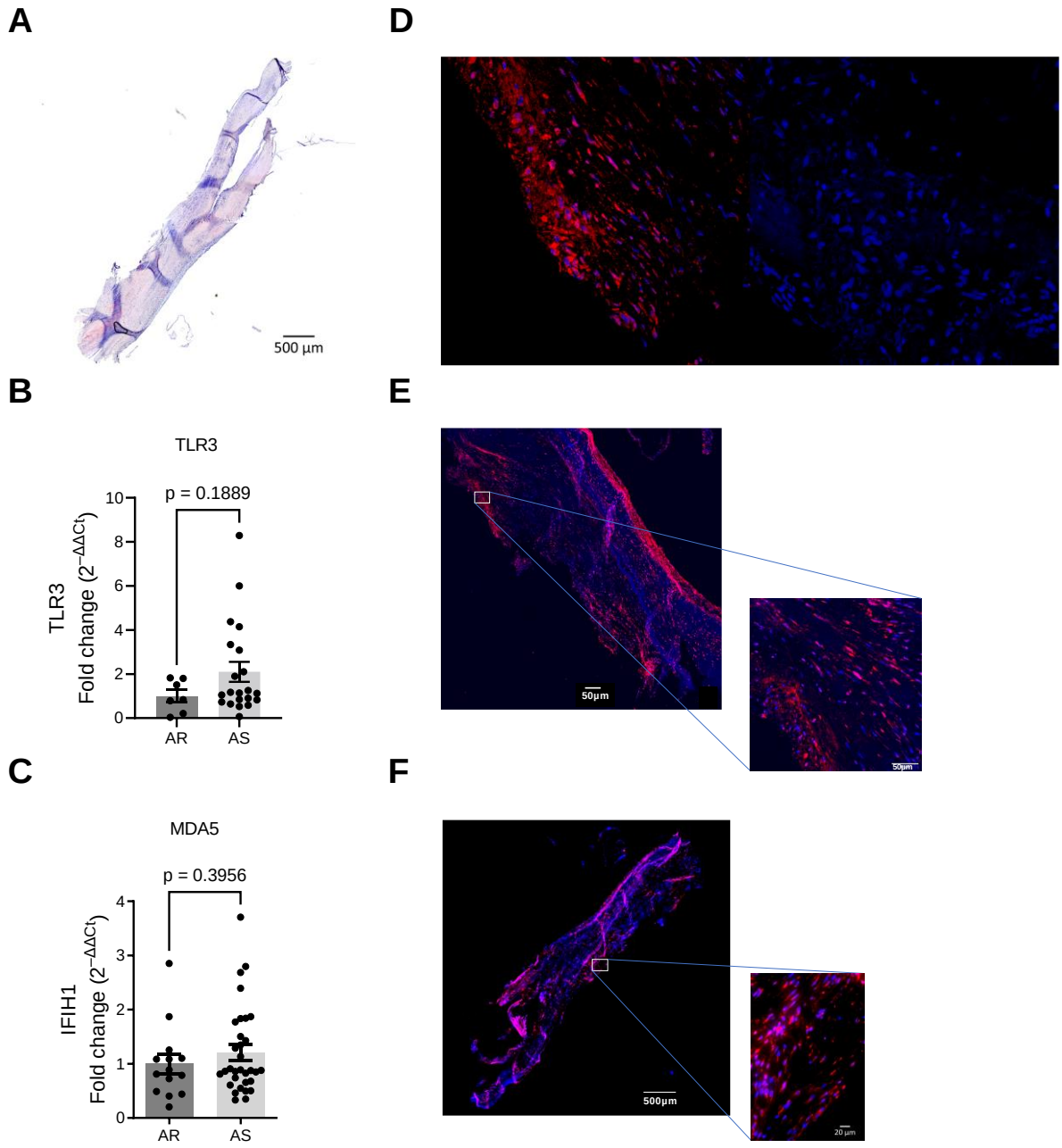

Figure 15 TLR3 and MDA5 gene expression of explanted human aortic valves

A: *Cross-section of stenotic aortic valves were stained with HE to visualize the structure of the aortic valve tissue and cells and thereby to achieve an overview of the valve.* **B, C**: *TLR3 and IFIH1 (MDA5) gene expression of explanted human aortic valve tissue from patients was measured via qPCR analysis. TLR3 gene expression of explanted human aortic valves from AS patients was slightly, but not significantly, higher compared to control aortic valves from AR patients. The relative levels of target gene expression were calculated by the comparative Ct method (ΔΔCt method). Student´s t-test was used to analyze the statistical significance of gene expression.* ***D****: TLR3 and MDA5 expression in human stenotic aortic valves were visualized via immunofluorescence staining. For control, sections were stained only with secondary antibody. Thereby, any background fluorescence was excluded and staining could be confirmed.* ***E:*** *TLR3 expression in human stenotic aortic valves were visualized via immunofluorescence and could be*

observed throughout all layers of the valve. Microscopic images were conducted in the Microscopy Core Facility of the Medical Faculty. ***F****: MDA5 expression in human stenotic aortic valves were visualized via immunofluorescence and could be observed throughout all layers of the valve.*

AR= Aortic regurgitation; AS= Aortic valve stenosis; HE= Hematoxylin/Eosin; MDA5= Melanoma differentiation-associated protein; TLR3= Toll- like receptor 3

Images were modified from (Niepmann et al. 2023).

3.2. Activation of pattern recognition receptors in valvular interstitial cells

To investigate if VICs respond to PRR stimulation, VICs were treated with specific agonists of selected membrane-bound and cytosolic PRRs (Table 5 in chapter 2.5.4). Afterwards, the culturing medium was changed to PCM to induce calcification. This experimental approach was employed to gain an understanding of the gene expression profiles associated with the selected receptors in VICs and was performed in cooperation within the TRR259 with Project A03 (PhD student Madeleine Graef, research group of Prof. Dr. Gunther Hartmann; Institut für Klinische Chemie und Klinische Pharmakologie, Universitätsklinikum Bonn). Here, selected PRRs were stimulated and their subsequent gene expression was measured and compared to the neg control (Figure 16). Stimulation of the PRRs depicted in figure 16 led to an upregulation of mRNA expression when compared to unstimulated cells.

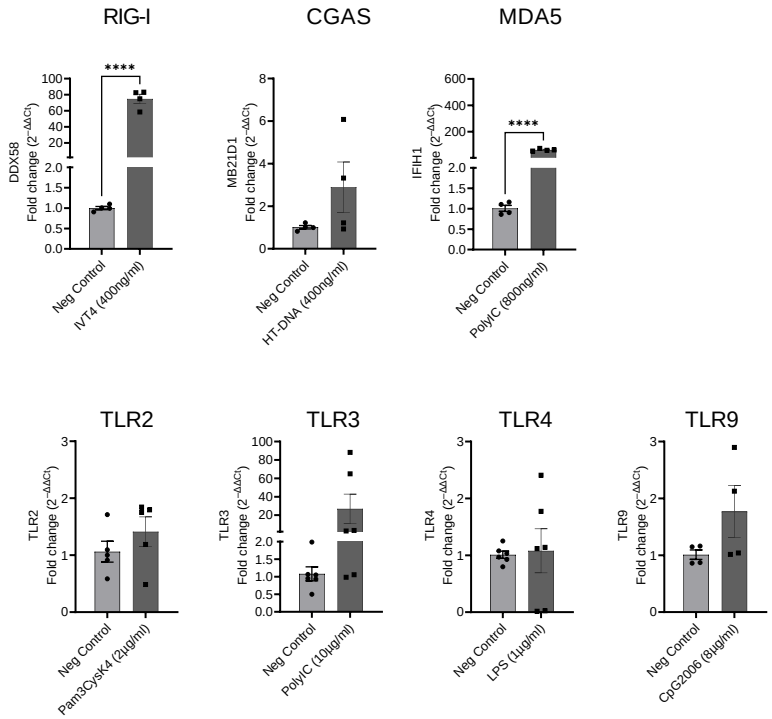

Figure 16 Gene expression of selected pattern recognition receptors

*Gene expression of selected PRRs after activation. VICs were treated with specific agonists of selected membrane-bound and cytosolic PRRs. Afterwards, the culturing medium was changed to PCM to induce calcification. RNA was isolated after 7 days and qPCR was performed. The relative levels of target gene expression were calculated by the Comparative Ct Method (ΔΔCt Method). Student´s t-test was used to analyze the statistical significance of gene expression data. Bars displayed the relative expression normalized by neg control ± SEM. n=2-3; ****p< 0.00005;*

BM= Basal medium; PCM= Pro-calcifying medium; MDA5= Melanoma differentiation-associated protein 5; RIG-I= Retinoic acid inducible gene I; TLR= Toll-like receptor; IVT4= 5' Triphosphate double-stranded RNA; HT-DNA= Deoxyribonucleic acid sodium salt from herring testes; MB21D1= Mab-21 domain-containing 1/cyclic GMP-AMP; PolyIC= Polyinosinic:polycytidylic acid; Pam3CysK4 =Pam3CysSerLys4; LPS= Lipopolysaccharide; CpG2006= TLR9 ligand; PRR= Pattern recognition receptor

Next, calcification, as well as inflammation, were detected after activation of the receptors using gene expression of *BMP2, RUNX2*, and *IL6*. Untreated control cells (neg control) showed an effect of calcification after the addition of PCM compared to BM in gene expression of the pro-inflammatory marker *IL6*. In addition, changing the medium to PCM increased the osteogenic markers *RUNX2* and *BMP2*. All conditions were compared with untreated control cells in BM (Figure 17).

RIG-I activation and changing the medium to PCM resulted in a slight but not significant increase in *IL6* and *RUNX2* gene expression. Compared to neg control cells, *BMP2* expression showed increased expression in both media after RIG-I receptor activation. However, *BMP2* gene expression remained unchanged between BM and PCM.

Activation of cGAS (*MB21D*) resulted in increased levels of *IL6*. The addition of PCM doubled *IL6* gene expression compared to BM. Osteogenic markers showed no significant difference between BM and PCM after cGAS activation. However, *BMP2* gene expression was upregulated in BM and PCM after stimulation of this receptor compared to the neg control in BM.

After activation of MDA5, *IL6* and *BMP2* gene expression were increased in both media, whereas *RUNX2* expression remained unchanged, compared to the neg control. Within the two media, PCM showed higher *IL6*, *RUNX2,* and *BMP2* gene expression after MDA5 activation in comparison to BM.

Activation of TLR 2, 3, 4, and 9, resulted in an increased gene expression level of *IL6*, *RUNX2,* and *BMP2* after adding PCM compared to the BM condition. In comparison to the neg control, *RUNX2* gene expression remained unchanged. In conclusion, these results suggest that activation of PRRs affects calcification in VICs.

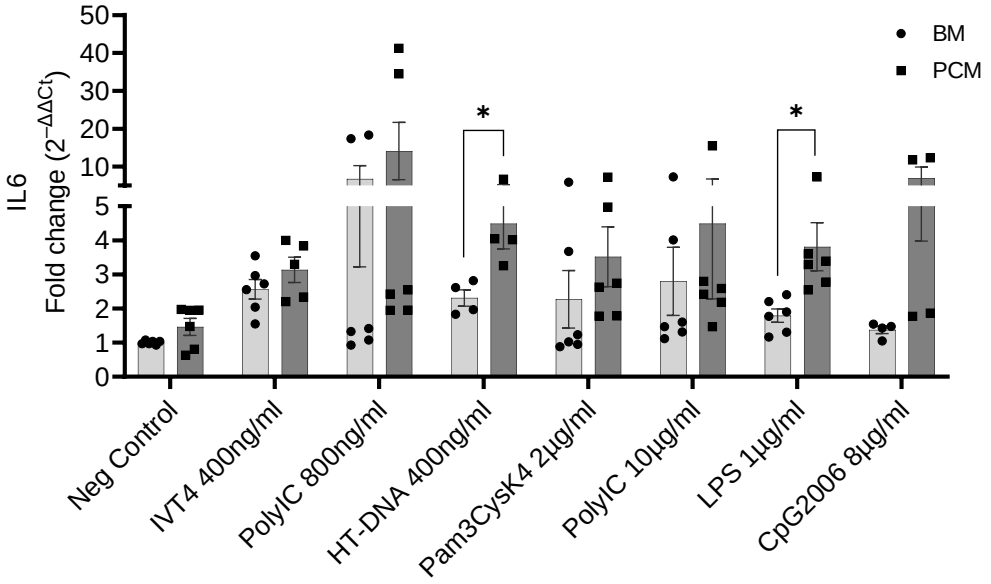
IL6
Fold change ($2^{-\Delta\Delta Ct}$)
BM
PCM
*
*
Neg Control
IVT4 400ng/ml
PolyIC 800ng/ml
HT-DNA 400ng/ml
Pam3CysK4 2µg/ml
PolyIC 10µg/ml
LPS 1µg/ml
CpG2006 8µg/ml

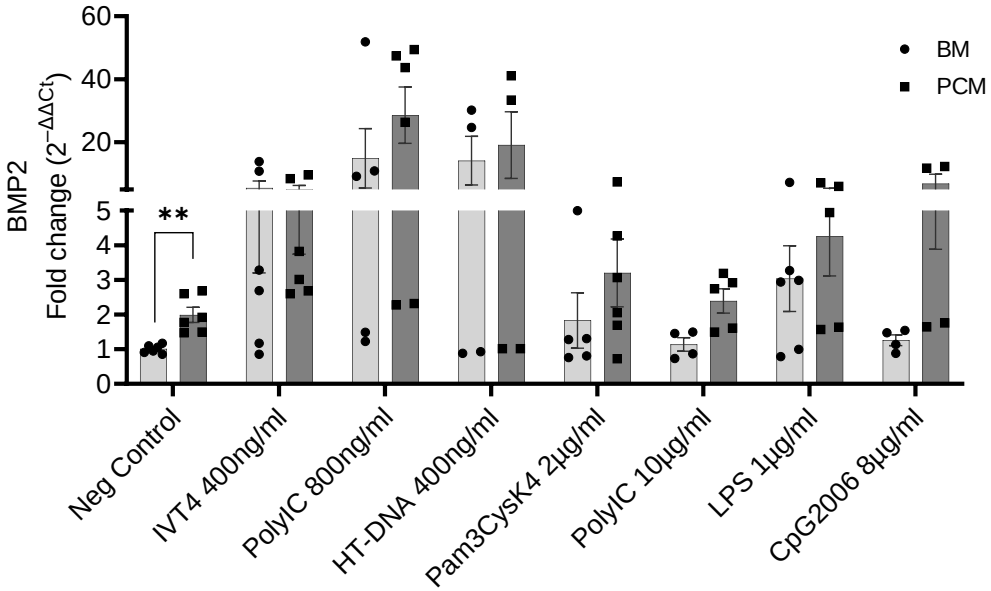
BMP2
Fold change ($2^{-\Delta\Delta Ct}$)
BM
PCM
**
Neg Control
IVT4 400ng/ml
PolyIC 800ng/ml
HT-DNA 400ng/ml
Pam3CysK4 2µg/ml
PolyIC 10µg/ml
LPS 1µg/ml
CpG2006 8µg/ml

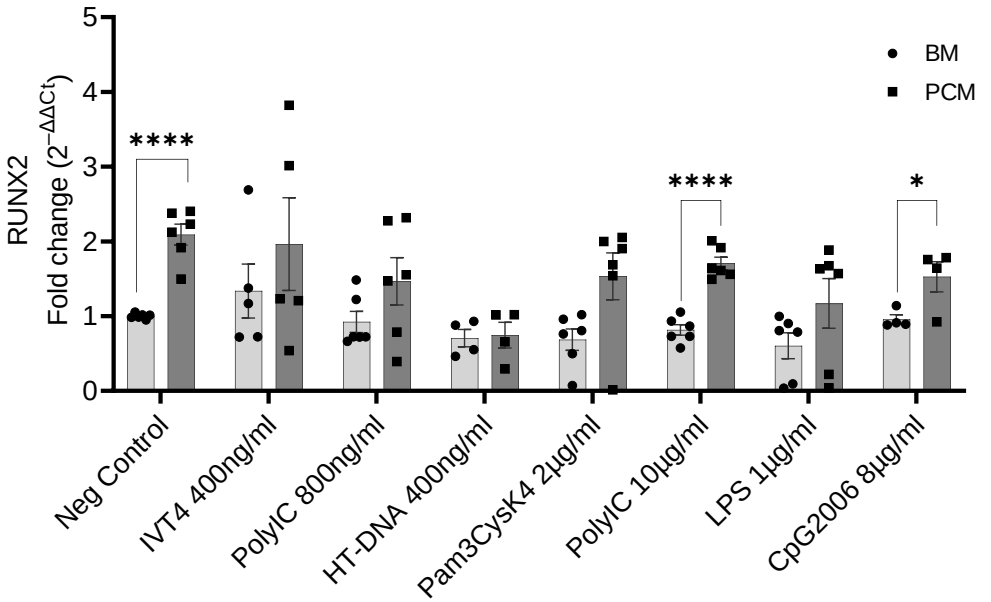
RUNX2
Fold change ($2^{-\Delta\Delta Ct}$)
BM
PCM
****
****
*
Neg Control
IVT4 400ng/ml
PolyIC 800ng/ml
HT-DNA 400ng/ml
Pam3CysK4 2µg/ml
PolyIC 10µg/ml
LPS 1µg/ml
CpG2006 8µg/ml

Figure 17* Gene *expression after activating certain pattern recognition receptors

Calcification, as well as inflammation, were detected after activation of the selected PRRs. After stimulating the cells, the medium was changed to induce calcification in VICs. After 7 days, RNA was isolated and qPCR was performed. The relative levels of target gene expression were calculated by the Comparative Ct Method (ΔΔCt Method). ***A****: IL6 gene expression after activating selected PRRs.* ***B****: BMP2 gene expression after activating selected PRRs.* ***C****: RUNX2 gene expression after activated PRRs. Student´s t-test was used to analyze the statistical significance of gene expression data. Bars displayed the relative expression normalized by neg control in BM ± SEM. n=2-3; *p < 0.05, **p < 0.005, ****p < 0.00005*

BM= Basal medium; BMP2= Bone morphogenetic protein 2; IL6= Interleukin 6; PCM= Pro-calcifying medium; MDA5= Melanoma differentiation-associated protein 5; RIG-I= Retinoic acid inducible gene I; RUNX2= Runt-related transcription factor 2; TLR= Toll-like receptor; IVT4= 5'Triphosphate double-stranded RNA; HT-DNA= Deoxyribonucleic acid sodium salt from herring testes; PolyIC= Polyinosinic:polycytidylic acid; Pam3CysK4 =Pam3CysSerLys4; LPS= Lipopolysaccharide; CpG2006= TLR9 ligand

3.2.1 The role of TLR3 in valvular interstitial cells

This study primarily investigated the involvement of TLR3 in the progression of AS. The expression of TLR3 was demonstrated in the human aortic valve and its gene expression was found to be elevated in AS patients compared to the control group (Figure 15). Additionally, an *in vitro* examination of the PRRs provided initial insights into the potential role of TLR3 in calcification processes in VICs. Following, VICs were transfected with PolyI. 48 hours after transfection and 7 days after changing the medium, images of cells were recorded with a microscope and cell viability as well as Caspase 3/7 activity were measured. The transfection led to visibly less viability after 48 hours and 7 days, compared to neg control (Figure 18 A). This result of reduced viability could be confirmed by performing an alamarBlue assay (Figure 18 B). Caspase 3/7 activity initially elevated 48 hours after PolyIC transfection followed by a subsequent decrease after 7 days compared to control cells (Figure 18 C).

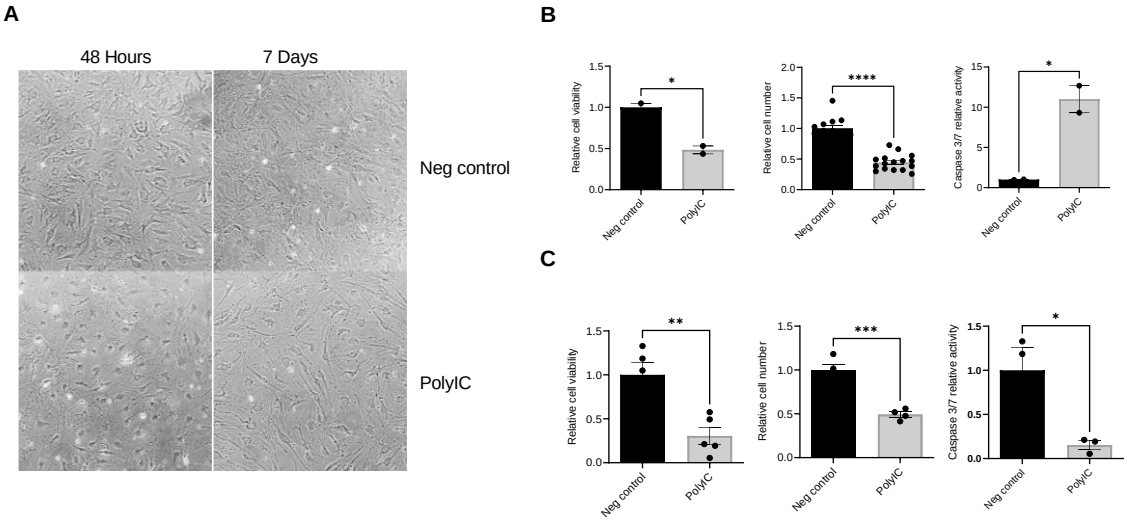

Figure 18 Valvular interstitial cells 48 hours and 7 days after transfection

VICs were transfected with PolyIC, or kept untreated. Cell viability, Caspase 3/7 activity, and cell number were analyzed. ***A****: Representative Images of VICs after Transfection. PolyIC transfected VICs showed less viability compared to untreated control cells at 48 hours after transfection and 7 days after changing the medium.* ***B:*** *48 hours after transfection and* ***C:*** *7 days after transfection. Student´s t-test was used to analyze the statistical significance. Bars displayed the relative value normalized by neg control ± SEM. n=2; *p < 0.05; **p< 0.005¸***p< 0.0005, ****p< 0.00005. The graph was modified from (Niepmann et al. 2023).*
PolyIC= Polyinosinic:Polycytidylic acid; VICs= Valvular interstitial cells

An endogenous knockdown of TLR3 was conducted to assess its specific contribution to VIC calcification. TLR3 siRNA, PolyIC, or scrambled siRNA as control were transfected into VICs for 48 hours. Subsequently, calcification was induced by changing the medium to PCM for 7 days. However, TLR3 siRNA transfected cells showed an increase in cell viability compared to PolyIC treatment. No significant differences between the two media, BM and PCM could be observed but a similar pattern of cell viability (Figure 19 A). Furthermore, the relative Caspase 3/7 activity was decreased in PolyIC transfected cells compared to untreated control or siRNA transfected cells 7 days after inducing calcification (Figure 19 B). This result remained consistent when compared to the data presented in figure 18, emphasizing the reproducible effect of TLR3. Caspase 3 and 7 both are crucial in the process of apoptosis (Brentnall et al. 2013) and therefore appropriate markers for apoptotic responses. Thus, TLR3 activation resulted in more cell death, which in turn led to calcification. TLR3 knockdown might prevent this process.

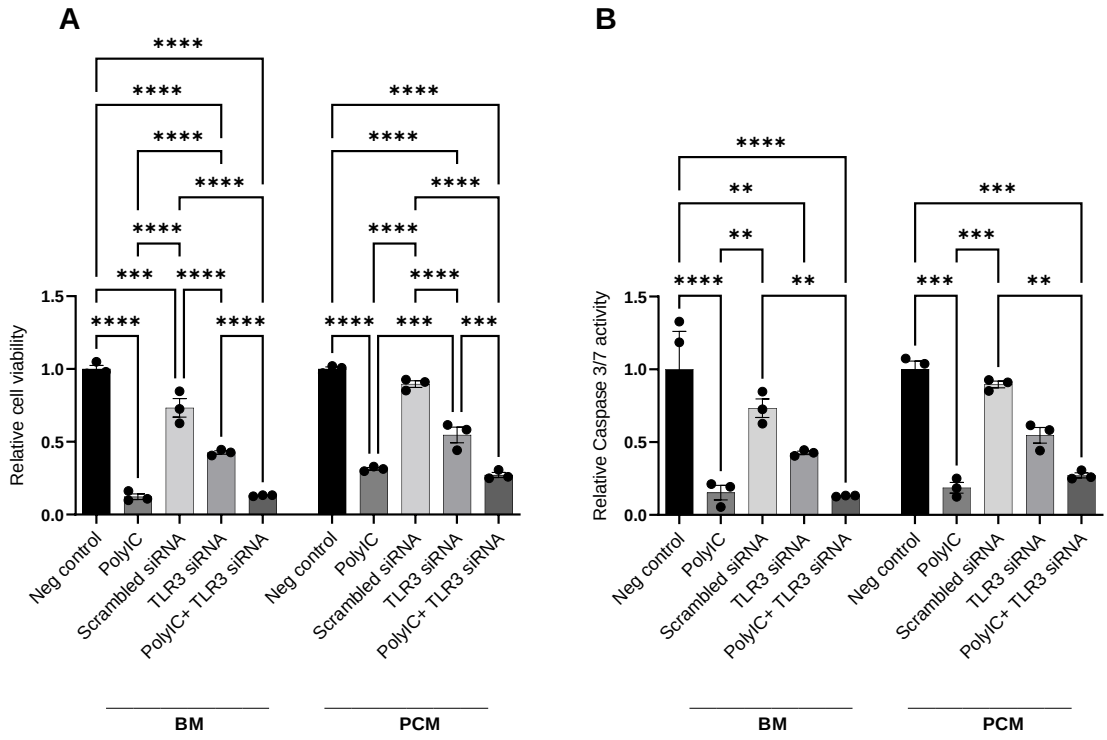

Figure 19 Relative cell viability and Caspase 3/7 activity of transfected valvular interstitial cells

VICs were transfected with siRNA, PolyIC, scrambled siRNA, or untreated. Afterwards, calcification was induced by changing the medium to PCM. ***A:*** *7 days after calcification induction, cell viability was measured using alamarBlue.* **B:** *7 days after calcification induction, Caspase 3/7 activity was measured using Caspase 3/7 Glo Assay*

*A 2-way ANOVA test with Tukey's post test for multiple comparisons was used to analyze the statistical significance of Caspase activity. Bars displayed the relative caspase activity normalized by neg control within each medium ± SEM. n=3; *p< 0.05, ** p< 0.005, *** p< 0.0005 ****p< 0.00005.*

BM= Basal medium; PCM= Pro-calcifying medium; PolyIC= Polyinosinic: Polycytidylic acid; VICs= Valvular interstitial cells. The graph was modified from (Niepmann et al. 2023).

Calcification, a key driver in the development of AS, is a focal point in these experimental approaches. Important markers associated with calcification, such as *RUNX2* and *BMP2*, were measured in the following *in vitro* experiments. Following 7 days of inducing calcification in transfected cells, RNA isolation was carried out and subsequent qPCR measurements were performed. TLR3 siRNA transfected cells showed a knockdown of *TLR3* in BM and PCM. Scrambled siRNA resulted in a higher *TLR3* expression compared to neg control. PolyIC treatment resulted in an increased *TLR3* gene expression whereas the combination with the TLR3 knockdown could blunt this response. The other receptors *IFIH1* (MDA5) and *DDX58* (RIG-I) showed an increased gene expression after activation with PolyIC, whereas the TLR3 knockdown did not show a decreased gene expression of these receptors compared to neg

control. The combination of TLR3 knockdown together with PolyIC treatment led to a decreased *IFIH1* (MDA5) and *DDX58* (RIG-I) gene expression compared to PolyIC-treated cells. When analyzing the osteogenic markers *BMP2* and *RUNX2* as well as *IL6* as a pro-inflammatory marker, the gene expression was upregulated after PolyIC treatment and could be blunted when combining PolyIC with TLR3 knockdown. In PCM, *RUNX2* was not affected by TLR3 stimulation but cells cultured in PCM generally showed higher gene expression levels (Figure 20).

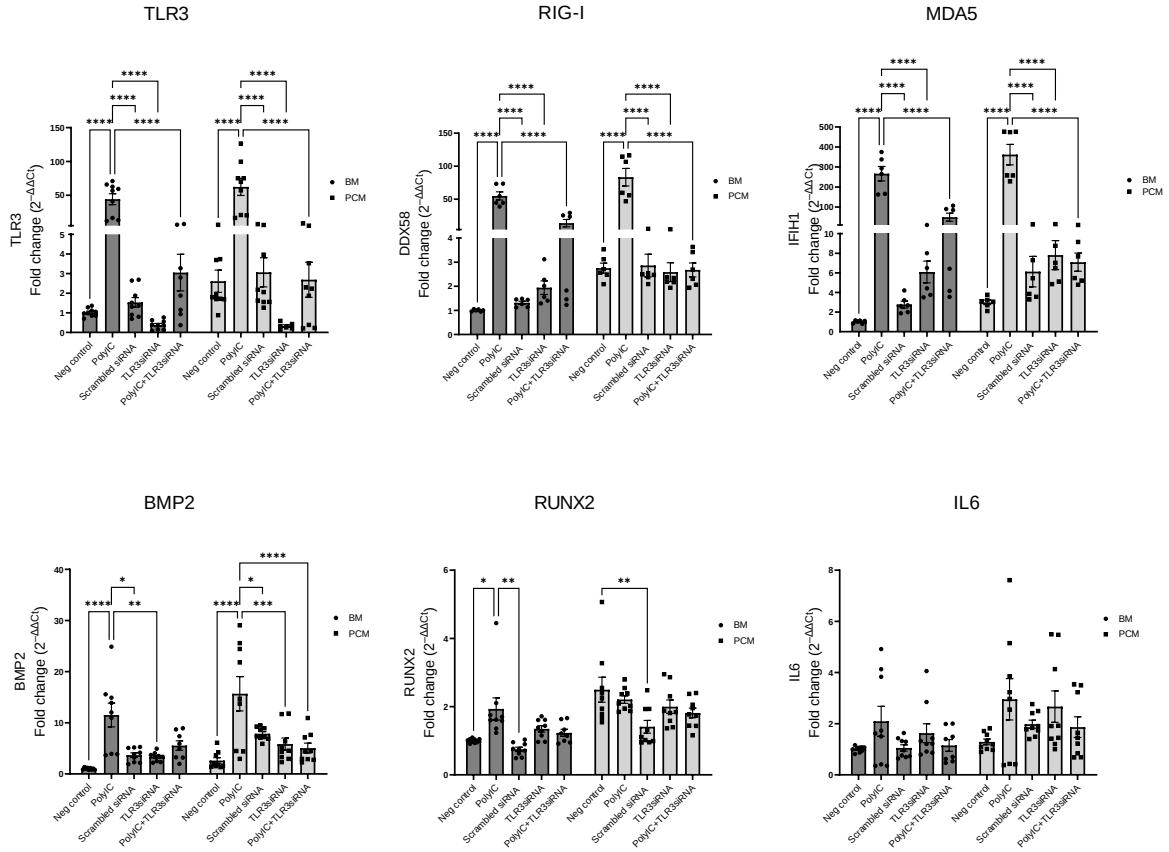

Figure 20 Gene expression in transfected valvular interstitial cells

*TLR3 siRNA, PolyIC, or scrambled siRNA as neg control were transfected into cells for 48 hours. Subsequently, calcification was induced by changing the media. After 7 days, RNA was isolated and qPCR was performed. The relative levels of target gene expression were calculated by the Comparative Ct Method (ΔΔCt Method). A 2-way ANOVA test with Tukey's post test for multiple comparisons was used to test the statistical significance of qPCR data. Bars displayed the fold change of gene expression normalized by control in BM ± SEM. n=2-3; *p < 0.05, ** p< 0.005, *** p< 0.0005 ****p< 0.00005. The graph is modified from (Niepmann et al. 2023).*

BM= Basal medium; BMP2= Bone morphogenetic protein 2; IL6= Interleukin 6; MDA5= Melanoma differentiation-associated protein 5; PCM= Pro-calcifying medium; PolyIC= Polyinosinic:Polycytidylic acid; RIG-I= Retinoic acid inducible gene I; RUNX2= Runt-related transcription factor 2; TLR3= Toll-like receptor 3;

3.2.2. Inhibition of TLR3 using C4a could prevent calcification in valvular interstitial cells

In addition to endogenous inhibition of TLR3 expression, this study also aimed to investigate the impact of pharmacological inhibition of TLR3 on calcification in VICs. For this, the specific TLR3 inhibitor C4a was used in the following *in vitro* studies. VICs were treated with PolyIC, C4a, or PolyIC+C4a for 72 hours. Afterwards, calcification was induced by changing the medium to PCM. First, upon treatment with PolyIC, *TLR3* expression was upregulated in VICs while incubation with a combination of PolyIC+C4a resulted in a downregulation of *TLR3*. To verify a successful VIC calcification, osteogenic markers *BMP2* and *RUNX2* were used. Upon PolyIC treatment, *BMP2* expression increased while inhibition of TLR3 with C4a blunted this response. There was no significant increase of *RUNX2* associated with PolyIC treatment. *IL6* showed a similar response to *TLR3* gene expression, indicating an involvement of inflammation. *IFIH1* (MDA5) and *DDX58* (RIG-I) gene expression were analyzed to exclude an off-target effect of treatment with C4a. After PolyIC treatment, *IFIH1* (MDA5) and *DDX58* (RIG-I) gene expression were increased. Concomitant treatment with PolyIC+C4a showed no effect on *IFIH1* and *DDX58* gene expression compared to PolyIC treatment (Figure 21 A) indicating a specific C4a binding to TLR3. In addition to assessing the expression of calcification markers at the mRNA level, protein-level analysis was also performed in this study. Cells were stained with BMP2 antibody and immunofluorescence was analyzed. PolyIC-treated cells showed an increased BMP2 signal compared to control or C4a treated cells showing a reduced BMP2 detection (Figure 21 B). Western blot for BMP2 verified this upregulated protein expression after PolyIC treatment compared to the other conditions (Figure 21 C).

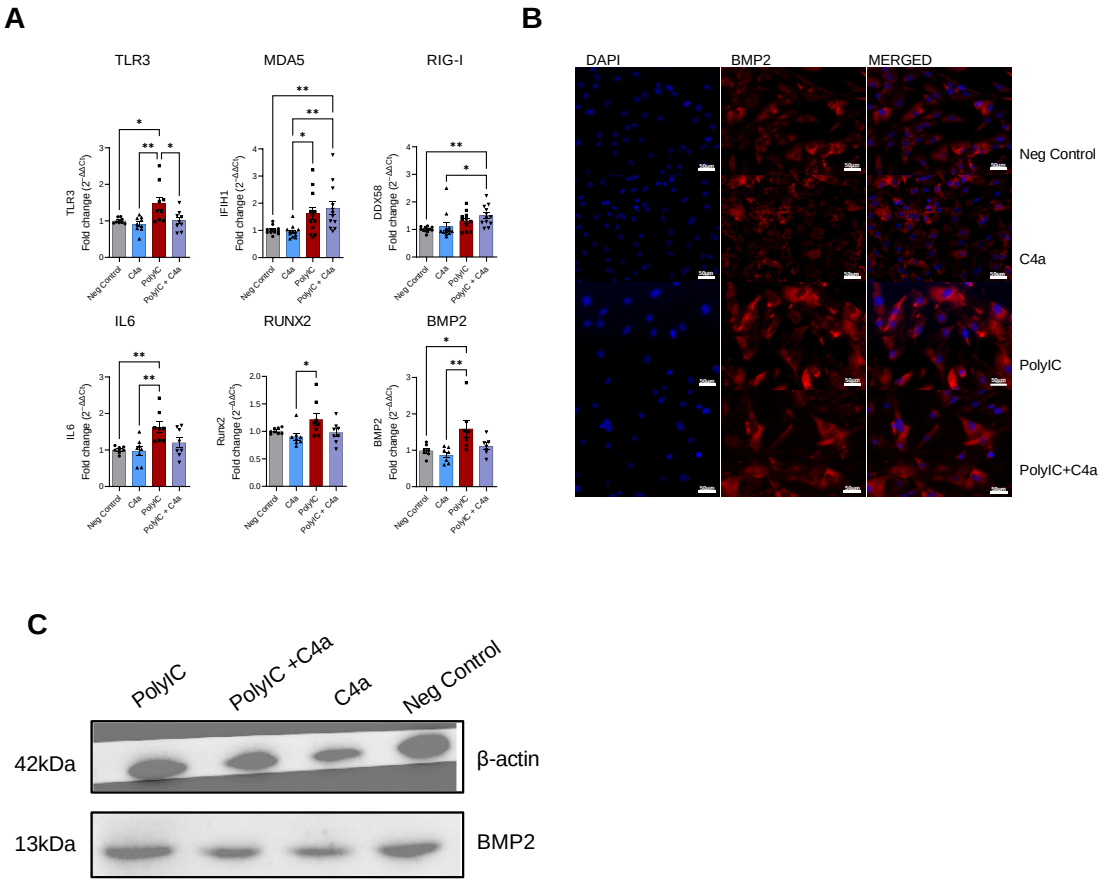

Figure 21 Gene expression, immunofluorescence staining, and Western blot of treated valvular interstitial cells *VICs were treated with PolyIC, C4a, or both to investigate the influence of PolyIC and C4a treatment. Afterwards, calcification was induced by changing the medium to PCM for 7 days.* ***A:*** *RNA was isolated and qPCR was performed. The relative levels of target gene expression were calculated by the Comparative Ct Method (ΔΔCt Method). 2-way ANOVA test with Tukey's post test for multiple comparisons was used to test the statistical significance of qPCR data. Bars displayed the fold change of gene expression normalized by neg control ± SEM. n=3; *p < 0.05, ** p< 0.005, *** p< 0.0005.* ***B:*** *Cells were fixed and stained with anti BMP2 and DAPI.****C:*** *Western blot for BMP2 was performed to verify immunofluorescence staining.*
BMP2= Bone morphogenetic protein 2; C4a= Compound 4a; IL6= Interleukin 6; MDA5= Melanoma differentiation-associated protein 5; PCM= Pro-calcifying medium; PolyIC= Polyinosinic:Polycytidylic acid; RIG-I= Retinoic acid inducible gene I; RUNX2= Runt-related transcription factor 2;TLR3= Toll-like receptor 3;

Next, to visualize calcium nodule formation in VICs, Alizarin Red S staining was performed after 21 days of calcification induction. PolyIC stimulated cells as well as control cells showed more calcification than C4a treated VICs (Figure 22 A). As a result, C4a exhibited a protective effect against the process of calcification, while the PolyIC-stimulated and control cells demonstrated calcification. AlamarBlue as well as Caspase 3/7 Glo assay were performed to decipher differences in cell viability and apoptotic responses between the treatments. PolyIC

treatment caused less viability as well as reduced Caspase 3/7 activity 7 days after calcification induction. These findings were consistent with the results reported in chapter 3.2.1 of this study. There was no significant difference between PolyIC and PolyIC+C4a treatment (Figure 22 B). These results indicate a PolyIC mediated calcification that was independent of decreasing cell viability. In conclusion, these results revealed a potential role of TLR3 in the process of calcification.

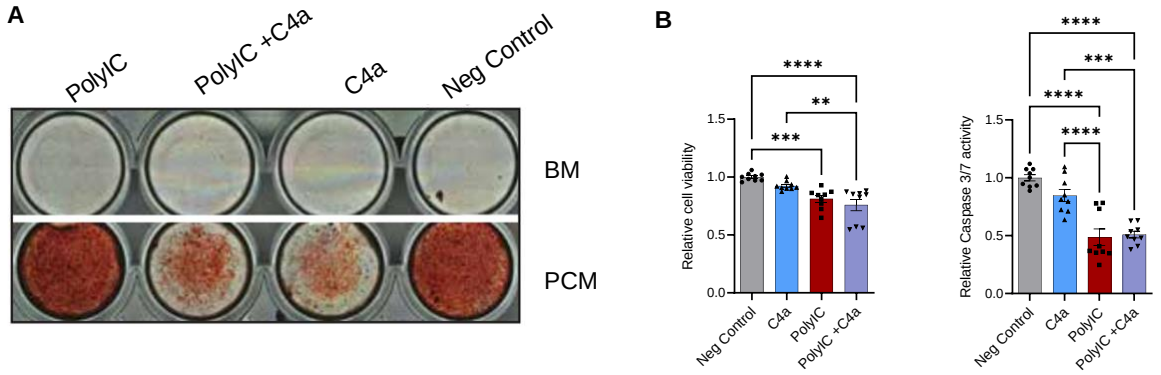

Figure 22 PolyIC treatment of valvular interstitial cell showed increased calcification which could be reversed by incubation with C4a

VICs were stimulated with PCM every other day after treatment with PolyIC, C4a, or both. ***A:*** *Alizarin Red S showed a strong calcium nodule staining in PolyIC treated cells, whereas it was reduced upon incubation with C4a. The image was modified from (Niepmann et al. 2023).* ***B:*** *The cell viability as well as apoptosis was significantly decreased when incubating cells with C4a, PolyIC, or both. One-way ANOVA test with Tukey's post test for multiple comparisons was used to analyze the statistical significance of cell viability, or Caspase activity. Bars displayed the fold change of cell viability, or Caspase 3/7 activity normalized by control ± SEM. n=3; *p < 0.05, ** p< 0.005, *** p< 0.0005 ****p< 0.00005.*

BM= Basal medium; C4a= Compound 4a; PCM= Pro-calcifying medium; PolyIC= Polyinosinic:Polycytidylic acid; VICs= Valvular interstitial cells

3.3 Establishment of endothelial to mesenchymal transition protocol

In recent years, accumulating evidence has highlighted the significant involvement of EndMT in the pathogenesis of AS. However, the existing literature on *in vitro* induction of EndMT has shown inconsistent results, necessitating the establishment of a standardized protocol. In this study, a comprehensive protocol for the induction of EndMT in VECs was developed. The protocol design included testing specific stimuli, time points, and concentrations based on a thorough review of the literature. Detailed information on the stimuli, time points, and concentrations used in the study can be found in table 10 in the Supplementary Appendix (Chapter 6.1, figures 55, 56, 57). Once the protocol was finalized, immunocytochemistry was

performed to confirm the expression of different endothelial and mesenchymal markers (Figure 23A). Furthermore, cell viability was measured using the alamarBlue assay (Figure 23 B).

Microscopic images revealed distinct alterations in cell morphology following stimulation. Treatment with TGFβ1+IL1β or TNFα induced a noticeable shift towards a mesenchymal-like phenotype, characterized by changes in cellular appearance, such as elongated and spindle-shaped morphology, when compared to the neg control group. These morphological changes provided first visual evidence of the transition towards a mesenchymal phenotype in response to TGFβ1+IL1β or TNFα stimulation. Cells were stained with CD31 (endothelial marker) and Vimentin (mesenchymal marker) antibodies for immunofluorescence imaging. The control cells, which were not subjected to any stimulation, exhibited protein synthesis of CD31. However, this CD31 expression decreased following stimulation. When TGFβ1+IL1β or TNFα were added, there was a notable increase in Vimentin expression, suggesting a shift towards a mesenchymal phenotype in the VECs after 7 days. The stimulation with TGFβ1+IL1β still displayed detectable CD31 expression, although the majority of cells showed immunofluorescence detection of Vimentin. In contrast, TNFα stimulation primarily resulted in Vimentin expression without significant CD31 detection (Figure 23 A).

Regarding the cell viability, TGFβ1+IL1β treated cells showed significantly less viability after 7 days compared to control cells, TGFβ1 only, or TNFα. There was no difference in TGFβ1 and TNFα stimulation compared to unstimulated cells (Figure 23 B). These findings suggest that the concomitant treatment of TGFβ1 and IL1β negatively impacts cell viability, while individual stimulation with TGFβ1 or TNFα does not significantly affect cell viability compared to the unstimulated condition.

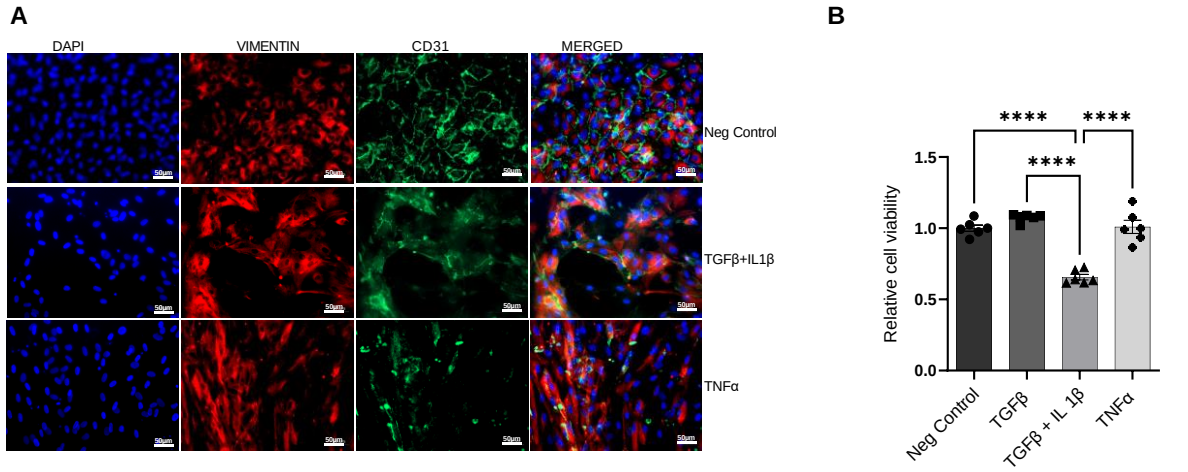

Figure 23 Immunocytochemistry and alamarBlue assay in stimulated valvular endothelial cells

VECs were stimulated with TGFβ1+IL1β and TNFα, or kept unstimulated for 7 days. **A** *Cells were fixed and stained with anti CD31, anti Vimentin, and DAPI. Stimulated cells revealed less CD31*

synthesis compared to neg control. **B***: AlamarBlue assay was performed to measure the cell viability. One-way ANOVA test with Tukey's post test for multiple comparisons was used to analyze the statistical significance of cell viability. Bars displayed viability normalized by control in EndMT medium ± SEM. n=3; ****p< 0.00005*

EndMT= Endothelial to mesenchymal transition; IL= Interleukin; CD31= Platelet and endothelial cell adhesion molecule 1; TGFβ1= Transforming growth factor-beta 1; TNFα= Tumor necrosis factor-alpha; VEC= Valvular endothelial cells

3.3.1 Proteomic data

In order to gain comprehensive insight into the expressed proteins, a proteomic analysis was performed at the Core Facility Analytical Proteomics and Core Unit for Bioinformatics Data Analysis (P-459-NW PS01+02). The analysis included stimulation of the cells with TGFβ1, TGFβ1+IL1β, and TNFα in comparison to unstimulated cells. This unbiased approach allowed a thorough examination of protein expression patterns. The proteomic analysis was performed after completion of the EndMT protocol, which is described in the previous chapter and further detailed in chapter 6.1 of the supplementary appendix. In total, 2 proteomic analyses were conducted. First, one batch, corresponding to one donor of VECs, was used to confirm the reproducibility of the results. In a second experiment, 4 different batches, so 4 different donors were used. Thus, VECs from **A:** 4 different donors, or **B:** one donor with 4 replicates, were stimulated with TGFβ1, TGFβ1+IL1β, TNFα, or vehicle for 7 days. The results showed high aberrations within the 4 donors whereas one donor revealed repetitious accuracy within the technical replicates in all analyses.

In regard to TGFβ1 and TGFβ1+ IL1β conditions, in both analyses, MMRN1, ECI2, and NEK7 were significantly upregulated in TGFβ1 stimulated cells compared to TGFβ1+IL1β stimulation. Among these proteins, MMRN1 could be found in platelets and in the endothelium of blood vessels and it functions as extracellular matrix or adhesive protein (Tasneem et al. 2009).

The addition of IL1β led to an upregulation of mesenchymal markers as for instance VCAM1 and Transgelin, which were also used in this study. Still, Transgelin seemed to be donor dependent as its expression was only observed within the analysis for all 4 donors. Moreover, Transgelin expression was inaccuracy within the donors confirming the lack of expression in the second analysis (Figure 24 B). Regarding the analysis of the single donor, eNOS and VWF expression could be found in an upregulated expression within the TGFβ1 stimulation compared to TGFβ1+IL1β. These 2 endothelial markers were also used within the experiments in this

study for investigating endothelial characteristics. In conclusion, IL1β seemed to be a crucial factor for EndMT induction.

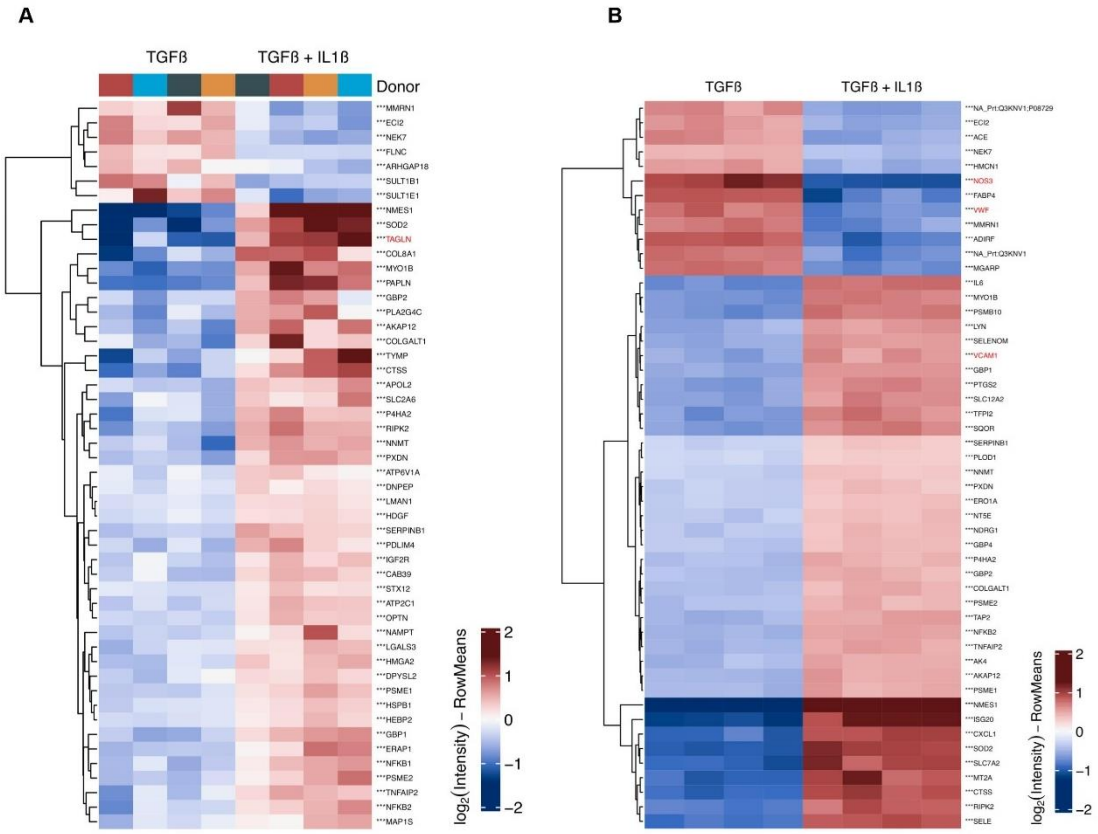

Figure 24 Comparison of TGFβ1+IL1β versus TGFβ1 stimulation in valvular endothelial cells

*VECs from **A**: 4 different donors, or **B**: one donor with 4 replicates, were stimulated with TGFβ1 or TGFβ1+IL1β for 7 days. Proteomic analysis was performed in the Core Facility Analytical Proteomics and Core Unit for Bioinformatics Data Analysis. The results showed high aberrations within the 4 donors whereas one donor revealed repetitious accuracy within the technical replicates.*

VECs= Valvular endothelial cells; TGFβ1= Transforming growth factor-beta 1; IL1β= Interleukin 1 beta; TNFα= Tumor necrosis factor-alpha

In regard to TNFα stimulation compared to TGFβ1+IL1β stimulated VECs, obviously more inflammation markers showed an increased expression (ISG, MX1, MX2, IFIT, IL1β, etc.). Interestingly, the in here investigated PRR RIG-I as well as MDA5 were also higher expressed after TNFα stimulation. Furthermore, STING1 was also significantly expressed in TNFα stimulated cells (Figure 25). The associated pathway of STING will be addressed again in the discussion. Transgelin seemed to be IL1β dependent, which could be confirmed in the following experiments as well as in the comparison between TGFβ1 and TGFβ1+IL1β (Figure 24).

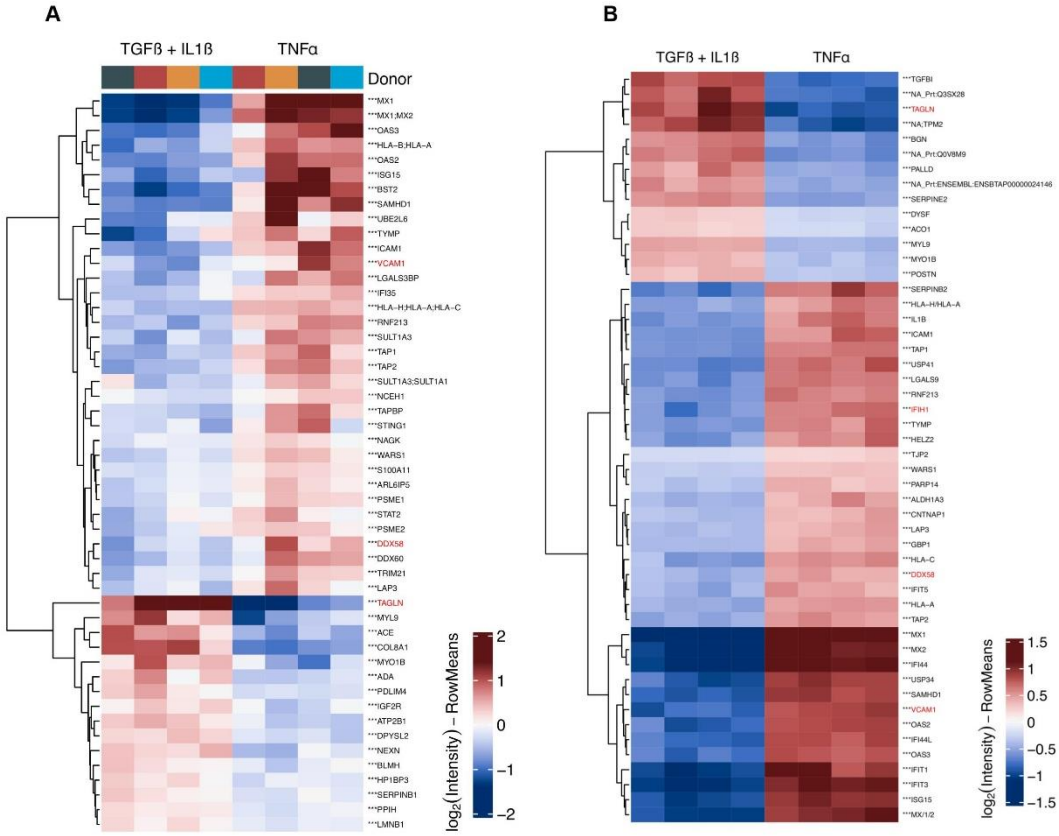

Figure 25 Comparison of TGFβ1+IL1β versus TNFα stimulation in valvular endothelial cells

*VECs from **A**: 4 different donors, or **B**: one donor with 4 replicates, were stimulated with TNFα or TGFβ1+IL1β for 7 days. Proteomic analysis was performed in the Core Facility Analytical Proteomics and Core Unit for Bioinformatics Data Analysis. The results showed high aberrations within the 4 donors whereas one donor revealed repetitious accuracy within the technical replicates.*

VECs= Valvular endothelial cells; TGFβ1= Transforming growth factor-beta 1; IL1β= Interleukin 1 beta, TNFα= Tumor necrosis factor-alpha

3.4 The role of TLR3 in the process of endothelial to mesenchymal transition

This study identified the presence of TLR3 in VICs. Moreover, TLR3 was subjected to further investigation to elucidate its involvement in the process of EndMT. First, in order to achieve an

overview of the endogenous role of TLR3 in the process of EndMT, TLR3 siRNA, PolyIC, or scrambled siRNA were transfected into VECs for 24 hours. *TLR3* gene expression as well as EndMT markers such as *NOS3*, *PECAM1*, and *VWF* as endothelial markers and *VCAM1*, *ACTA2*, and *TAGLN* as mesenchymal markers, were measured (Figure 26). TLR3 siRNA transfection resulted in a reduced gene expression compared to neg control. PolyIC transfection led to an upregulated *TLR3* gene expression that could be downregulated again after knockdown with siRNA. The endothelial markers were reduced after PolyIC transfection compared to the other conditions. TLR3 knockdown in turn resulted in a higher gene expression compared to PolyIC treated cells. Only *VWF* gene expression was lower in PolyIC+TLR3 siRNA compared to only PolyIC treatment. Regarding mesenchymal markers, PolyIC treatment led to a higher gene expression compared to the other conditions. Interestingly, *ACTA2* expression was higher after TLR3 knockdown (Figure 26).

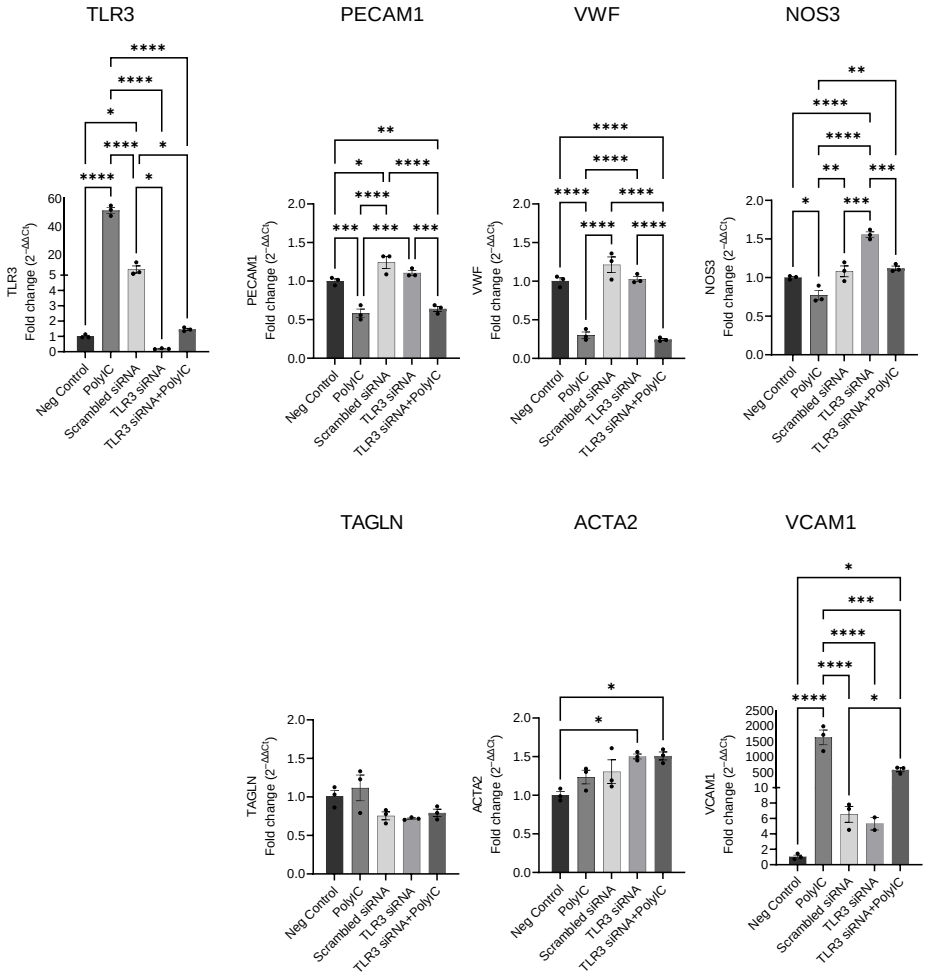

Figure 26 Gene expression of transfected valvular endothelial cells

TLR3 siRNA, PolyIC, or scrambled siRNA were transfected into cells for 24 hours. RNA was isolated and qPCR was performed. The relative levels of target gene expression were calculated

*by the Comparative Ct Method (ΔΔCt Method). One-way ANOVA test with Tukey's post test for multiple comparisons was used to test the statistical significance of qPCR data. Bars displayed the fold change of gene expression normalized by neg control ± SEM. n=1 *p < 0.05, ** p< 0.005, *** p< 0.0005 ****p< 0.00005.*

ACTA2= Smooth muscle alpha-2 actin; C4a= Compound 4a; NOS3= Nitric oxide synthase 3; PECAM1= Platelet endothelial cell adhesion molecule-1; PolyIC= Polyinosinic:Polycytidylic acid; TAGLN= Transgelin; TLR3= Toll-like receptor 3; VCAM1= Vascular cell adhesion molecule 1; VEC= Valvular endothelial cell; VWF= Von Willebrand factor

3.4.1 TLR3 inhibition with C4a in the process of endothelial to mesenchymal transition

In addition to performing knockdown experiments targeting TLR3, the study also employed pharmacological inhibition of the receptor. For this, VECs were treated with PolyIC to activate TLR3 and C4a to specifically inhibit TLR3 signaling. This approach aimed to investigate the TLR3 activation and inhibition in VECs and potential modulation of the EndMT process. Different time points were investigated after treatment in contrast to untreated neg control cells. 72 hours after treatment, microscopic images were recorded to visualize the cell morphology (Figure 27). Control cells as well as C4a-treated cells showed a normal endothelial cell shape whereas PolyIC-treated cells obtained a mesenchymal characteristic cell shape with an increased cell elongation. In addition, these VECs adopted similar directions after PolyIC treatment. PolyIC+C4a treatment resulted in a similar pattern. This indicated a first impression of TLR3-mediated EndMT.

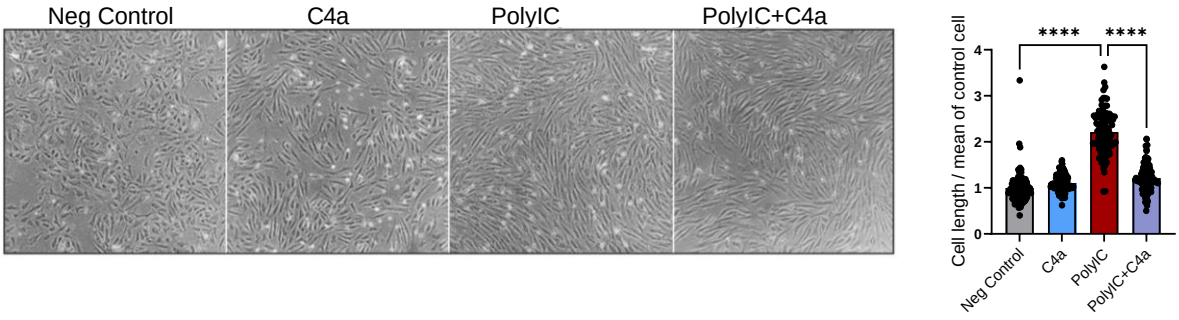

Figure 27 Representative images of treated valvular endothelial cells

*Cells were treated with PolyIC, C4a, PolyIC+C4a, or vehicle (neg control). PolyIC treated cells revealed a significantly increased cell length and an ordered direction compared to untreated, or C4a treated cells. One-way ANOVA test with Tukey's post test for multiple comparisons was used to test the statistical significance. Bars displayed the difference in cell length normalized by neg control ± SEM. **** p< 0.00005 Graph and image were modified from (Niepmann et al. 2023).*

C4a= Compound 4a; PolyIC= Polyinosinic:Polycytidylic acid

To ensure the reliability and reproducibility of the results of this chapter, all data graphs, illustrating the results, have been included as blots in the supplemental appendix in chapter 6.2. These blots provide the assessment of statistical significance and additional information observed in the data.

TLR3 gene expression was investigated after different time points in VECs treated with PolyIC, C4a, or vehicle for 24 hours. Afterwards, medium was changed to EndMT medium without VEGF or hydrocortisone. *TLR3* was higher expressed after PolyIC treatment compared to control, C4a-treated, or PolyIC+C4a-treated cells after 24, 48, and 72 hours. 5 days after treatment, PolyIC still resulted in a higher *TLR3* mRNA level in comparison to untreated control cells. Nevertheless, the general gene expression of *TLR3* was reduced compared to earlier time points. Thus, PolyIC treatment resulted in a time dependent *TLR3* gene expression that lasted approximately 72 hours to 5 days (Figure 28). Similar results could be found regarding the *DDX58* (RIG-I) and *IFIH1* (MDA5) mRNA levels: PolyIC treatment elicited an initial upregulation of gene expression within the first 72 hours. However, subsequent analysis revealed a downregulation of gene expression upon prolonged exposure to PolyIC (Figure 28).

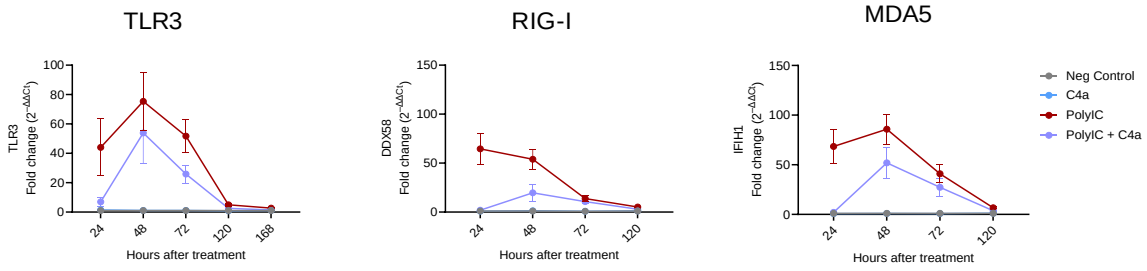

Figure 28 TLR3, RIG-I, MDA5 gene expression in valvular endothelial cells at different time points

VECs were treated with PolyIC, C4a, or both for 24 hours. Afterwards, medium was changed to EndMT medium. TLR3, DDX58 (RIG-I), and IFIH1 (MDA5) gene expression levels in VECs were measured by qPCR after certain time points. The relative levels of target gene expression were calculated by the Comparative Ct Method (ΔΔCt Method). Superimposed symbols displayed the fold change of gene expression normalized by neg control ± SEM. n=3

DDX58= DEAD (Asp-Glu-Ala-Asp) box polypeptide 58; IFIH1= Interferon induced with helicase C Domain 1; C4a= Compound 4a; EndMT= Endothelial to mesenchymal transition; MDA5= Melanoma differentiation-associated protein 5; PolyIC= Polyinosinic:Polycytidylic acid; RIG-I= Retinoic acid inducible gene I; TLR3= Toll-like receptor 3; VECs= Valvular endothelial cells

To further investigate the role of TLR3 in the process of EndMT, both endothelial and mesenchymal markers were measured in VECs (Figure 29). For this, cells were treated with

PolyIC as well as C4a for 24 hours. The endothelial marker *PECAM1* was downregulated within the first 48 hours after PolyIC, C4a, and Poly+C4a treatment in comparison to neg control. *VWF* gene expression showed a downregulation within the first 72 hours compared to untreated control cells. *NOS3* gene expression did not show significant differences after 24 hours. 48 hours after PolyIC treatment, cells showed lower *NOS3* mRNA levels compared to untreated control cells or C4a treated cells. All 3 markers showed a similar pattern: By day 5, the cells seemed to have regained their endothelial phenotype. *VCAM1* was upregulated in the first 72 hours after the addition of PolyIC, showing a treatment-dependent result, whereas C4a co-treatment resulted in a blunted response 24 hours after treatment. *ACTA2* gene expression was upregulated by PolyIC, but there was no major difference from C4a treatment. *TAGLN* was downregulated 24 hours after C4a treatment. After 48 hours, PolyIC treatment showed a downregulation compared to untreated control cells as well as C4a treated cells. In general, similar to the analysis of endothelial markers, gene expression of mesenchymal markers showed a reverse trend within 7 days of treatment.

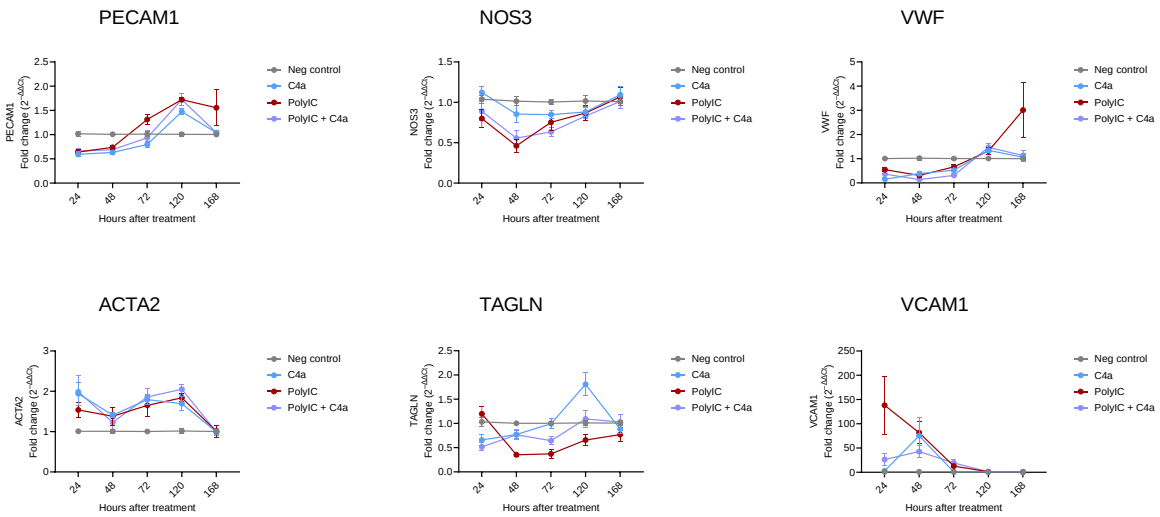

Figure 29 Gene expression in treated valvular endothelial cells

VECs were treated with PolyIC, C4a, or both for 24 hours. The medium was then changed to EndMT medium. After certain time points, RNA was isolated and qPCR was performed. Relative levels of target gene expression were calculated using the comparative Ct method (ΔΔCt method). The superimposed symbols indicate the fold change in gene expression normalized to the neg control ± SEM. n=3

C4a= Compound 4a; EndMT= Endothelial to mesenchymal transition; NOS3= Nitric oxide synthase 3; PECAM1= Platelet endothelial cell adhesion molecule-1; PolyIC= Polyinosinic:Polycytidylic acid; RIG-I= Retinoic acid inducible gene I; TAGLN= Transgelin; VCAM1= Vascular cell adhesion molecule 1; VEC= Valvular endothelial cell; VWF= Von Willebrand factor

To verify these results, cells were stained with anti VCAM1 antibody, 72 hours after addition of PolyIC, C4a, or both. Treatment with PolyIC resulted in a change in cell length and direction of order, as shown in figure 30 A. In some regions, VCAM1 staining appeared to be more specific in PolyIC-treated cells, but it was also expressed in C4a-treated and untreated control cells. Western blot was performed 24 hours after treatment and revealed a higher VCAM1 expression after PolyIC treatment compared to the treatment with PolyIC+C4a (Figure 30 B). In C4a treated cells as well as untreated control cells (neg control), VCAM1 was not detected. Furthermore, CD31 (*PECAM1*) expression was measured by Western Blot and showed less expression after PolyIC treatment compared to the other conditions. These results confirmed the observations of the time dependent gene expression pattern (Figure 29).

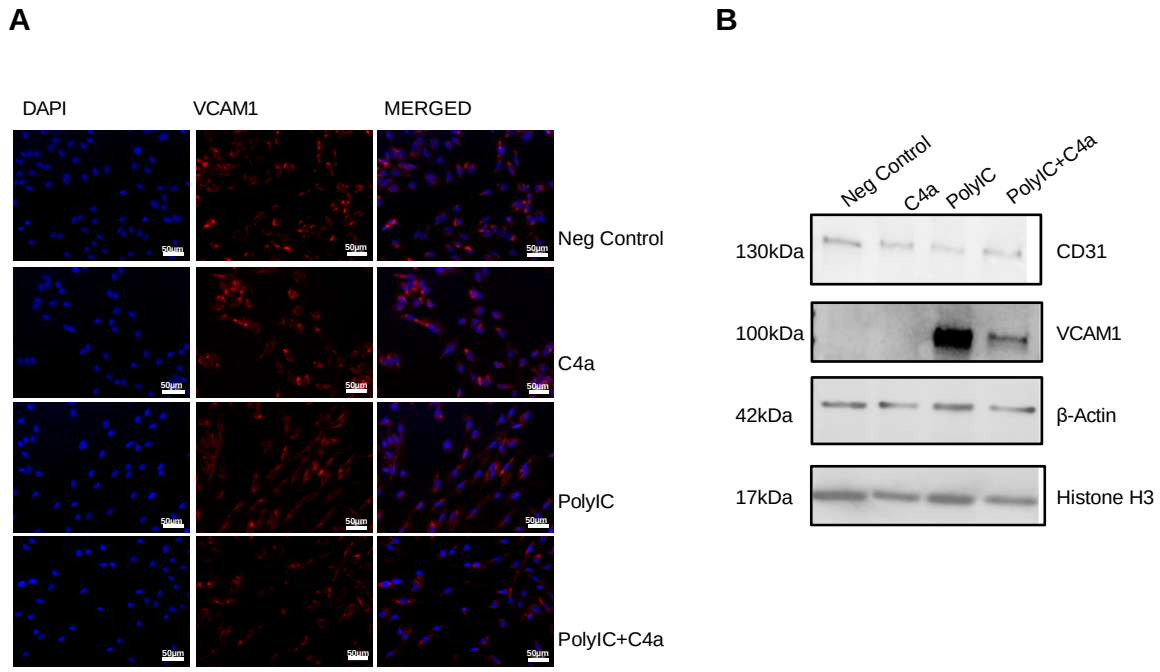

Figure 30 Immunofluorescence staining and Western blot of valvular endothelial cells

VCAM1 expression of VECs treated with PolyIC, C4a, both, or untreated. ***A****: Immunofluorescence staining.* ***B****: Western blot was performed to confirm CD31 and VCAM1 expression of VECs treated with PolyIC, C4a, or both, compared to untreated cells.*

C4a= Compound 4a; PolyIC= Polyinosinic:Polycytidylic acid; TLR3= Toll-like receptor 3; VCAM1= Vascular cell adhesion molecule 1

3.4.2 Endothelial to mesenchymal transition induction after TLR3 activation/inhibition

A slight response to TLR3 activation in the manner of EndMT was demonstrated in section 3.4.1. However, the transition to mesenchymal cells did not last long and the cells appeared to revert to their endothelial phenotype.

In a next experimental investigation, the involvement of TLR3 in the process of EndMT was explored in conjunction with the EndMT stimulation, that is shown in chapter 3.3. VECs were treated with PolyIC, C4a, both, or left untreated as a control. In addition, after treatment, EndMT was induced by adding TGFβ1+IL1β or TNFα. EndMT processing could be assumed by observing decreased endothelial and increased mesenchymal marker gene expression via qPCR analysis. *VWF* and *NOS3* showed decreased gene expression after the addition of TGFβ1+IL1β or TNFα. *PECAM1* showed a slightly reduced gene expression after changing medium. Within 7 days, *PECAM1* gene expression increased again. *VCAM1* showed an effect immediately after the change of media including TGFβ1+IL1β or TNFα. *TAGLN* and *ACTA2* gene expression increased significantly on day 5 (Figure 31).

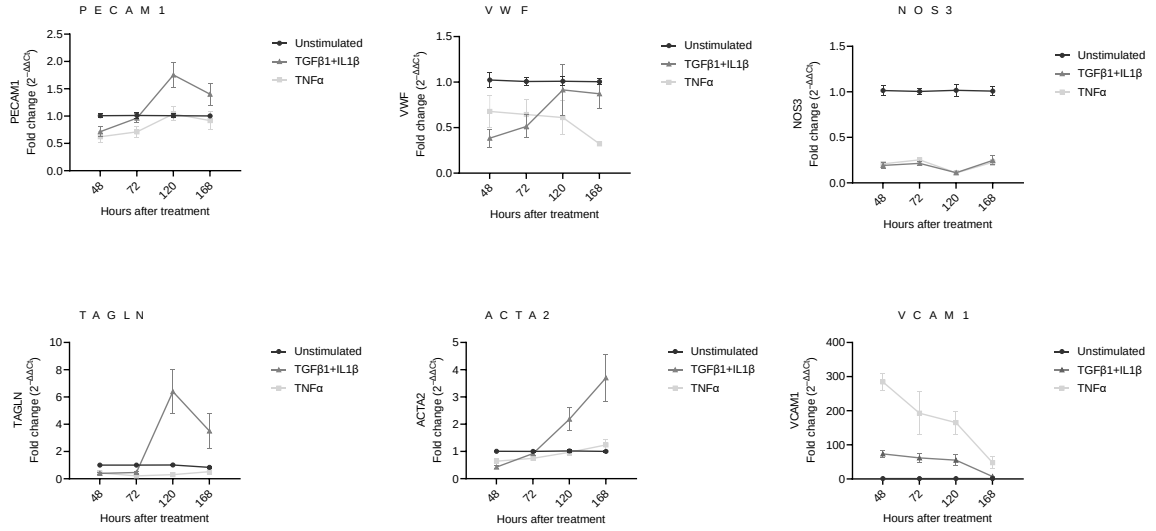

Figure 31 Gene expression after endothelial to mesenchymal transition induction in valvular endothelial cells

Gene expression of endothelial and mesenchymal markers after TGFβ1+IL1β, TNFα stimulation, or left unstimulated. Relative levels of target gene expression were calculated using the comparative Ct method (ΔΔCt method). The superimposed symbols displayed the fold change of gene expression normalized unstimulated controls ± SEM. n=3

ACTA2= Smooth muscle alpha-2 actin; NOS3= Nitric oxide synthase 3; PECAM1= Platelet endothelial cell adhesion molecule-1; TAGLN= Transgelin; TGFβ1= Transforming growth factor-beta 1; TNFα= Tumor necrosis factor-alpha; VCAM1= Vascular cell adhesion molecule 1; VWF= Von Willebrand factor

EndMT induction with TGFβ1+IL1β, or TNFα resulted in a higher *TLR3, IFIH1* (MDA5), and *DDX58* (RIG-I) gene expression compared to unstimulated control cells (Figure 32).

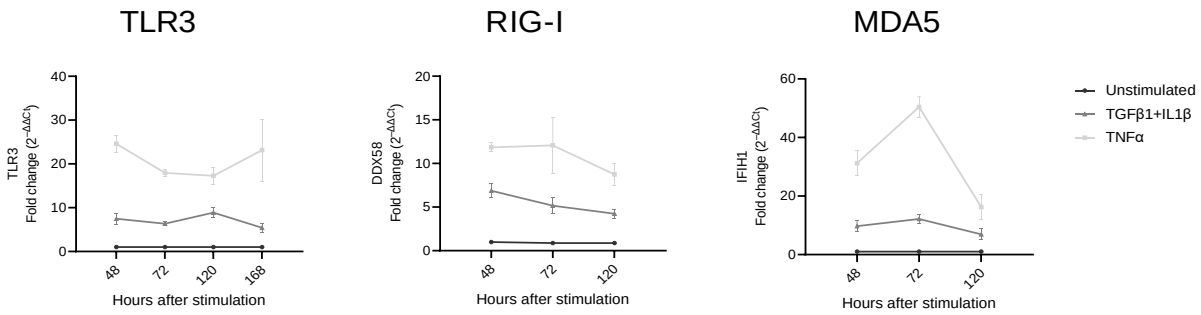

Figure 32 TLR3, RIG-I, and MDA5 gene expression in valvular endothelial cells

TLR3, DDX58 (RIG-I), and IFIH1 (MDA5) gene expression in VECs after TGFβ1+IL1β, or TNFα stimulation compared to unstimulated cells. Relative levels of target gene expression were calculated using the comparative Ct method (ΔΔCt method). The superimposed symbols indicate the fold change in gene expression normalized to unstimulated cells ± SEM. n=3

DDX58= DEAD (Asp-Glu-Ala-Asp) box polypeptide 58; IFIH1= Interferon induced with helicase C Domain 1; MDA5= Melanoma differentiation-associated protein 5; RIG-I= Retinoic acid inducible gene I; TGFβ1= Transforming growth factor-beta 1; TLR3= Toll-like receptor 3; TNFα= Tumor necrosis factor-alpha; VEC= Valvular endothelial cell

After demonstrating decreased and increased endothelial marker and mesenchymal marker, respectively (Figure 32), cells were treated with PolyIC, C4a, or both, and subsequently stimulated with TGFβ1+IL1β to induce EndMT. Gene expressions of *TLR3*, *DDX58* (RIG-I), and *IFIH1* (MDA5) revealed similar findings: PolyIC treatment resulted in an increased mRNA level compared to the other conditions, whereas the C4a-treated cells showed a consistent result compared to untreated cells (Figure 33).

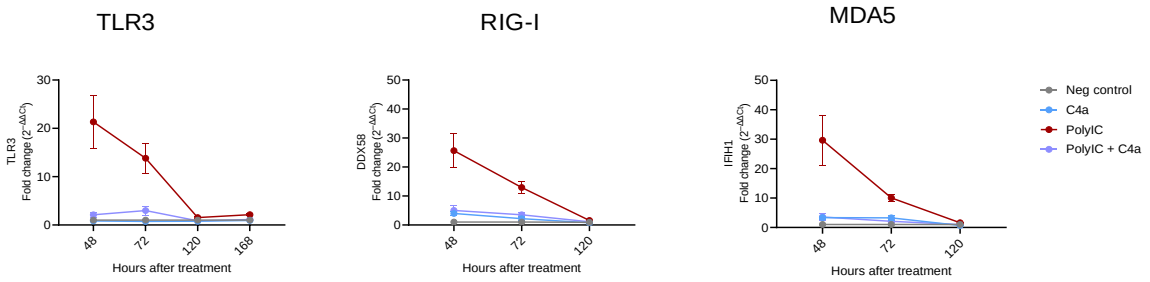

Figure 33 TLR3, RIG-I, and MDA5 gene expression in valvular endothelial cells at selected time points after endothelial to mesenchymal transition induction with TGFβ1+IL1β

VECs were treated with PolyIC, C4a, or both for 24 hours. The medium was then changed to EndMT medium supplemented with TGFβ1+IL1β. After certain time points, RNA was isolated and qPCR was performed. Relative levels of target gene expression were calculated using the comparative Ct method (ΔΔCt method). The superimposed symbols indicate the fold change in gene expression normalized to the neg control ± SEM. n=3

C4a= Compound 4a; DDX58= DEAD (Asp-Glu-Ala-Asp) box polypeptide 58; EndMT= Endothelial to mesenchymal transition; IFIH1= Interferon induced with helicase C domain 1; MDA5= Melanoma differentiation-associated protein 5; PolyIC= Polyinosinic:Polycytidylic acid; RIG-I= Retinoic acid inducible gene I; TGFβ1= Transforming growth factor-beta 1; TLR3= Toll-like receptor 3; VEC= Valvular endothelial cell

Focusing on EndMT marker, PolyIC treatment resulted in decreased gene expression of *VWF*, *PECAM1,* and *NOS3* compared to C4a treatment and untreated control cells. C4a treatment appeared to affect *VWF* and *PECAM1* expression within the first 3 days, but by 5 days after treatment there were no differences compared to untreated control cells. In comparison to control cells, PolyIC treatment showed no effect on mesenchymal gene expression after TGFβ1+IL1β stimulation. In fact, C4a treatment may affect *ACTA2* and *TAGLN* gene expression rather than PolyIC. Interestingly, *VCAM1* gene expression decreased upon 48 hours after PolyIC treatment (Figure 34), whereas unstimulated cells showed higher *VCAM1* mRNA levels within the first 2-3 days (Figure 29).

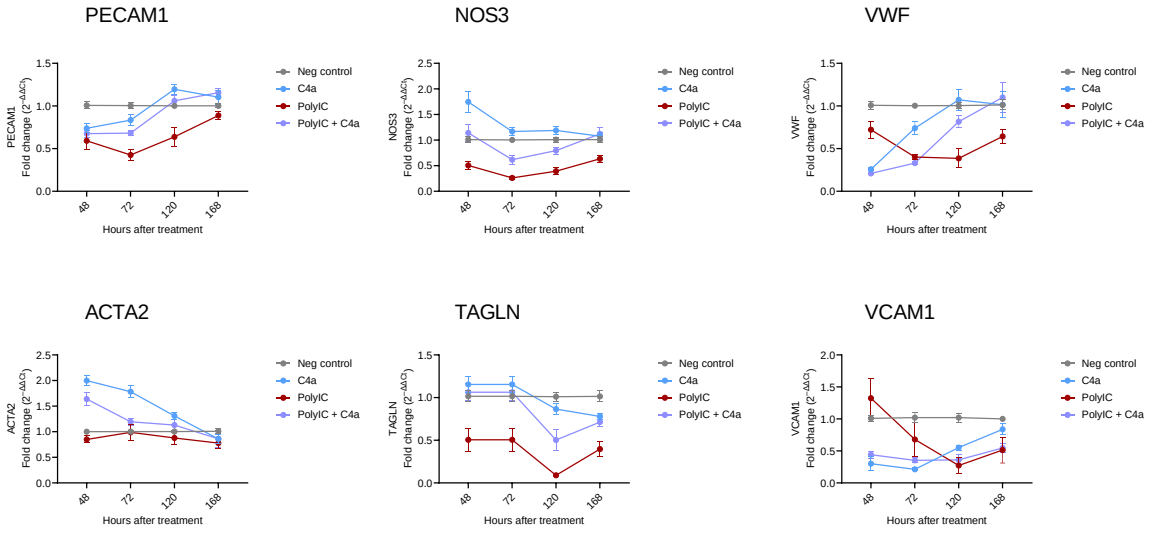

Figure 34 Gene expression in treated valvular endothelial cells after endothelial to mesenchymal transition induction with TGFβ1+IL1β

Gene expression in VECs treated with PolyIC, C4a or both for 24 hours. The medium was then changed to EndMT medium supplemented with TGFβ1+IL1β. After certain time points, RNA was isolated and qPCR was performed. Relative levels of target gene expression were calculated

using the comparative Ct method (ΔΔCt method). The graphs show the fold change in gene expression normalized to the neg control ± SEM. n=3

ACTA2= Smooth muscle alpha-2 actin; C4a= Compound 4a; EndMT= Endothelial to mesenchymal transition; NOS3= Nitric oxide synthase 3; PECAM1= Platelet endothelial cell adhesion molecule-1; PolyIC= Polyinosinic:Polycytidylic acid; TAGLN= Transgelin; TGFβ1= Transforming growth factor-beta 1; TLR3= Toll-like receptor 3; VCAM1= Vascular cell adhesion molecule 1; VEC= Valvular endothelial cell; VWF= Von Willebrand factor

In another experiment, VECs were stimulated with TNFα to induce EndMT, 24 hours after PolyIC or C4a treatment. 48h after PolyIC treatment, mRNA levels of *TLR3*, *DDX58* (RIG-I), and *IFIH1* (MDA5) increased and were blunted with C4a treatment. From day 5 onwards, no significant differences were detected among the various treatments in terms of *TLR3*, *DDX58* (RIG-I), and *IFIH1* (MDA5) gene expressions (Figure 35).

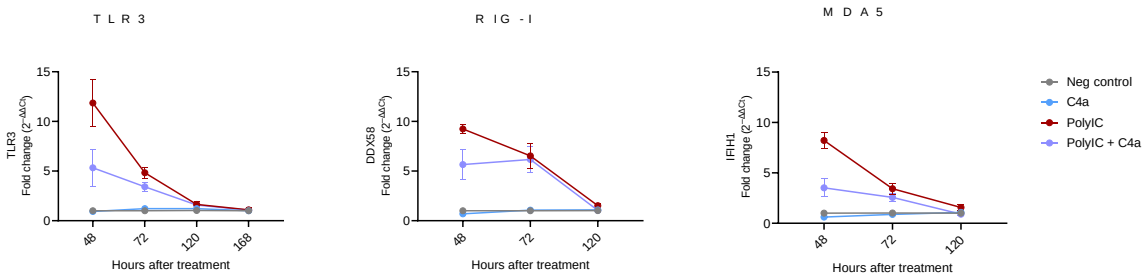

Figure 35 TLR3, RIG-I, and MDA5 gene expression in valvular endothelial cells at selected time points after endothelial to mesenchymal transition induction with TNFα

Cells were treated with PolyIC, C4a or both for 24 hours. The medium was then changed to EndMT medium supplemented with TNFα. After certain time points, RNA was isolated and qPCR was performed. Relative levels of target gene expression were calculated using the comparative Ct method (ΔΔCt method). The graphs showed the fold change in gene expression normalized to the neg control ± SEM. n=3

C4a= Compound 4a; DDX58= DEAD (Asp-Glu-Ala-Asp) box polypeptide 58; EndMT= Endothelial to mesenchymal transition; IFIH1= Interferon induced with helicase C domain 1; MDA5= Melanoma differentiation-associated protein 5; PolyIC= Polyinosinic:Polycytidylic acid; RIG-I= Retinoic acid inducible gene I; TLR3= Toll-like receptor 3; TNFα= Tumor necrosis factor-alpha; VEC= Valvular endothelial cell

Next, mRNA levels from EndMT marker were quantified and analyzed. According to endothelial markers, PolyIC treatment resulted in decreased gene expression of *PECAM1*, *NOS3,* and *VWF* within 7 days. By the seventh day after treatment, the cells appeared to have regained their endothelial phenotype. Focusing on *VWF* expression, C4a treatment may have a

greater effect within the first 3 days. These data were comparable to those obtained with TGFB1+IL1β stimulation and unstimulated cells: Regarding *ACTA2* and *TAGLN* gene expression, VECs were more responsive to C4a treatment in contrast to PolyIC treatment (Figure 36).

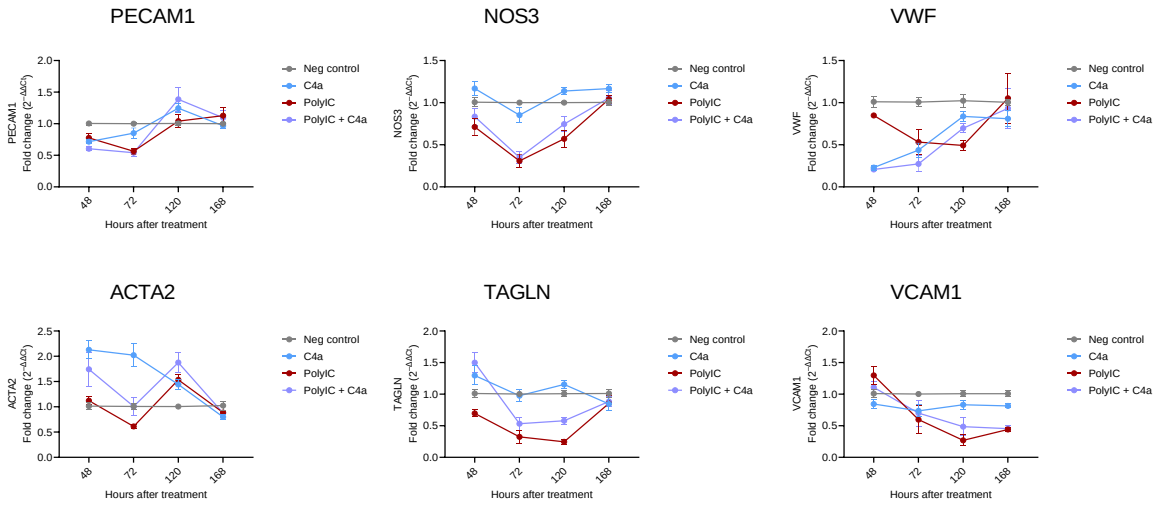

Figure 36 Gene expression in treated valvular endothelial cells after endothelial to mesenchymal transition induction with TNFα

Gene expression in VECs treated with PolyIC, C4a or both for 24 hours. The medium was then changed to EndMT medium supplemented with TNFα. After certain time points, RNA was isolated and qPCR was performed. Relative levels of target gene expression were calculated using the comparative Ct method (ΔΔCt method). The graphs show the fold change in gene expression normalized to the neg control ± SEM. n=3

ACTA2= Smooth muscle alpha-2 actin; C4a= Compound 4a; EndMT= Endothelial to mesenchymal transition; NOS3= Nitric oxide synthase 3; PECAM1= Platelet endothelial cell adhesion molecule-1; PolyIC= Polyinosinic:Polycytidylic acid; TAGLN= Transgelin; TNFα= Tumor necrosis factor-alpha; VCAM1= Vascular cell adhesion molecule 1; VEC= Valvular endothelial cell; VWF= Von Willebrand factor

3.5 TLR3 in *in vivo* experiments

Basic research aims to investigate the target of interest not only at the cellular level but also within the broader system context. Thus, in addition to *in vitro* experiments, TLR3 was also studied in mice. Within 3 main experiments, the role of TLR3 in the pathogenesis of AS was investigated using C57BL/6 mice and AS was induced by the wire injury method (Niepmann et al. 2019). These 3 experiments investigated the TLR3 activation with PolyIC, the endogenous activation of TLR3, and receptor inhibition with C4a. Over a period of 6 weeks, several parameters, such as peak systolic velocity, ejection fraction (EF), and mean pressure gradient

were measured every 2 weeks. After sacrifice, hearts were isolated and sections were stained with hematoxylin and eosin to measure valve size. Von Kossa staining was used to confirm calcification. Sirius Red staining was used to visualize collagen and fibrotic areas. CD68 immunofluorescence staining was performed to examine macrophage infiltration.

3.5.1 PolyIC treatment in wild type mice

After wire injury, WT mice were treated daily with PolyIC to activate TLR3. Control animals received NaCl. After 2, 4, and 6 weeks, ultrasound examinations were performed by Dr. Sven Niepmann with the help of Ann-Sophie Boucher. 6 weeks after surgery, the mice were sacrificed, blood samples were taken, the heart was explanted, and cryosections were prepared for staining.

3.5.1.1 Echocardiography

To assess the development of AS in mice, ultrasound examinations were performed. A clear trend of increasing peak velocity and mean pressure gradient after stimulation with PolyIC could be demonstrated. The ejection fraction initially appeared to increase after 2 weeks, but the trend reversed and left ventricular function remained unchanged in these 2 groups (Figure 37).

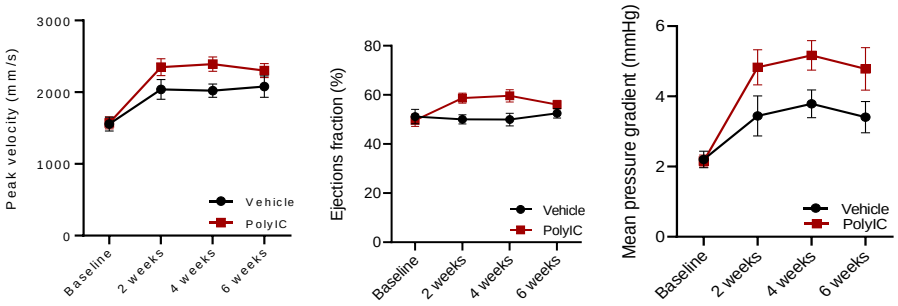

Figure 37 Echocardiography data of wild type mice treated with PolyIC compared to control mice

After wire injury, WT mice were treated daily with PolyIC to activate TLR3. Control animals received NaCl. Echocardiography was performed every other week. Wire injury as well as echocardiography were performed by Dr. Sven Niepmann; n=7-8. Graphs were modified from (Niepmann et al. 2023).

PolyIC= Polyinosinic:Polycytidylic acid; WT= Wild type

3.5.1.2 Histologic analysis of aortic valves

Mice were euthanized 6 weeks after wire injury and histological stainings of the aortic valves were performed. No significant differences in aortic valve area were observed in PolyIC-treated mice compared to controls. Sirius Red staining of murine aortic valves did not display significant differences in fibrotic areas in PolyIC-treated mice compared to control. Von Kossa

staining as a calcification marker of murine aortic valves did not differ in PolyIC-treated mice compared to control. CD68 staining of murine aortic valves displayed a slight but no significant increase in macrophage infiltration in PolyIC-treated mice compared to control animals (Figure 38).

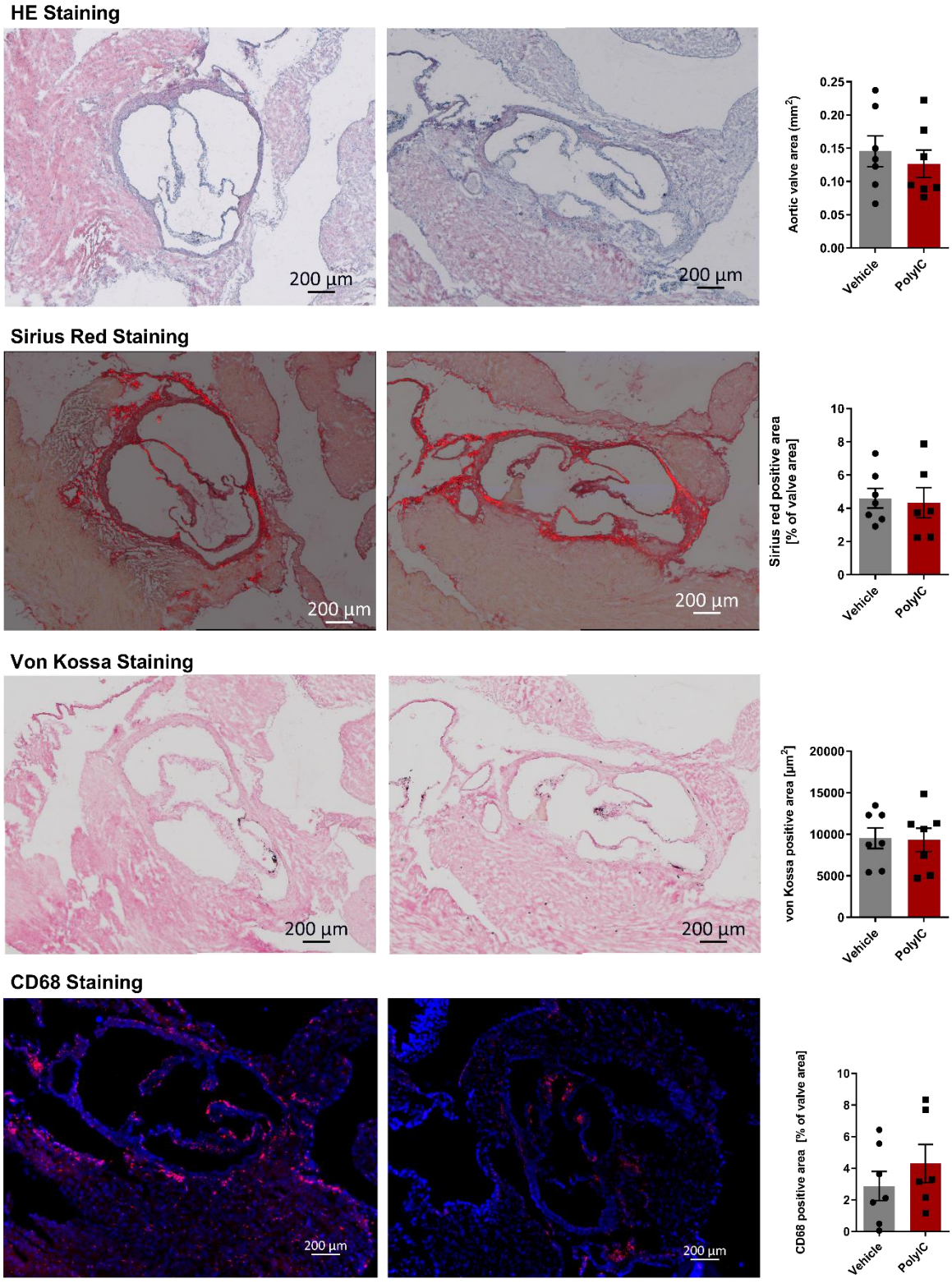

Figure 38 Histological stainings of murine aortic valves: wild type mice treated with PolyIC

After wire injury, WT mice were treated daily with PolyIC to activate TLR3. Control animals received NaCl. 6 weeks after surgery, mice were euthanized and histological stainings of the aortic valve area were performed. Student´s t-test was used to test the statistical significance; ±SEM; n=7

HE= Hematoxylin/Eosin; PolyIC= Polyinosinic:Polycytidylic acid

3.5.2 TLR3$^{-/-}$ compared to wild type mice

To elucidate the endogenous role of TLR3, TLR3$^{-/-}$ mice were used in the following experiment, while WT mice served as the control group. Dr. Sven Niepmann and the technical assistants induced AS in mice by performing wire injury. No pharmaceutical intervention was used in this experiment. A possible endogenous effect of TLR3 is demonstrated in the following data.

3.5.2.1 Echocardiography

Figure 39 shows the ultrasound studies performed by Dr. Sven Niepmann every other week. Doppler measurements showed a higher transaortic valve peak velocity and mean pressure gradient in WT mice compared to TLR3-deficient mice, confirming the absence of AS in knockout animals after wire injury. The ejection fraction remained unchanged.

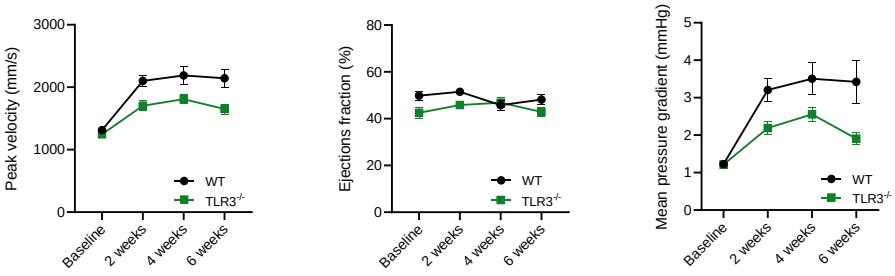

Figure 39 Echocardiography data of TLR3-/- mice compared to control mice

AS was induced by wire injury in WT and TLR3 knockout mice. Wire injury as well as echocardiography every other week were performed by Dr. Sven Niepmann; n=19-20. Graphs were modified from (Niepmann et al. 2023).

TLR3= Toll-like receptor 3

3.5.2.2 Histological analysis

Mice were euthanized 6 weeks after wire injury and histological stainings of the aortic valve area were performed. The knockout resulted in significantly smaller aortic valve area. In addition, CD68 staining, a marker for macrophage infiltration, showed reduced inflammation in TLR3-deficient mice. However, this monocyte invasion into the valves did not correlate with

fibrosis or calcification as shown by Sirius Red and von Kossa staining, respectively (Figure 40).

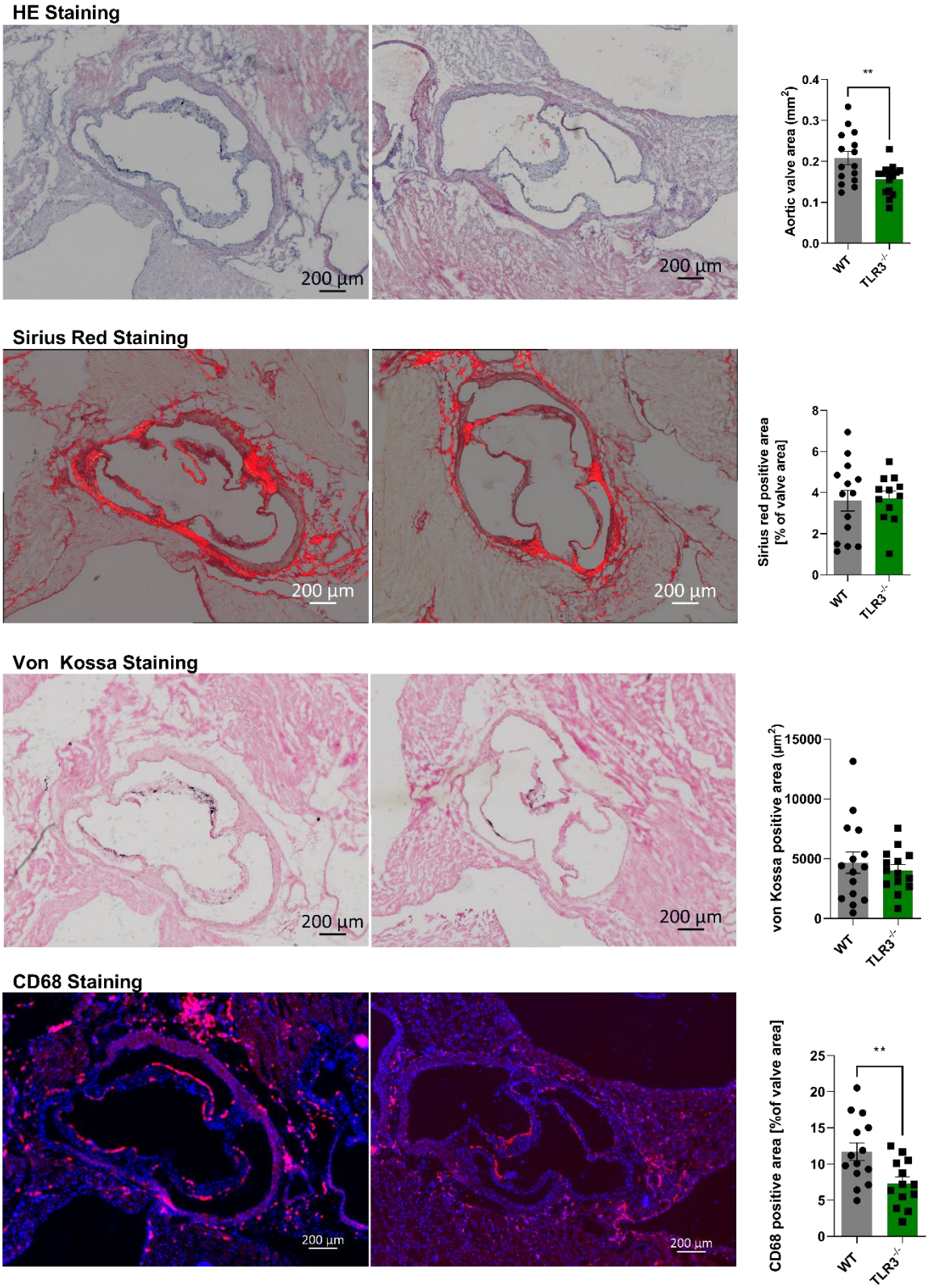

Figure 40 Histological stainings of murine aortic valves: wild type mice compared to TLR3$^{-/-}$ mice

*AS was induced by wire injury in WT and TLR3 knockout mice. 6 weeks after wire injury, mice were euthanized and histological stainings of the aortic valve area were performed. Student´s t-test was used to test the statistical significance; ± SEM. n=14-15; **p< 0.005;*
HE= Hematoxylin/Eosin; TLR3= Toll-like receptor3; WT= Wild type
Graph and image were modified from (Niepmann et al. 2023).

3.5.3 C4a treatment in wild type mice

Next to the TLR3 knockout, this study also investigated the pharmacological inhibition of TLR3. For this, the TLR3/dsRNA complex inhibitor C4a was used and injected after wire injury every other day into WT mice to inhibit TLR3. For control, mice were injected with PBS. Echocardiography was performed every 2 weeks by Dr. Sven Niepmann with the help of Ann-Sophie Boucher. After sacrifice, the hearts were explanted and cryosections were prepared for staining.

3.5.3.1 Echocardiography

TLR3 inhibition by C4a injection resulted in reduced AS development compared to the control group. We could see a lower transaortic valve peak velocity as well as a lower mean pressure gradient after 2 weeks in C4a treated mice. Ejection fraction and therefore left ventricular function remained unchanged in these 2 groups (Figure 41).

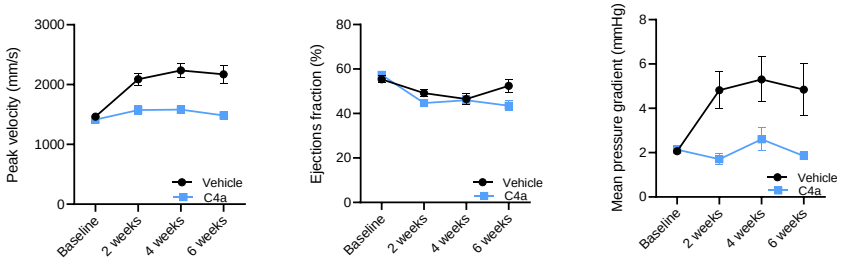

Figure 41 Echocardiography data of wild type mice treated with C4a compared to control mice
AS was induced by wire injury in WT mice. Afterwards, mice were injected with C4a every other day. Wire injury as well as echocardiography were performed by Dr. Sven Niepmann; n=12-16. Graphs were modified from (Niepmann et al. 2023)

3.5.3.2. Histological analysis

Mice were euthanized 6 weeks after wire injury and histological stainings of the aortic valves were performed. Histological sections showed a prevention of valve thickening in C4a-treated mice compared to control animals. In addition, TLR3 inhibition might reduce aortic valve fibrosis as shown by Sirius Red staining. CD68, a marker of macrophage infiltration, was less

expressed in the aortic valves of C4a-treated mice compared to the control group, confirming an anti-inflammatory effect of C4a. There was a slight trend towards reduced calcification of aortic valves in C4a-treated mice. However, von Kossa staining did not show a significant difference (Figure 42).

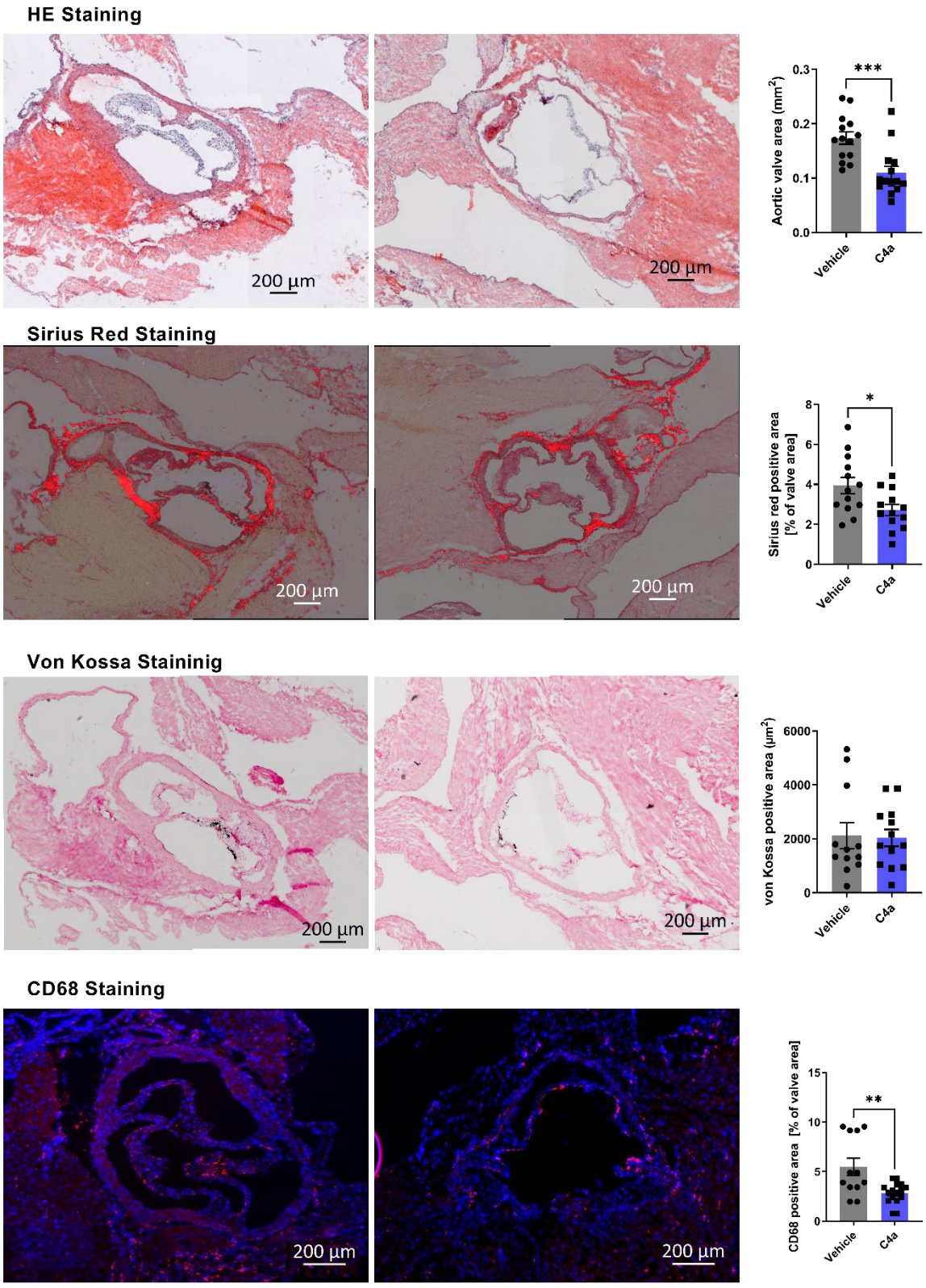

Figure 42 Histological stainings of murine aortic valves: wild type mice treated with C4a

*AS was induced by wire injury in WT mice. Afterwards, C4a was injected every other day. 6 weeks after wire injury, mice were euthanized and histological stainings of the aortic valve area were performed. Student´s t-test was used to test the statistical significance ± SEM. n=12-16*p< 0.05¸**p< 0.005, ***p< 0.0005*

C4a= Compound 4a; HE= Hematoxylin/Eosin

3.6 MDA5 in *in vivo* experiments

3.6.1 MDA5$^{-/-}$ compared to wild type mice

This study successfully identified the expression of MDA5 in human aortic valve tissue and further suggested its potential involvement in calcification processes in VICs. In order to investigate its role in a comprehensive system, a mouse model was employed. Knockout mice lacking MDA5 were utilized in subsequent experiments, with wild-type mice serving as the control group. AS was induced by wire injury as described above and performed by Dr. Sven Niepmann. No pharmaceutical intervention was used in this experiment.

3.6.1.1 Echocardiography

Figure 43 shows the ultrasound examinations performed by Dr. Sven Niepmann with the help of Ann-Sophie Boucher at 2, 4, and 6 weeks after surgery. Peak velocity and mean pressure gradient were higher in WT compared to MDA5$^{-/-}$ mice. The ejection fraction was unchanged (Figure 43).

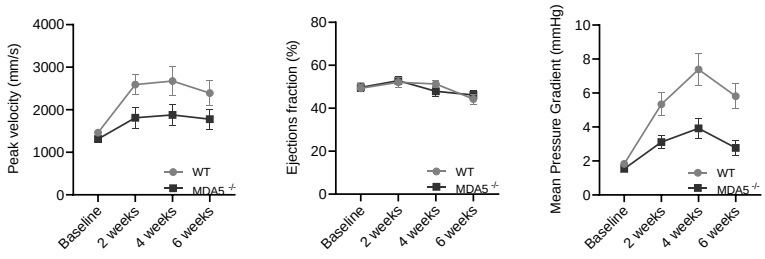

Figure 43 Echocardiography data of MDA5 $^{-/-}$ mice compared to control mice

AS was induced in MDA5 knockout mice compared to WT. Wire injury as well as echocardiography were performed by Ann-Sophie Boucher and Dr. Sven Niepmann. n=16

MDA5= Melanoma differentiation-associated protein 5; WT= Wild type

3.6.1.2 Histological analysis

Mice were euthanized 6 weeks after wire injury and histological stainings of the aortic valves were performed. HE staining technique was used to assess the aortic valve area and it showed no change in the thickness of the valves. Further, Sirius Red staining gave no significant

evidence of fibrosis. In terms of inflammation, WT and knockout mice did not reveal differently infiltrating macrophages as measured by CD68 staining. However, von Kossa staining showed that MDA5 knockout resulted in less calcification compared to WT animals (Figure 44).

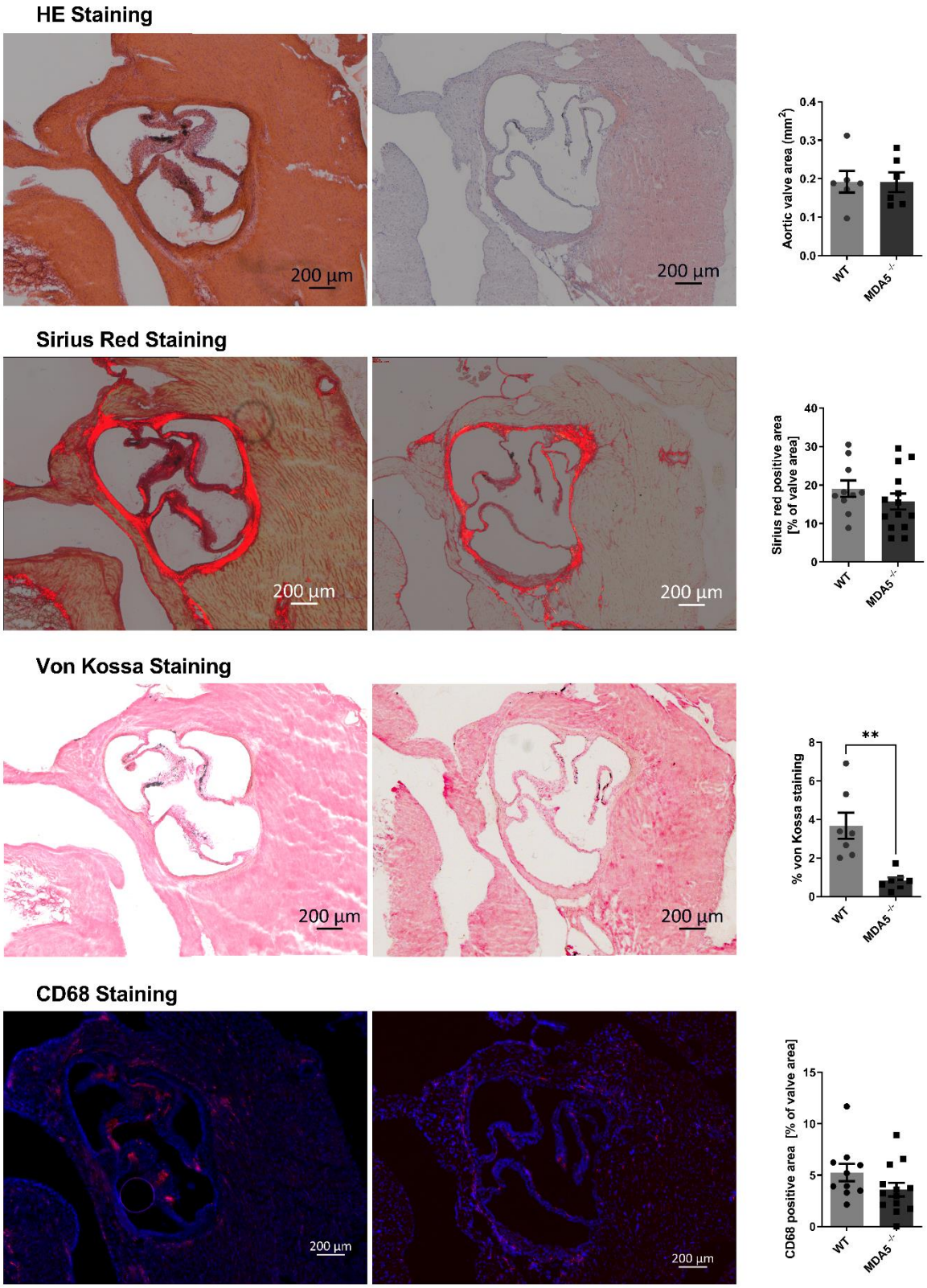

Figure 44 Histological stainings of murine aortic valves: wild type mice compared to MDA5$^{-/-}$ mice

*AS was induced by wire injury in WT and MDA5 knockout mice. 6 weeks after wire injury, mice were euthanized and histological stainings of the aortic valve area were performed. HE staining was performed by Ann-Sophie Boucher. Student´s t-test was used to test the statistical significance ± SEM. n=6-16 **p< 0.005*
HE= Hematoxylin/Eosin; MDA5= Melanoma differentiation-associated protein 5; WT= Wild type

The role of cholesterol in the development of aortic valve stenosis

Not only does the immune system play a critical role in the development of AS, but also lipid metabolism. In particular, CC have been shown to play a key role in the development of atherosclerosis and can be solubilized by CD to prevent atherosclerotic plaque formation (Zimmer et al.2016). This prompted us to investigate the role of CC and CD in AS patients and in VICs and VECs.

3.7 Measurement of cholesterol crystal dissolution rate in human blood plasma

This study aimed to evaluate the potential of dissolving cholesterol crystals in human blood spiked with different concentrations of CD or vehicle. Blood samples were taken in the clinic from patients who had undergone catheterization. In this study, only data from patients suffering from AS are presented below. As no immediate dissolution was observed, some plasma samples started to dissolve CC after 0.5 hours. After 4 hours of incubation at 37°C, slightly more samples showed a dissolution effect. After the addition of 10mM of CD, it was shown that approximately 60% of the CC were dissolved after 0.5 hours (Figure 45). After 2 hours, approximately 80% were dissolved with this concentration. After 4 hours, there was no difference and the dissolution rate remained at approximately 80% after the addition of 10mM CD. 1mM CD resulted in a dissolution of approximately 40% after 2 hours and increased up to approximately 60% after 4 hours. The lowest concentration with 0.1mM showed an increased dissolution after 4 hours, but the result was not significant (Figure 45).

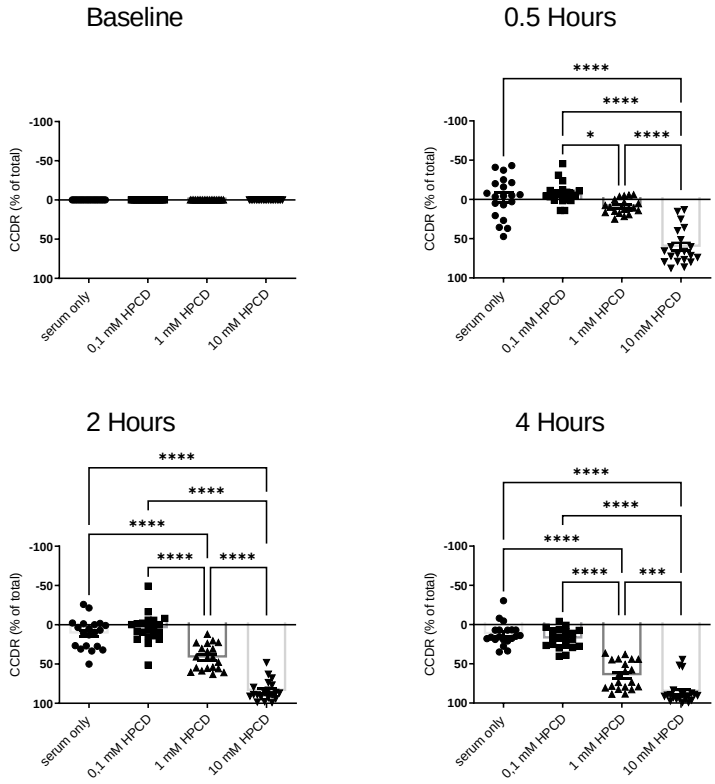

Figure 45 Cholesterol crystal dissolution rate in human plasma

*Patient´s blood was collected in the clinic. CC were added to the plasma as well as various concentrations of CD. CCDR was measured by flow cytometry. One-way ANOVA test with Tukey's post test for multiple comparisons was used to test the statistical significance. ***p< 0.0005, ****p< 0.00005; n=20*

CC= Cholesterol crystals; CCDR= Cholesterol crystal dissolution rate; CD= Cyclodextrin

3.8 Cholesterol crystal uptake

Next, CC were investigated in *in vitro* studies. To record CC in cells, VICs and VECs were treated with CC and incubated at 37°C in a humidified 5% CO_2 atmosphere. Images were taken immediately after treatment (Baseline) and after 8 hours of incubation. At the beginning, CC were floating around whereas 8 hours post treatment, CC were found inside the cells. Thus, within 8 hours, the cells ingested the crystals (Figure 46, 47).

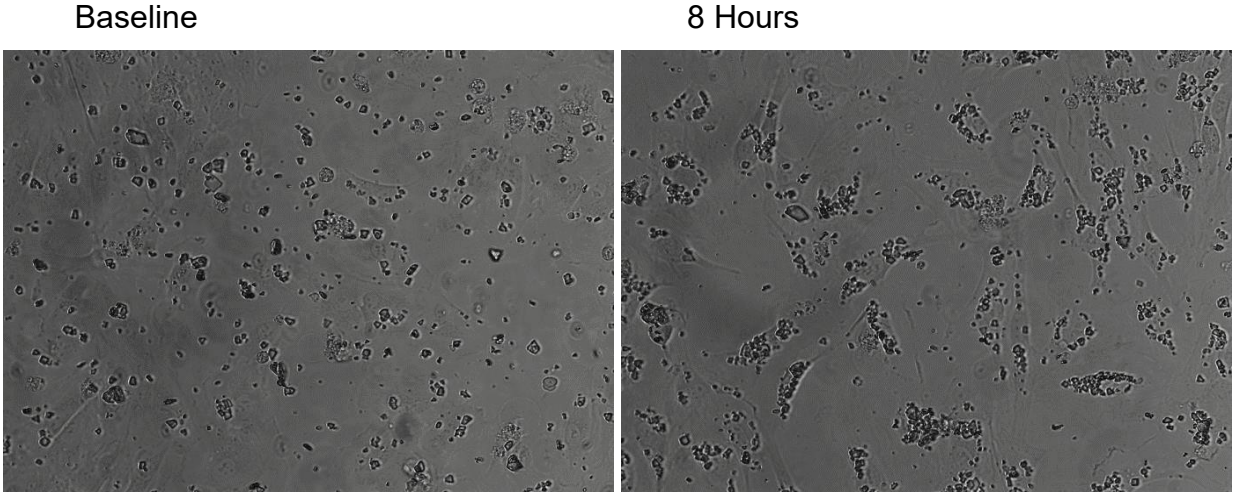

Figure 46 Representative image of valvular endothelial cells phagocytosing cholesterol crystals

VECs were treated with CC. 8 hours after treatment, CC could be observed being ingested by cells and ordered within the cell.

CC= Cholesterol crystals; VECs= Valvular endothelial cells

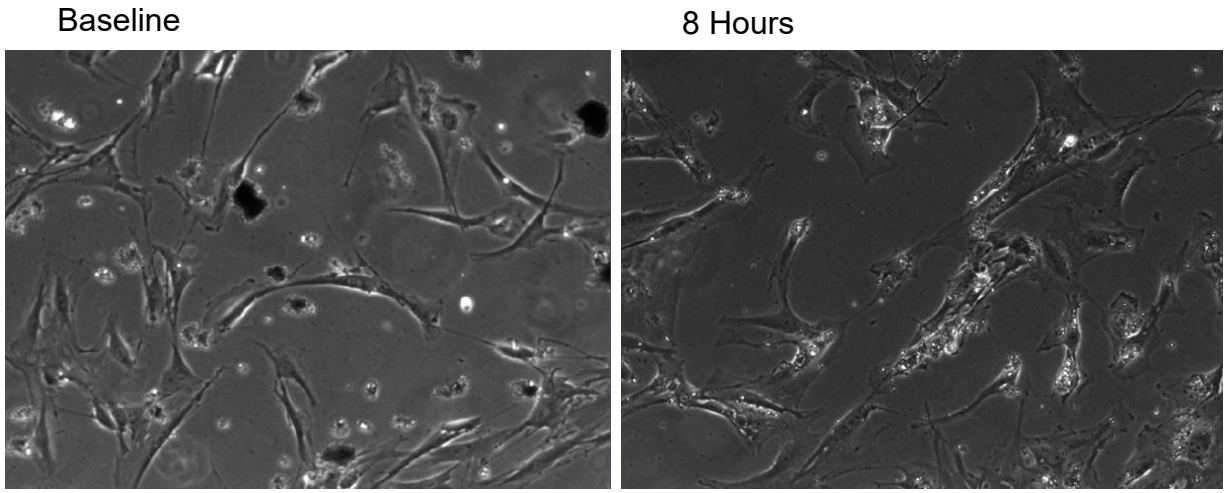

Figure 47 Representative image of valvular interstitial cells phagocytosing cholesterol crystals

VICs were treated with CC. 8 hours post treatment, CC could be observed being ingested by cells and ordered within the cell.

CC= Cholesterol crystals; VICs= Valvular interstitial cells

After the addition of CD into the medium, a dissolution of the CC was observed (Figure 48).

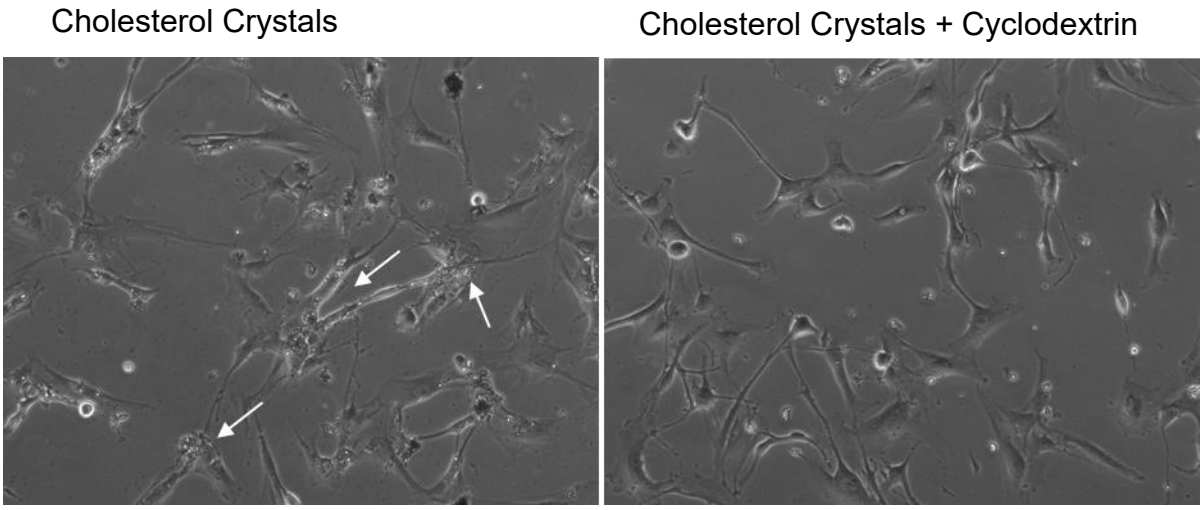

Figure 48 Valvular interstitial cells were treated with cholesterol crystals

VICs were treated with CC and CD. 8 hours post treatment, CC were mainly dissolved. CC= Cholesterol crystals; CD= Cyclodextrin; VICs= Valvular interstitial cells

3.9 Cholesterol crystals in valvular interstitial cells

As calcification is one of the key mechanisms for AS, this study aimed to investigate the role of CC as well as CD in this process. VICs were treated with both CC and CD and calcification was induced by changing the medium for 7 days. With regard to the osteogenic markers *RUNX2* and *BMP2,* changing the medium to PCM resulted in an overall higher gene expression of these 2 genes. However, no significant difference within the treatment was observed. For *BMP2* in BM, CC treatment resulted in an increased gene expression compared to the other conditions, whereas for *BMP2* in PCM, CD treatment caused an increased but not significant gene expression compared to untreated control cells, or CC treated cells. Regarding pro-inflammatory markers, CC treatment resulted in an elevated *IL1β* gene expression in BM whereas it increased in PCM after adding CD (Figure 49).

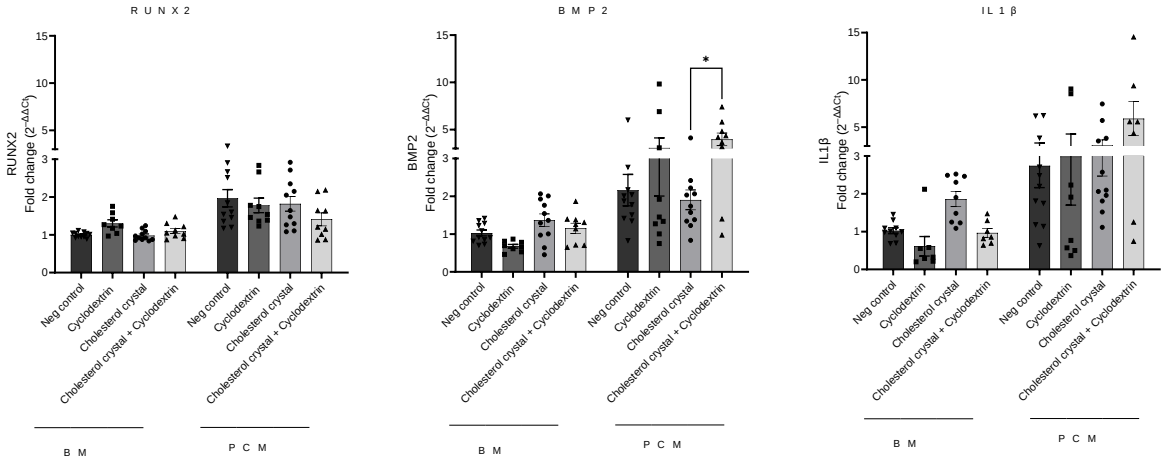

Figure 49 Gene expression in cholesterol crystals cyclodextrin treated valvular interstitial cells

*CC and CD were added to the cells and calcification was induced by changing the medium to PCM. 7 days after calcification induction, RNA was isolated and qPCR was performed. The relative levels of target gene expression were calculated by the Comparative Ct Method (ΔΔCt Method). 2-way ANOVA test with Tukey's post test for multiple comparisons was used to test the statistical significance of qPCR data. Bars displayed the fold change of gene expression normalized by neg control in BM ± SEM; n=3; *p< 0.05*

BM= Basal medium; BMP2= Bone morphogenetic protein 2; RUNX2= Runt-related transcription factor 2; IL1β= Interleukin 1 beta; PCM= Pro-calcifying medium

3.10 Cholesterol crystals in valvular endothelial cells

Another key mechanism in the development of AS is EndMT. In order to investigate CC in this process, CC were added to the cells for 7 hours. Gene expression of endothelial markers showed a slightly decreased expression after the addition of CC to the cells. *VCAM1* was upregulated in CC-treated cells compared to untreated cells. Inflammatory marker *IL6* showed no difference, whereas *IL1β* gene expression was upregulated in cells that were treated with CC in comparison to control cells (Figure 50 A).

VECs were stained with anti VCAM1 7 hours after CC treatment. VCAM1 expression seemed to be higher in CC treated cells compared to control cells, although VCAM1 expression could be observed in these cells as well (Figure 50 B).

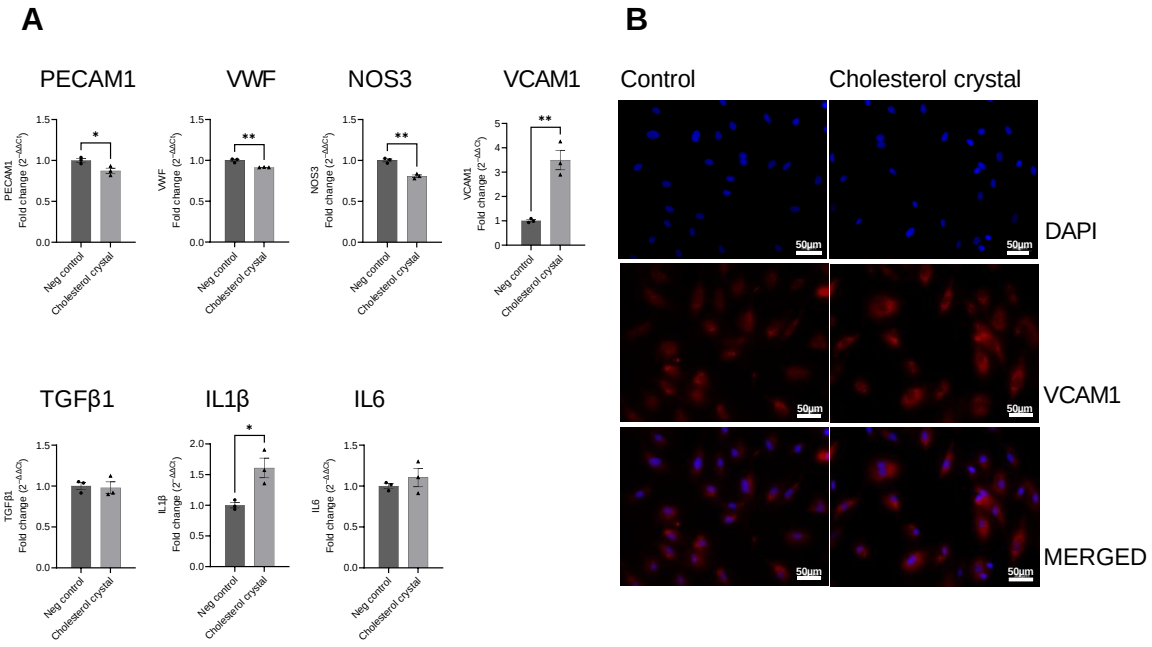

Figure 50 Gene expression and immunofluorescence in cholesterol crystals treated valvular endothelial cells

VECs were harvested 7 hours after treatment with CC. ***A:*** *RNA was isolated RNA was isolated and qPCR was performed. The relative levels of target gene expression were calculated by the Comparative Ct Method (ΔΔCt Method). Student´s t-test was used to test the statistical significance of qPCR data. Bars displayed the fold change of gene expression normalized by neg control ± SEM. n=1; *p< 0.05, **p< 0.005.* ***B****: VCAM1 expression in VECs treated with CC compared to untreated control cells.*

CC= Cholesterol crystals; VCAM1= Vascular cell adhesion protein 1; VEC=Valvular endothelial cells; IL= Interleukin; NOS3= Nitric oxide synthase 3; PECAM1= Platelet endothelial cell Adhesion molecule-1; VWF= Von Willebrand factor; TGFβ1= Transforming growth factor-beta 1

After 7 hours of treatment with CC, the medium was changed to EndMT medium and CD was added. After 5 days, RNA was isolated and EndMT as well as proinflammatory markers were measured. Regarding endothelial markers, *PECAM1* as well as *VWF* gene expression were upregulated in CC treated cells compared to the other conditions and control cells. No significant difference was observed after the addition of CD compared to neg control. *TAGLN* as a mesenchymal marker showed an upregulated gene expression in CD treated cells. CC treatment resulted in a downregulated expression of *TAGLN*. *ACTA2* showed no difference between the treatments whereas *VCAM1* was upregulated by CD treatment. Thus, the addition of CD led to an upregulation of mesenchymal markers. Regarding inflammatory markers, *IL1β* revealed a similar gene expression as *TAGLN* and CD treatment resulted in an upregulated mRNA level. There was no difference in *IL6* expression (Figure 51).

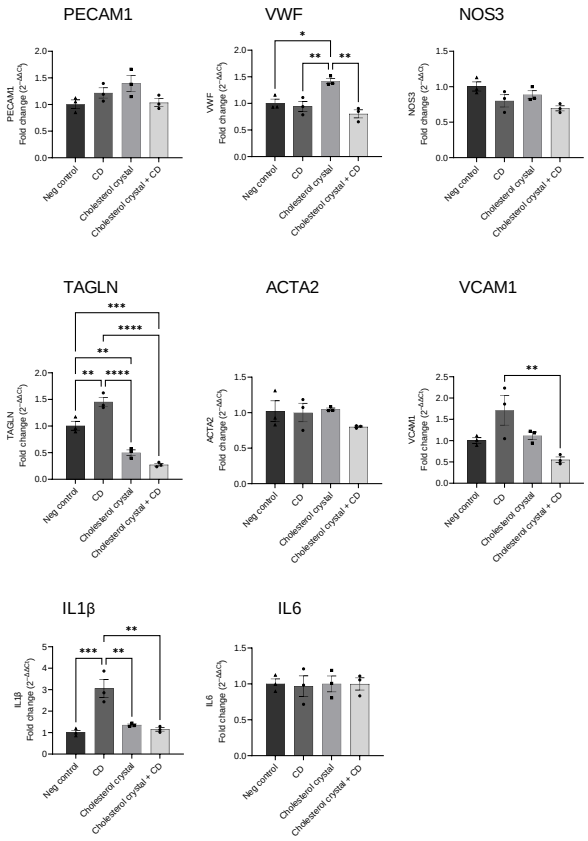

Figure 51 Gene expression in valvular endothelial cells after treatment with CC and CD

*After 7 hours of incubation with CC, Medium was changed into EndMT medium supplemented with CD, or vehicle for control. After 5 days, RNA was isolated and qPCR was performed. The relative levels of target gene expression were calculated by the Comparative Ct Method (ΔΔCt Method). One-way ANOVA test with Tukey's post test for multiple comparisons was used to test the statistical significance of qPCR data. Bars displayed the fold change of gene expression normalized by unstimulated neg control ± SEM. n=1; *p< 0.05, **p< 0.005, ***p< 0.0005, ****p< 0.00005*

CC= Cholesterol crystals; CD= Cyclodextrin; VECs= Valvular endothelial cells; ACTA2= Smooth muscle alpha-2 actin; EndMT= Endothelial to mesenchymal transition; NOS3= Nitric oxide synthase 3; PECAM1= Platelet endothelial cell adhesion molecule-1; TAGLN= Transgelin; VCAM1= Vascular cell adhesion molecule 1; VWF= Von Willebrand factor

To study the process of EndMT in VECs that were treated with CC and subsequently with CD the EndMT medium was supplemented with TGFβ1+IL1β and TNFα. First, the process of EndMT was partially confirmed: *NOS3* as an endothelial marker showed a downregulated expression in TGFβ1+IL1β and TNFα condition compared to unstimulated cells. *PECAM1* and *VWF* showed an upregulated gene expression in TGFβ1+IL1β stimulated cells. For *VWF*, TNFα stimulated VECS did show an EndMT effect and its gene expression was downregulated compared to unstimulated control cells. Regarding mesenchymal markers, the stimulation with

TGFβ1+IL1β demonstrated an EndMT effect as *TAGLN*, *ACTA2*, and *VCAM1* demonstrated an upregulated gene expression. After TNFα stimulation, only *ACTA2* and *VCAM1* were upregulated suggesting a successful EndMT induction, whereas *TAGLN* mRNA level was downregulated compared to unstimulated cells (Figure 52).

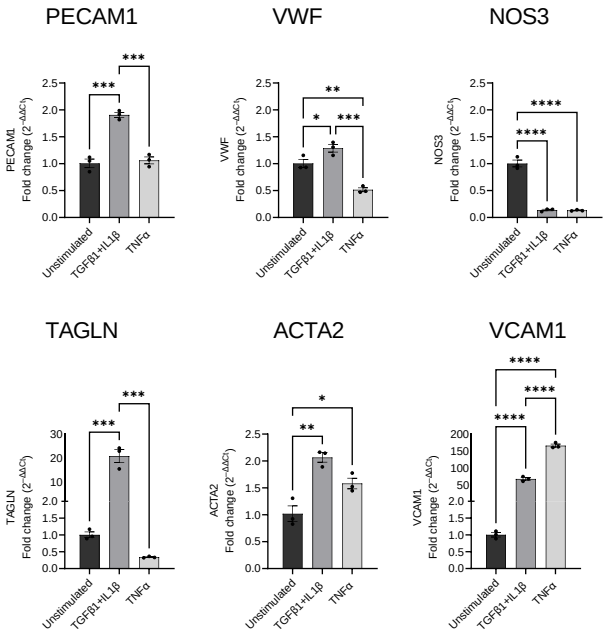

Figure 52 Endothelial to mesenchymal transition induction in valvular endothelial cells

*VECs were stimulated with TGFβ1+IL1β, or TNFα, to induce EndMT, or left unstimulated. After 5 days, RNA was isolated and qPCR was performed. The relative levels of target gene expression were calculated by the Comparative Ct Method (ΔΔCt Method). One-way ANOVA test with Tukey's post test for multiple comparisons was used to test the statistical significance of qPCR data. Bars displayed the fold change of gene expression normalized by unstimulated control ± SEM. n=1; *p< 0.05, **p< 0.005, ***p< 0.0005, ****p< 0.00005*

EndMT= Endothelial to mesenchymal transition; TGFβ1= Transforming growth factor-beta 1; TNFα= Tumor necrosis factor-alpha; VECs= Valvular endothelial cells; ACTA2= Smooth muscle alpha-2 actin; NOS3= Nitric oxide synthase 3; PECAM1= Platelet endothelial cell adhesion molecule-1; TAGLN= Transgelin; VCAM1= Vascular cell adhesion molecule 1; VWF= Von Willebrand factor

The next graph shows qPCR data of CC and CD treated cells in EndMT medium supplemented with TGFβ1+IL1β. *PECAM1* and *VWF* revealed a similar pattern and CD treatment resulted in a downregulated gene expression compared to CC treated and untreated control cells. *NOS3* gene expression showed an upregulated gene expression in cells that were treated with both CC and CD. The mesenchymal markers *TAGLN, ACTA2,* and *VCAM1* demonstrated a decreased mRNA level after CC+CD treatment compared to untreated control cells. The CD single

treatment resulted in a downregulated *ACTA2* and *VCAM1* gene expression. Treatment with CC did not show significant effects but resulted in a decreased *VCAM1* gene expression (Figure 53).

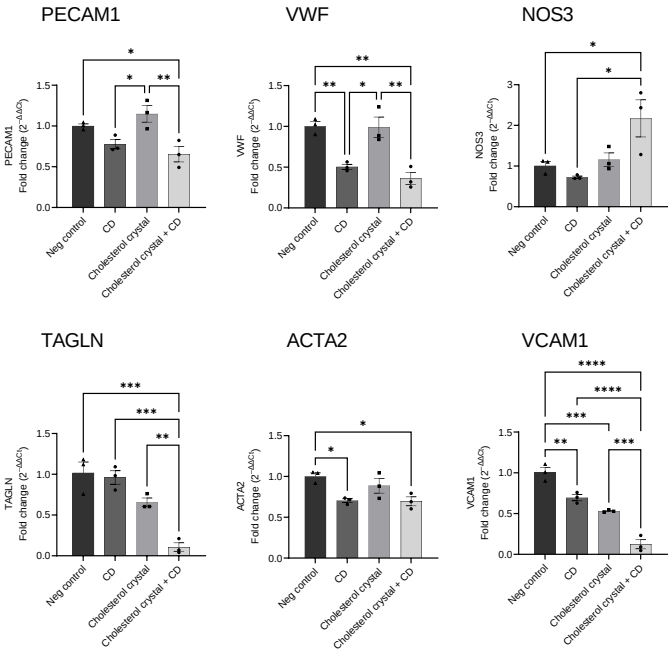

Figure 53 Gene expression in valvular endothelial cells after treatment with CC and CD and stimulation with TGFβ1+IL1β

*VECs were treated with CC for 7 hours. Afterwards, medium was changed to EndMT medium supplemented with TGFβ1+IL1β. In addition, the medium was supplemented with CD. After 5 days, RNA was isolated and qPCR was performed. The relative levels of target gene expression were calculated by the Comparative Ct Method (ΔΔCt Method). One-way ANOVA test with Tukey's post test for multiple comparisons was used to test the statistical significance of qPCR data. Bars displayed the fold change of gene expression normalized by neg control ± SEM. n=1; *p< 0.05, **p< 0.005, ***p< 0.0005, ****p< 0.00005*

CC= Cholesterol crystals; CD= Cyclodextrin; EndMT= Endothelial to mesenchymal transition; TGFβ1= Transforming growth factor-beta 1; VECs= Valvular endothelial cells; ACTA2= Smooth muscle alpha-2 actin; NOS3= Nitric oxide synthase 3; PECAM1= Platelet endothelial cell adhesion molecule-1; TAGLN= Transgelin; VCAM1= Vascular cell adhesion molecule 1; VWF= Von Willebrand factor

After stimulation with TNFα, a similar gene expression pattern was shown in comparison to cells after stimulation with TGFβ1+IL1β (Figure 54 compared to Figure 53). CD treatment resulted in a downregulation of *PECAM1* and *VWF*. The treatment with CC did not result in any significant difference in the expression of endothelial markers compared to the untreated cells. *NOS3* gene expression was upregulated in CC- and CC+CD-treated cells. *ACTA2* showed no difference between the treatments after TNFα stimulation. CC treatment resulted in downregulated *TAGLN* expression, whereas single treatment with CD did not change anything.

VCAM1 was downregulated after CD and showed a slight, but not significant downregulation after CC treatment, compared to untreated control cells (Figure 54).

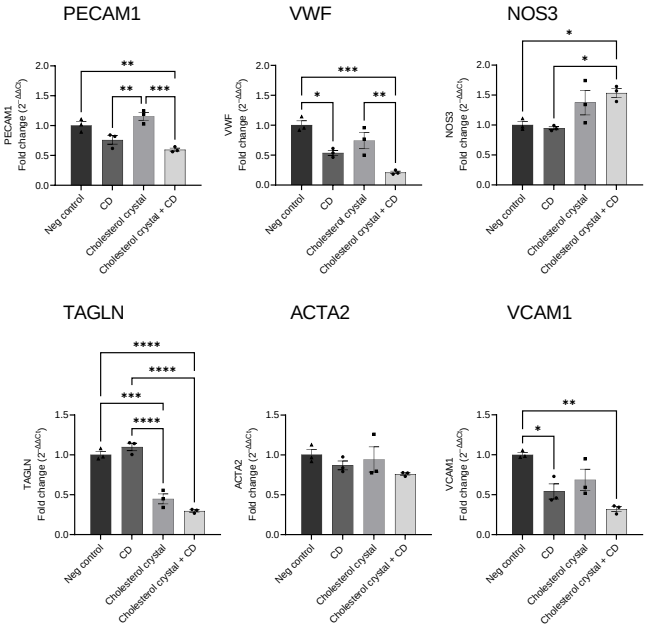

Figure 54 Gene expression in valvular endothelial cells after treatment with CC and CD and stimulation with TNFα

*VECs were treated with CC for 7 hours. Afterwards, the medium was changed to EndMT medium supplemented with TNFα. In addition, the medium was supplemented with CD. After 5 days, RNA was isolated and qPCR was performed. The relative levels of target gene expression were calculated by the Comparative Ct Method (ΔΔCt Method). One-way ANOVA test with Tukey's post test for multiple comparisons was used to test the statistical significance of qPCR data. Bars displayed the fold change of gene expression normalized by neg control ± SEM.n=1; *p< 0.05, **p< 0.005, ***p< 0.0005, ****p< 0.00005*

CC= Cholesterol crystals; CD= Cyclodextrin; EndMT= Endothelial to mesenchymal transition; TNFα= Tumor necrosis factor-alpha VECs= Valvular endothelial Cells, ACTA2= Smooth muscle alpha-2 actin; NOS3= Nitric oxide synthase 3; PECAM1= Platelet endothelial cell adhesion molecule-1; TAGLN= Transgelin; VCAM1= Vascular cell adhesion molecule 1; VWF= Von Willebrand factor

These initial results did not yield substantial information and thus require verification and expansion through additional experiments to obtain more conclusive findings about CC and CD in the process of EndMT and with that, in the development of AS.

4. Discussion

Patients with symptomatic AS usually exhibit symptoms such as breathlessness, dizziness, and angina pectoris, and their overall exercise tolerance is reduced. The diagnosis of AS typically begins with a physical examination if there are indications of the condition. One possible indicator is the presence of a typical systolic murmur. The primary test used for diagnosis is echocardiography (Otto et al 2021). Once AS has been diagnosed, patients need to monitor their condition with regular tests and attend scheduled medical visits. They may also require making lifestyle modifications or using medication to treat other cardiovascular symptoms until valve replacement is recommended. The disease process is individual for each patient and can take several years. However, the process can accelerate, and waiting too long can lead to irreversible heart damage and death. AS is perhaps associated with age, gender, lifestyle factors such as smoking, alcohol consumption, and diet, as well as damage from infections and chronic illnesses. It is a degenerative disease with a low survival rate, if untreated. Approximately 25% of people by the age of 65 have a thickened aortic valve and 3% over the age of 75 have severe AS (Stewart et al. 1997; Lindroos et al. 1993; Chambers 2009; Lee and Choi 2016). The prevalence of heart disease, particularly AS, is increasing due to modern lifestyles and dietary patterns. Unfortunately, the only treatment currently available for AS is valve replacement. In this area, treatment options have improved in recent years with the development of TAVR and minimal invasive surgery. However, although TAVR is a low risk procedure and an essential treatment for AS, CAVD rates are projected to rise 240% worldwide by 2040 and the TAVR treatment will not be able to cover all the cases (Blaser et al. 2021; Danielsen et al. 2014). Therefore, it is crucial to understand the pathomechanisms of such a disease in order to find medical treatment and perhaps prevent the development of AS. The most common causes of AS are CAVD of tricuspid or bicuspid valve and rheumatic heart disease. Rare causes include for instance homozygous familial hypercholesterolemia, congenital heart disease (except bicuspid aortic valve), chest irradiation, rheumatic heart disease, and renal failure (Kurtz and Otto 2010). In recent years, there have been promising trials of statin therapy to slow down the progression of AS (Moura et al. 2007; Rosenhek et al. 2004; Lee and Choi 2016). However, these trials showed negative results and such treatment cannot be applied to every individual (Rossebø et al. 2008; Cowell et al. 2005; Lee and Choi 2016).

4.1 *In vitro* experiments

Our laboratory purchased valve cells from the company Lonza. These cells were isolated from healthy aortic valves using highly standardized and optimized techniques, resulting in high

levels of purity. The sex of the cells was critical because only female cells were examined in this study. Regarding aortic valve calcification in terms of sex, it has been shown that men develop more calcification than women (Saeed et al. 2020). Saeed and colleagues called in their review for sex-specific drugs because of differences in valve pathology and parameters that appeared to be sex-specific (Saeed et al. 2020). Therefore, experiments in male cells would be required to confirm the results shown in this study and may show a different or greater effect on calcification.

Another limitation of the *in vitro* experiments is the medical history of the cell donors. The cells were highly aberrant, due to their high heterogeneity, putative external factors, and other diseases that may influence the progression of AS. Regarding the disease progression, which is linked to several other diseases, such as kidney disease, rheumatic fever, and inflammation, as well as oscillatory stress and environmental factors, *in vitro* experiments do not take all these factors into account, but focus on one parameter or even a single gene. In addition, in cell culture experiments, cells are grown in a plastic dish that is not comparable to their real environment. Cell-cell communication with other cell types via cytokines and chemokines for signaling is very important for certain cell types, such as ECs. This communication is also missing in such cell culture experiments. Still, *in vitro* experiments give a first idea of a specific target and can investigate if specific signaling pathways are involved in certain aspects of disease development. These findings must be confirmed in other more complex systems. For this, animal models are used such as the mouse.

4.1.1 Endothelial to mesenchymal transition

Recent studies have provided evidence that ECs undergo a transition towards mesenchymal cells during EndMT. These mesenchymal cells include chondrogenic and osteogenic cells, which are crucial in the development of CVD and atherosclerosis. With regard to the process of EndMT in VECs, which may be important for the development of AS, this work demonstrated the establishment of an EndMT protocol in VECs. Therefore, several stimuli, including BMPs, TGFβ1, Il1β, and TNFα were tested based on previous publications (Figures 61, 62, 63 in chapter 6.1). While BMP signaling has been shown to induce EndMT (Medici et al. 2010; Yao et al. 2013; Yao et al. 2021), this study provided evidence that VECs undergo EndMT when stimulated with a combination of TGFβ1+Il1β, as well as TNFα as a single stimulant. TGFβ is considered to be a main driver of EndMT. TGFβ is also a critical factor in many cellular processes, for instance, cell proliferation, apoptosis, differentiation, autophagy, and the immune response (Meng et al. 2016; Böttinger and Bitzer 2002). Thus, global inhibition of TGFβ would

have too many side effects in a whole living system. Aside from the disturbed signaling homeostasis, it might be interesting to investigate TGFβ and its downstream targets in specific cell types.

4.2 The role of the innate immune system and its pattern recognition receptors in the development of aortic valve stenosis

Previous studies have shown that the immune system is crucial in AS and more studies have focused on investigating the connection between inflammation and valvular calcification (Aikawa and Otto 2012; New and Aikawa 2011).

Therefore, the aim of this research project was to investigate the potential role of TLR3 as an important member of the PRR family and part of the innate immune system. Further, we wanted to develop an understanding of the process of EndMT and calcification.

TLRs are transmembrane signaling receptors containing an extracellular domain with a conserved structure for ligand recognition at the N- terminus and for intracellular signaling at the C-terminus (Takeuchi and Akira 2010; Akira and Takeda 2004; Kaisho and Akira 2006). TLR3 is localized in the endosomal compartment and recognizes intracellular patterns such as viral-derived molecules and host nucleic acids (García-Rodríguez et al. 2018). Compared to the other members of the TLR family, TLR3 only uses the adaptor protein TRIF for its downstream signaling. It was found that a synthetic analog of dsRNA termed PolyIC is able to activate the TLR3-TRIF-NF-κB pathway in human VICs and, thereby, upregulating inflammatory mediators (Zhan et al. 2017). As mentioned in the introduction, Zhan and colleagues demonstrated PolyIC mediated upregulation of calcification markers and showed calcium deposit formation by human VICs. Thus, PolyIC promotes a pro-osteogenic effect by activating TLR3 mediated NF-κB pathway (Zhan et al. 2017; Zhan et al. 2015).

In our study, TLR3 expression in the human aortic valve could be confirmed by immunofluorescence staining (Figure 15). Further, TLR3 gene expression was slightly higher in aortic valve tissue of AS patients, compared to patients with AR (Figure 15).

4.2.1 Pattern recognition receptors

In cooperation with Project A03 from TRR259 (PhD student Madeleine Graef, research group of Prof. Gunther Hartmann; Institut für Klinische Chemie und Klinische Pharmakologie, Universitätsklinikum Bonn), various PRRs were stimulated in VICs and their expression profiles examined. Furthermore, these collaborative experiments provided an overview of PRRs and their potential role in calcification. Interestingly, TLR2 and TLR4 seemed to play a role in

calcification in VICs (Yang et al. 2009). Yang and colleagues reported a higher gene expression of *TLR2* and *TLR4* in aortic VICs compared to pulmonary VICs (Yang et al. 2009). At the same time, they demonstrated a correlation between higher TLR2 and TLR4 levels in aortic VICs and increased *BMP2* expression. Upon TLR2 and TLR4 inhibition they could reveal a reduced gene expression of the osteogenic markers. Overall, they concluded that the innate immune system plays a crucial role in aortic valve calcification and thus in AS (Yang et al. 2009). Our study also revealed elevated *BMP2* and *RUNX2* gene expression after incubation of VICs with TLR2 and TLR4 agonists (Figure 16). Therefore, it might be interesting to consider these receptors in future experiments to holistically study the underlying mechanisms in the development of aortic disease.

Next, in figure 17 of this study, it was shown that cGAS influenced VIC calcification. qPCR results did not only present higher *IL6* gene expression but also *BMP2* expression was elevated after stimulation (Figure 17). This is consistent with recent literature showing that the cGAS-STING pathway may also play an important role in CVD and metabolic disorders. Oduro and colleagues mentioned that this pathway is crucial in several heart diseases, such as chronic sterile inflammation, fibrosis, cardiac remodeling, aortic degeneration, left ventricular dysfunction, coagulation, impaired endothelial function, senescence and lytic cell death (Oduro et al. 2022). cGAS and STING are both cytosolic receptors and belong to the PRR of the innate immune system. The cGAS-STING pathway recognizes dsDNA and is important for defense against viruses, mycobacteria and intracellular parasites. Upon recognition of dsDNA, cGAS dimerizes to form cyclic GMP-AMP (cGAMP), which binds to STING. Activation of STING triggers phosphorylation of the TF IRF3, which in turn enters the nucleus and binds to its specific promoter for inflammatory genes such as IFNβ (Nakhaei et al. 2010). Oduro addresses other publications and explains that a continuous active cGAS-STING pathway via IRF3 as well as IFN-I signaling is involved in CVD and metabolic diseases. Still, this raises questions about the signaling, other cofactors, and IFN type I affecting cardiovascular and metabolic health which is still unknown. In conclusion, this pathway might be an important factor in CVD and can lead to further interesting results.

TLR9 was also examined in this study. Its activation exhibited a notable upregulation in the gene expression levels of the osteogenic markers, such as *BMP2* and *RUNX2*, alongside the pro-inflammatory marker *IL6* (Figure 17). TLR9 is a DNA sensing receptor and is located in intracellular compartments. In its immature condition, TLR9 is located in the endoplasmic reticulum or the Golgi apparatus and is transferred via a facilitator protein toward cell surface. At the cell surface, it is associated with an adaptor protein for delivery to the endosome

(Martínez-García et al. 2018). TLR9 activates NF-κB and/or IRF7 nuclear translocation and thereby the production of cytokines and IFN type I (Amadio et al. 2021). It is possible to assume that these two signaling pathways may connect in phagocytes. Amadio and colleagues called this phenomenon "cross-sensing" (Amadio et al. 2021). Perhaps these receptors are also connected in their response regarding CVD.

Another cross-sensing might exist between RIG-I, MDA5, and TLR3. Both RIG-I and MDA5 are RLRs and are cytosolic nucleic acid sensors (Jabłońska et al. 2018). RIG-I and MDA5 recognize viral ssRNA and dsRNA. Activated MDA5 and RIG-I results in type I IFN and pro-inflammatory cytokine production via IRF 3 and 7, and NF-κB signaling (Loo and Gale 2011). TLR3 also recognizes dsRNA (Takeda and Akira 2015). Still, it is assumed, that RIG-I mostly only detects viral genomes in the aortic wall. However, TLR3, on the contrary, is also activated by a non-viral mechanism, such as self-RNA from damaged or necrotic tissue (Jabłońska et al. 2018). It could be shown that both RIG-I and TLR3 are important regarding aortic diseases. The aim of this study was to investigate the role of TLR3. Thus, given that these 3 receptors detect dsRNA and might be linked in their sensing, this study provides qPCR measurements of all 3 receptors when activating TLR3.

4.2.2 TLR3 in valvular interstitial cells

Valvular calcification is crucial in the process of AS development and a major factor contributing to valve stiffness. After valve replacement, the majority of patients showed dystrophic calcification, which occurs for instance, after tissue damage. Other, but less frequent cases, displayed lamellar or endochondral bone tissue, resulting in increased collagen remodeling (Freeman and Otto 2005). Calcium deposits accumulated in the aortic valves cause them to narrow and thereby, restrict the blood flow. To test whether TLR3 has an effect on calcification in VICs, cells were treated with PolyIC. On the other hand, a TLR3 knockdown was performed using siRNA. PolyIC treatment gave rise to an upregulation of *TLR3* in those cells compared to untreated control cells. This response could be blunted with the knockdown of the gene. Interestingly, the scrambled siRNA used as transfection control, also resulted in an upregulated *TLR3* gene expression, as the siRNA is a 21 base pair long dsRNA with 2 nucleotide single stranded overhangs. This allows it to activate the receptor (Pirher et al. 2017; Kleinman et al. 2008; Cho et al. 2009). Thus, all data points were compared to untreated control cells (neg control). Osteogenic markers *BMP2* and *RUNX2* as well as pro-inflammatory marker *IL6* revealed a similar pattern: PolyIC treatment led to an upregulated gene expression, whereas siRNA-mediated knockdown resulted in a downregulation (Figure 20). Furthermore, PolyIC

treatment also enhanced *DDX58* (RIG-I) as well as *IFIH1* (MDA5) gene expression that was blunted by TLR3 siRNA (Figure 20). This observation indicated that PRR signaling may contribute to increased levels of osteogenic markers *RUNX2* and *BMP2* in humans. However, the results of the TLR3 siRNA transfection pointed to an independent role of TLR3 regarding to calcification in VICs.

In another experiment, TLR3 was pharmacologically inhibited by a small molecule called C4a (Cheng et al. 2011). Indeed, PolyIC treatment resulted in an upregulation of *TLR3* gene expression that could be blunted by adding C4a. Moreover, a similar pattern could be observed regarding pro-inflammatory markers as well as osteogenic markers (Figure 21). This result confirmed a TLR3 specific response. Alizarin Red S also confirmed these results and showed increased calcification in PolyIC treated and untreated cells compared to C4a treatment (Figure 22). Regarding cell viability, treating cells with PolyIC resulted in reduced viability compared to neg controls while C4a treatment did not affect naive cell viability. Caspase 3/7 activity was decreased after 7 days indicating that the cells recovered from initial PolyIC treatment. Concurrent with *TLR3* gene expression, *DDX58* (RIG-I) and *IFIH1* (MDA5) showed increased mRNA levels upon PolyIC and PolyIC+C4a treatment in VICs, compared to untreated control cells revealed that PolyIC treatment activated those receptors (Figure 21).

4.2.3 TLR3 in valvular endothelial cells

The endothelium has a crucial part in the inflammation of the vascular system and further, of the aorta and aortic valves. Especially, endothelial shear stress and blood flow affect the aortic valves and the wall leading to a secretion of cytokines and adhesion molecules by ECs that results in EndMT/EMT as well as recruitment and infiltration of immune cells. In order to get an idea of the role of PRRs in the process of EndMT, we considered the role of TLR3 in VECs and performed a TLR3 knockdown compared to treatment with PolyIC as well as control cells. PolyIC treatment resulted in downregulation of endothelial markers, whereas mesenchymal markers showed an upregulated gene expression (Figure 26) On the other hand, TLR3 knockdown resulted in increased endothelial marker gene expression whereas mesenchymal markers, except for ACTA2, showed a lower expression in PolyIC-treated VECs. In conclusion, TLR3 signaling affects EndMT (Figure 26).

In the next experimental approach, TLR3 was treated with PolyIC, C4a, or PolyIC+C4a in order to activate and inhibit the functioning of this receptor. First, only the effect of the treatments was analyzed after selected time points. This suggested a time-dependent outcome: Not only

TLR3 gene expression increased within the first 48 hours and decreased after 72 hours up to 5 days but also PolyIC treatment gave rise to a downregulation of endothelial markers in the first 2 days. After 72 hours, though, it seemed that cells gained back their endothelial phenotype. A concomitant result could be found in the gene expression of the mesenchymal marker *VCAM1* which was upregulated after PolyIC treatment but went down after 5 days. *ACTA2* and *TAGLN* both did not show significant differences with respect to EndMT induction with PolyIC treatment (Figure 29). Regarding the cell morphology, PolyIC treatment resulted in a change of cell shape in comparison to control cells and VECs seemed to differentiate into mesenchymal cells. In conclusion, this study showed a first impression of TLR3 inducing EndMT.

This study demonstrated the effective initiation of EndMT in VECs through the application of TGFβ1+IL1β and TNFα. Consequently, in the subsequent stage of the experiment, the induction of EndMT was employed using these stimulations after PolyIC/C4a treatment, to explore the involvement of TLR3 following the induction of EndMT.

In terms of TGFβ1+IL1β stimulation 24 hours after PolyIC treatment, we could see an effect in the gene expression of endothelial markers. All 3 markers were downregulated compared to untreated neg control cells within 7 days after PolyIC/C4a treatment. Still, no effect could be shown in mesenchymal markers except for *VCAM1* gene expression, after 48 hours (Figure 34). In case of TNFα stimulation 24 hours after PolyIC treatment, we observed again a time-dependent result: After 5 days, endothelial markers were upregulated again. No noteworthy effects could be explored regarding mesenchymal markers after treatment and TNFα stimulation (Figure 36).

In conclusion, TLR3 influenced EndMT, since TLR3 mRNA levels were highly upregulated immediately after treatment. This resulted in a downregulation of endothelial- and elevated mesenchymal markers. In turn, a decreased TLR3 gene expression 72 hours and 5 days after treatment again showed upregulated endothelial mRNA levels, and mesenchymal markers showed decreased gene expression. Thus, it seemed that VEC-derived mesenchymal-like cells were able to regain their endothelial phenotype. Recent studies could confirm this reverse transition of mesenchymal-like cells back to endothelial function, which in turn could prevent or reduce vascular calcification (Yao et al. 2021). In their research, osteoblasts lost osteogenic capacity in bone formation while cells enhanced their integration into vascular endothelium structure. Nevertheless, after regaining endothelial function, the gene expression profiles of ECs compared to those osteoblast-like derived ECs did not match (Yao et al. 2021). From this, it can be concluded that the transition of these cell fates was not complete. Based on this study and the result described above, further questions emerge to investigate how to guide the EndMT and

the process of cells regaining back the endothelial phenotype after TLR3 activation as well as inhibition.

Nevertheless, the mesenchymal marker *VCAM1* showed an upregulation in the mRNA level after treatment. Other mesenchymal markers that were measured in this study include *TAGLN* and *ACTA2*. *TAGLN* is mainly expressed in SMCs (Tsuji-Tamura et al. 2021). *ACTA2* is also expressed in SMCs, but it is also used as a marker for myofibroblast formation (Shinde et al. 2017). As there was no significant result in *TAGLN* and *ACTA2* gene expression in VECs treated with PolyIC/C4a and stimulated with TGFβ1+IL1β/TNFα but *VCAM1* mRNA level was upregulated, this study aimed to address the following research questions: How is VCAM1 linked to PolyIC induced EndMT and is TLR3 involved in this? VCAM1 belongs to the immunoglobulin superfamily in the peripheral blood and is a crucial mediator of vascular endothelial inflammation. It is expressed in SMCs and is a biomarker for vascular endothelial inflammatory damage (Braun et al. 1999; Hastings et al. 2009; Troncoso et al. 2021; Su et al. 2022). Thus, it could be an important factor to understand the underlying effects.

In order to gain more information on the role of TLR3 and the cross-sensing between TLR3, MDA5, and RIG-I, the gene expression of *DDX58* (RIG-I) and *IFIH1* (MDA5) was measured parallel to *TLR3* after PolyIC/C4a treatment. Indeed, *DDX58* (RIG-I) and *IFIH1* (MDA5) mRNA levels increased upon PolyIC treatment and were downregulated when adding C4a, similar to *TLR3* gene expression. Further experiments are needed to fully understand the underlying mechanisms and putative linked signaling pathways.

Another important field in regard to VECs in AS is to investigate the above-mentioned shear stress. ECs are exposed to different blood flow conditions, oxygen tension, or cyclic stretch that can influence intracellular signaling (Aman et al. 2016) for instance secretion of cytokines, and thereby, recruiting immune cells that are able to infiltrate the endothelium. Within the progress of aortic valve calcification, the valve becomes narrowed, the flow pattern undergoes a transition to a more turbulent phenotype characterized by elevated pressure gradients. The presence of turbulent oscillatory flow promotes endothelial dysfunction, facilitates the development of atherosclerotic lesions, and triggers the process of EndMT. Consequently, this can lead to increased immune cell infiltration and lipid deposition, creating a detrimental cycle characterized by enhanced calcification and increased turbulent flow. In this study, we performed *in vitro* experiments on a normal well plate without exposing the cells to shear stress or other forces. Thus, this study is limited to resting TLR3 mediated signaling with TNFα and

TGFβ1/IL1β stimulation and it notes the importance of investigating the impact of shear stress in the field of aortic diseases.

4.3 *In vivo* experiments

For *in vivo* experiments, AS was triggered by wire-induced aortic valve injury (Niepmann et al. 2019). This method gives an idea of AS in a whole living system and allows the analysis of several parameters. During the procedure, a wire is advanced into the apex of the left ventricle and retracted ten times, followed by 200 rotations. AS can be induced in any mouse without the need for genetic modification or a special diet. However, AS is induced by surgery and it should be noted that AS is usually a progressive disease that develops gradually over a period of years and is not caused by a single injury. What also plays a critical role in AS development are external factors, such as bicuspids, kidney diseases, and other heart diseases and lifestyle in general that was not considered in the present *in vivo* experiments.

Limitations within staining methods, such as von Kossa staining, need to be considered. Calcification was visually observed in unstained microscopic images of VICs. Similarly, in histological samples of murine aortic valves, the presence of dark particulate material, either pigmented cells or a calcification pattern, was evident in unstained, HE-stained, and von Kossa-stained microscopic images. However, it should be noted that the pigmented cells observed in these images could potentially be associated with the von Kossa staining used to detect calcification. Therefore, it is important to consider that such pigmented cells could lead to false positive results in the analysis of calcification using von Kossa staining. Previously published data have also addressed the issue of potential false impressions in the detection of calcification. This procedure proved effective in identifying patterns of dark particulate staining, which could indicate the presence of valve calcification or simply pigmented cells (Hinton et al. 2008; Mjaatvedt et al. 2005). Hinton and colleagues reported about the “false impression that calcification is present” (Hinton et al. 2008). They also detected these black particulate deposits and concluded, that Alizarin Red S might be the better method to detect calcification. This staining technique uses a dye that binds to calcium deposits, whereas the von Kossa staining method uses a silver nitrate solution that reacts with the calcium phosphate (Puchtler et al. 1969). Still, in our experiments, Alizarin Red staining also revealed the presence of dark particles in the same locations as observed in the unstained and HE-stained samples, creating the appearance of a potential false positive result. Further investigation and validation through additional staining techniques or analyses would be necessary to clarify the nature of these particles and confirm the presence of calcification. But such pigmented cells were shown on all aortic valve

cusps, so we can conclude this as a constant limitation that must be considered when interpreting the data. Another putative means for detecting calcification is osteosense staining. It is a fluorescent dye that binds to hydroxyapatite formed during mineralization.

4.3.1 TLR3 in mice

In this study, we used WT and knockout mice with C57/BL6-J background. Thereby, these *in vivo* experiments showed the exogenous activation and inhibition of TLR3 with PolyIC and C4a, respectively. Furthermore, a global TLR3 knockout was used in order to investigate the role of TLR3 in the progression of AS.

To activate TLR3, WT mice were treated daily with PolyIC over a period of 6 weeks after surgery. Control animals were injected with NaCl. According to the ultrasound examinations, that were performed by Dr. Sven Niepmann, after 2, 4, and 6 weeks, we could observe a higher trans-aortic-valve peak velocity, as well as mean pressure gradient over the aortic valve in PolyIC-treated mice, compared to control mice (Figure 37). According to histological analysis, that considered the measurement of the valve area (HE), immune cell infiltration (CD68), calcification (von Kossa), and fibrosis (Sirius red), PolyIC treatment did not result in any changes compared to Placebo-treated mice. Under these premises, it was reasonable that TLR3 activation only led to marginal effects because the model might be independent of TLR3-activation. Further, it is possible, that there were high endogenous ligand concentrations before treatment and all binding sites were occupied already. Hence, there was no further increase in binding with a higher ligand concentration.

To investigate the potential role of endogenous TLR3 activation, knockout and control-WT mice underwent wire injury followed by ultrasound examinations every other week. No pharmacological intervention was performed. The transaortic- valve peak velocity was increased in both, knockout and WT mice, but despite this, the increase in peak velocity was observed to occur at a slower rate in TLR3 deficient mice in comparison to the WT animals (Figure 39). The same observations were made relating the mean pressure gradient whereas the ejection fraction remained unchanged. The histological analysis demonstrated less infiltration of monocytes into the aortic valves of $TLR3^{-/-}$ mice compared to control WT. No significant signs of fibrosis or calcification could be demonstrated (Figure 40). A putative reason for this could be the limited follow-up time of only 6 weeks after surgery as AS in humans develops over the years.

Next, WT mice were treated with C4a every other day after wire injury to pharmacologically inhibit TLR3. Ultrasound examination was performed after 2, 4, and 6 weeks by Dr. Sven

Niepmann, resulting in a lower peak velocity and mean pressure gradient over the aortic valve in C4a-treated mice, compared to the control group. Similar patterns could be elucidated in comparison to TLR3$^{-/-}$ mice. Histological analysis revealed smaller aortic valve cusps and reduced monocyte infiltration. Further, Sirius Red staining confirmed less fibrosis after C4a treatment. However, von Kossa staining, as a marker for calcification, did not show differences between the 2 groups. In conclusion, pharmacological inhibition of TLR3 with C4a led to a blunted pro-inflammatory response after wire injury and a suppressed AS development. Another study by Takemura and colleagues in 2014 focused on radiation-induced gastrointestinal syndrome, which is considered to be TLR3 dependent. Here, C4a was shown to sufficiently inhibit TLR3 and protected against gastrointestinal syndrome after radiation exposure. They highlighted C4a as a therapeutic clinical treatment for the prevention of such a syndrome (Takemura et al. 2014). Regarding AS, further studies are needed to confirm the effectiveness of C4a.

4.3.2 MDA5 in mice

The in vitro experiments also identified the gene expression of IFIH1 (MDA5) and DDX58 (RIG-I), suggesting their potential importance in the context of calcification and EndMT. Indeed, previous studies have shown that gain-of-function mutations in MDA5 and RIG-I lead to diseases such as SMS. Among others, SMS may be associated with aortic and valvular calcification. However, the background and other factors remain to be investigated. (Lu and MacDougall 2017; Soda et al. 2019). Activated MDA5 and RIG-I results in type I IFN and pro-inflammatory cytokine production via IRF 3 and 7, and NF-κB signaling (Loo and Gale 2011; Lu and MacDougall 2017). This prompted us to start questioning the role of MDA5 in AS. Regarding the *in vivo* model in this study, MDA5 deficient mice showed a lower peak velocity and mean pressure gradient compared to WT animals. Moreover, von Kossa staining revealed more calcification in WT in contrast to MDA5 deficient mice. These patterns indicated a putative development of AS. Still, more experiments are needed to verify an AS in this model. *In vivo* experiments regarding the role of RIG-I were not performed in this manner, as it was part of Project A03 from TRR259 (AG Gunther Hartmann; Institut für Klinische Chemie und Klinische Pharmakologie, Universitätsklinikum Bonn). Nevertheless, it might be still interesting to investigate putative compensations between TLR3, RIG-I, and MDA5.

4.4 Conclusion

The aim of this research project was to evaluate and establish protocols for cell types such as VICs and VECs and their respective roles regarding AS. This thesis provides an overview of the role of TLR3 in the development of AS in *in vitro* and *in vivo* experiments and highlights the importance of the innate immune system in this context. Further, this study demonstrated the efficacy of TLR3 inhibition in this aortic disease with C4a. It is an interesting and important outcome for future studies because of promising data that need to be verified within other experiments for instance in large animal models. Furthermore, TLR3 signaling needs to be studied more in-depth in this manner. Not only putative co-activation of TLR3 and other PRRs, but also downstream targets of TLR3 need to be investigated in more detail to exclude an inappropriate activation of downstream signaling, which can lead to chronic inflammatory diseases.

Another major area of interest within the field of aortic diseases is aortic aneurysms. In an aortic aneurysm, part of the aorta bulges out because of wall damage. In a study conducted by Jabłońska and colleagues, the expression levels of TLR3 and RIG-I in aortic tissue and blood were investigated in patients with abdominal aortic aneurysm (AAA) compared to healthy controls (Jabłońska et al. 2018). The results exhibited higher expression levels of TLR3 in their aortic tissue compared to both blood samples and healthy controls. This suggested that TLR3 may play a role in the development or progression of AAA. Furthermore, the expression of *DDX58* (RIG-I) was found to be elevated in AAA patients compared to the healthy group. Together, these findings provided valuable insights into the molecular mechanisms underlying AAA and suggested that TLR3 and RIG-I may contribute to the development of the disease. Further research is needed to investigate the specific roles of these receptors in AAA. Moreover, studies that elucidated VICs and VECs playing roles in aortic diseases led to address the following research questions regarding TLR3 experiments: Which cell types are sufficient in aortic diseases. In order to get insights about the role of TLR3 in specific cell types, we generated tissue-specific knockout mice using the cre/loxP system. Both AS and AAA research will use these knockout mice.

4.5 The role of cholesterol in the development of aortic valve stenosis

Cholesterol is a natural and essential resource for our body to produce hormones, maintain cell membranes and fat homeostasis. It is normally produced in the liver. Other main sources include animal-based foods, such as meats and dairy products, that contain saturated and trans fats. Although it is not possible to control genetic factors associated with hyperlipidemia that

contribute to atherosclerosis or other CVD, general lifestyle can be controlled by each individual. This includes diets, physical activity, smoking, and alcohol consumption to prevent the development of CVD. In fact, by replacing 3% of animal protein with vegetable protein in the general diet, studies have indicated a notable 10% decrease in mortality rates, primarily attributed to CVD (Spence et al. 2021).

It is not only high LDL-C levels that are important, low HDL-C levels also play a role in heart disease. For example, it has been shown that patients with low HDL-C levels (less than 40mg/dl for men and less than 50mg/dl for women) have a 40% higher rate of cardiac events (Gielen and Landmesser 2011). It is therefore not just a matter of reducing LDL-C to lower the risk of CVD, as the risk factor of low HDL-C is independent of LDL-C. Therefore, some clinical trials have suggested raising HDL-C levels to prevent CVD events (Mahdy Ali et al. 2012). In addition, the concentration of high HDL-C compared with LDL-C was thought to be a good indicator of cardiovascular risk. However, it has been shown that very high HDL-C levels do not show any beneficial compensation for elevated LDL-C (Hewing et al. 2012; Franczyk et al. 2021). High levels of HDL-C can also be a sign of dysfunctional and altered HDL-C and it promotes the development of CVD rather than being protective. The current European Society of Cardiology/European Atherosclerosis Society (ESC/EAS) dyslipidemia guidelines emphasized an increasing risk of CVD progression when HDL-C levels exceed 90mg/dL (Mach et al. 2020; Franczyk et al. 2021). Therefore, HDL-C levels above 90mg/dL are not reliable risk indicators. Accordingly, research should continue to focus on mechanisms to lower LDL-C rather than on raising HDL-C (Franczyk et al. 2021).

Cholesterol encompasses various derivatives undergoing regular and dynamic modifications. Thus, an alternative approach to preventing CVD associated with high cholesterol is not only focused on lowering LDL-C levels but also involves the dissolution of CC, namely with CD: As mentioned above, CD (HPβCD) has an affinity for cholesterol. It has been shown that it is able to shuttle cholesterol from cells to lipoproteins. At low concentrations, CD catalyzes the transfer from cells to serum lipoproteins. At higher concentrations, the CD itself is capable of removing cellular cholesterol (Atger et al. 1997; Liu et al. 2003). Previous studies demonstrated the possibility to solubilize CC in mice that developed atherosclerosis (Zimmer et al. 2016). They revealed that CD was able to reduce atherosclerotic plaque in mice. This study prompted us to find out, firstly whether CC are also crucial in the development of AS, and secondly, whether CD can be a putative treatment in this manner.

Here, the CCDR was tested in the blood plasma of AS patients. CC were added to the plasma. After 2 hours, the CC were partially dissolved by the plasma. When different concentrations of

CD were added, approximately 60% of the CC were dissolved already 0.5 hours after the addition of 10mM CD (Figure 45). After 2 hours, approximately 80% were dissolved. After 4 hours, there was no difference within the highest concentration (10mM) compared to the value after 2 hours and remained at approximately 80%, indicating possible saturation. 1mM CD resulted in approximately 40% dissolution after 2 hours and increased to 60% after 4 hours. The lowest concentration of 0.1mM showed an increased dissolution after 4 hours, but the result was not significant. In conclusion, CC were partially dissolved in plasma after 2 hours, but high concentrations of CD were more efficient at dissolving CC after 30 minutes.

4.5.1 Cholesterol crystals in valvular interstitial cells

With regard to CC in VICs, it was first observed that VICs were able to take up the CC (Figure. 47). Furthermore, this study showed the dissolution of CC after the addition of CD (Figure 48). The question that remained was whether this uptake and dissolution had an effect on the cells and on the process of calcification, which is known to be crucial for the development of AS. Upon the addition of CC to the cells, the gene expression of the osteogenic marker *BMP2* exhibited an increase compared to the other conditions in BM. Conversely, in PCM, CD induced a notable, yet statistically insignificant, upregulation of *BMP2* gene expression when compared to the control or CC-treated cells. The second osteogenic marker, *RUNX2* showed an elevated gene expression after CD addition in BM. In PCM, *RUNX2* expression decreased after CD addition compared to CC treatment, showing an effect of CD on CC solubilization. While slight changes were observed these did not reach statistical significance. To fully understand whether CC uptake may have an effect on the process of calcification in VICs further experiments are required. Regarding pro-inflammatory markers, CC treatment resulted in an elevated *IL1β* gene expression in BM which could be blunted with the addition of CD showing an anti-inflammatory effect of CD. Still, *IL1β* expression increased in PCM after adding CD. These results led to the remaining question of the effect of CD dissolving CC. Further experiments are required to determine the underlying reasons for the divergent outcomes observed between the two different media. Here, the supplements of PCM may react with CD, stressing and activating the cells that caused calcification.

4.5.2 Cholesterol crystals in valvular endothelial cells

This study showed the CC uptake in VECs after approximately 8 hours (Figure 46). It remained unclear, whether this uptake affected the process of EndMT, which is known to be crucial in AS. Therefore, VECs were treated with CC and EndMT was induced by the addition of TGFβ1+IL1β

or TNFα. After CC treatment, the endothelial markers were downregulated compared to untreated cells, whereas *VCAM1* was upregulated. Among pro-inflammatory markers, *IL1β* gene expression was increased in CC-treated cells compared to control cells. This result seemed to show a pro-inflammatory effect of CC treatment in VECs, and the cells might secrete IL1β to recruit other immune cells, for instance macrophages. In addition, the aortic valve is known to accumulate the highest amount of cholesterol, and as cholesterol levels increase, the saturation intensifies, thereby contributing to CC formation. CC formation and deposition in the valve trigger inflammation, which is a major driver of calcification through extensive macrophage infiltration (El-Khatib et al. 2020).

However, no EndMT effect was observed 5 days after CC treatment. *VCAM1* and *TAGLN* gene expression were upregulated in CD-treated cells compared to CC-treated and control cells. Thus, CD treatment was more likely to induce EndMT. Regarding *IL1β* expression, CD showed an effect similar to the *VCAM1* and *TAGLN* gene expression data.

TGFβ1+IL1β and TNFα stimulation both resulted in downregulated *NOS3* mRNA expression, whereas TGFβ1+IL1β stimulation did not show decreased gene expression of *PECAM1* and *VWF*. With regard to *VCAM1* and *ACTA2*, both TGFβ1+IL1β and TNFα stimulation resulted in increased gene expression. *TAGLN* expression was only upregulated in TGFβ1+IL1β stimulated cells, whereas *TNFα* did not show any increased gene expression, which was consistent with the proteomic data (Figure 24,25). Thus, the EndMT effect was only partially demonstrated and further experiments are needed to verify the upcoming results. CC treatment and additional TGFβ1+IL1β or TNFα stimulation did not show significant differences in the EndMT process. Interestingly, CD treatment resulted in decreased endothelial marker gene expression within the 2 stimulations (TGFβ1+IL1β and TNFα). CD treatment showed no difference to mesenchymal markers or resulted in downregulated gene expression. These results seemed to verify an interesting finding, namely that CD might play a more important role than CC in the process of EndMT. A potential reason could be a high concentration of CD and lower concentrations need to be tested in future studies. Nevertheless, these data need to be verified and confirmed by further experiments and only show a first pattern of CC not playing a role in EndMT. With more information on CC in the development of AS, *in vivo* experiments would also be interesting. Firstly, the study of CC in the aortic valve area, and secondly, the putative possibility of dissolving such crystals with CD treatment.

4.6 Conclusion

Overall, CC are critical in the development of atherosclerosis (Zimmer et al. 2016). Since lipids are known to play an important role in atherosclerosis and cardiovascular calcification (Hsu et al. 2022), it was of interest for this study to evaluate the effects of these crystals on AS disease progression. A recent study of approximately 350 patients with AS undergoing TAVR demonstrated CCDR as a novel biomarker for patients with AS. The study showed that high CC dissolvers had significantly fewer unplanned endovascular interventions than low CC dissolvers. Furthermore, low CC-dissolvers benefited more from statin treatment than high CC-dissolvers, while LDL-C and HDL-C levels were comparable in both groups (Atger et al. 1997; Al-Kassou et al. 2022). Moreover, based on these results (Figure 45), a clinical trial would be interesting to test whether it is beneficial to use CD for plaque prevention or to slow disease progression. People between the ages of 50 and 75 who have been diagnosed with any variant of CVD, for instance atherosclerosis or AS would be appropriate for this trial. Thereby, it is important to assess also other pre-diseases such as diabetes mellitus as well as kidney diseases. The aim of this study would be to assess the safety, tolerability, feasibility and pharmacokinetics of intravenously administered CD in patients suffering from various CVD. All participants would receive CD once monthly or weekly for at least 2 doses and follow-up would be based on safety and biochemical data assessed by adverse events, clinical laboratory tests, vital signs, physical examinations, ECG, plasma levels of LDL-C, HDL-C, and CD. Thus, the function of the aortic valves and participants generally would be screened. The advantage in this case is that CD is already present in certain medications and its side effects are well-known and minimal.

In conclusion, this study has identified CD as a potential treatment to promote the dissolution of CC in patient plasma. In addition, CD was also able to dissolve CC in the cell culture medium of VICs and VECs. This led us to the novel treatment idea of increasing cholesterol solubility and thereby reducing the CC-mediated inflammatory response. The *in vitro* experiments in VICs partially confirmed this strategy, showing patterns of CD decreasing gene expression of *BMP2* as an osteogenic marker in BM. Regarding the process of EndMT, no pattern of CD solubilizing CC could be observed after 5 days. Further research is needed in this direction to provide more results in the progression of the disease.

5. References

- Aikawa, Elena; Otto, Catherine M. (2012): Look more closely at the valve: imaging calcific aortic valve disease. In: *Circulation* 125 (1), S. 9–11. DOI: 10.1161/CIRCULATIONAHA.111.073452.
- Akira, Shizuo; Takeda, Kiyoshi (2004): Toll-like receptor signalling. In: *Nature reviews. Immunology* 4 (7), S. 499–511. DOI: 10.1038/nri1391.
- Al-Kassou, B.; Al-Kassou, L.; Mahn, T. H.; Luetjohann, D.; Shamekhi, J.; Willemsen, N. et al. (2022): Novel assay for quantifying the cholesterol crystal dissolution capacity of serum predicts outcomes in patients with severe aortic stenosis undergoing TAVR. In: *European heart journal* 43 (Supplement_2), Artikel ehac544.1623. DOI: 10.1093/eurheartj/ehac544.1623.
- Aluru, John Sukumar; Barsouk, Adam; Saginala, Kalyan; Rawla, Prashanth; Barsouk, Alexander (2022): Valvular Heart Disease Epidemiology. In: Medical sciences (Basel, Switzerland) 10 (2). DOI: 10.3390/medsci10020032.
- Amadio, Roberto; Piperno, Giulia Maria; Benvenuti, Federica (2021): Self-DNA Sensing by cGAS-STING and TLR9 in Autoimmunity: Is the Cytoskeleton in Control? In: *Frontiers in immunology* 12, S. 657344. DOI: 10.3389/fimmu.2021.657344.
- Aman, Jurjan; Weijers, Ester M.; van Nieuw Amerongen, Geerten P.; Malik, Asrar B.; van Hinsbergh, Victor W. M. (2016): Using cultured endothelial cells to study endothelial barrier dysfunction: Challenges and opportunities. In: *American journal of physiology. Lung cellular and molecular physiology* 311 (2), L453-66. DOI: 10.1152/ajplung.00393.2015.
- Arnett, Donna K.; Blumenthal, Roger S.; Albert, Michelle A.; Buroker, Andrew B.; Goldberger, Zachary D.; Hahn, Ellen J. et al. (2019): 2019 ACC/AHA Guideline on the Primary Prevention of Cardiovascular Disease: A Report of the American College of Cardiology/American Heart Association Task Force on Clinical Practice Guidelines. In: *Circulation* 140 (11), e596-e646. DOI: 10.1161/CIR.0000000000000678.
- Atger, V. M.; La Llera Moya, M. de; Stoudt, G. W.; Rodrigueza, W. V.; Phillips, M. C.; Rothblat, G. H. (1997): Cyclodextrins as catalysts for the removal of cholesterol from macrophage foam cells. In: *The Journal of clinical investigation* 99 (4), S. 773–780. DOI: 10.1172/JCI119223.

- Badimon, Lina; Vilahur, Gemma (2012): LDL-cholesterol versus HDL-cholesterol in the atherosclerotic plaque: inflammatory resolution versus thrombotic chaos. In: *Annals of the New York Academy of Sciences* 1254, S. 18–32. DOI: 10.1111/j.1749-6632.2012.06480.x.
- Barua, Rajat S.; Ambrose, John A.; Srivastava, Sudhesh; DeVoe, Mary C.; Eales-Reynolds, Lesley-Jane (2003): Reactive oxygen species are involved in smoking-induced dysfunction of nitric oxide biosynthesis and upregulation of endothelial nitric oxide synthase: an in vitro demonstration in human coronary artery endothelial cells. In: *Circulation* 107 (18), S. 2342–2347. DOI: 10.1161/01.CIR.0000066691.52789.BE.
- Bhat, Mohd Younis; Solanki, Hitendra S.; Advani, Jayshree; Khan, Aafaque Ahmad; Keshava Prasad, T. S.; Gowda, Harsha et al. (2018): Comprehensive ne2rk map of interferon gamma signaling. In: *Journal of cell communication and signaling* 12 (4), S. 745–751. DOI: 10.1007/s12079-018-0486-y.
- Blaser, Mark C.; Kraler, Simon; Lüscher, Thomas F.; Aikawa, Elena (2021): Multi-Omics Approaches to Define Calcific Aortic Valve Disease Pathogenesis. In: *Circulation research* 128 (9), S. 1371–1397. DOI: 10.1161/CIRCRESAHA.120.317979.
- Blunder, Stefan; Messner, Barbara; Scharinger, Bernhard; Doppler, Christian; Zeller, Iris; Zierer, Andreas et al. (2018): Targeted gene expression analyzes and immunohistology suggest a pro-proliferative state in tricuspid aortic valve-, and senescence and viral infections in bicuspid aortic valve-associated thoracic aortic aneurysms. In: *Atherosclerosis* 271, S. 111–119. DOI: 10.1016/j.atherosclerosis.2018.02.007.
- Bonilla, Francisco A.; Oettgen, Hans C. (2010): Adaptive immunity. In: *The Journal of allergy and clinical immunology* 125 (2 Suppl 2), S33-40. DOI: 10.1016/j.jaci.2009.09.017.
- Böttinger EP, Bitzer M (2002) TGF-beta signaling in renal disease. J Am Soc Nephrol 13:2600–2610. https://doi.org/10.1097/01.ASN.0000033611.79556.AE
- Braun, M.; Pietsch, P.; Schrör, K.; Baumann, G.; Felix, S. B. (1999): Cellular adhesion molecules on vascular smooth muscle cells. In: *Cardiovascular research* 41 (2), S. 395–401. DOI: 10.1016/s0008-6363(98)00302-2.

- Brentnall, Matthew; Rodriguez-Menocal, Luis; Guevara, Rebeka Ladron de; Cepero, Enrique; Boise, Lawrence H. (2013): Caspase-9, Caspase-3 and Caspase-7 have distinct roles during intrinsic apoptosis. In: *BMC cell biology* 14, S. 32. DOI: 10.1186/1471-2121-14-32.
- Brubaker, Sky W.; Bonham, Kevin S.; Zanoni, Ivan; Kagan, Jonathan C. (2015): Innate immune pattern recognition: a cell biological perspective. In: *Annual review of immunology* 33, S. 257–290. DOI: 10.1146/annurev-immunol-032414-112240.
- Bugge, Marit; Bergstrom, Bjarte; Eide, Oda K.; Solli, Helene; Kjønstad, Ingrid F.; Stenvik, Jørgen et al. (2017): Surface Toll-like receptor 3 expression in metastatic intestinal epithelial cells induces inflammatory cytokine production and promotes invasiveness. In: *The Journal of biological chemistry* 292 (37), S. 15408–15425. DOI: 10.1074/jbc.M117.784090.
- Cavassani, Karen A.; Ishii, Makoto; Wen, Haitao; Schaller, Matthew A.; Lincoln, Pamela M.; Lukacs, Nicholas W. et al. (2008): TLR3 is an endogenous sensor of tissue necrosis during acute inflammatory events. In: *The Journal of experimental medicine* 205 (11), S. 2609–2621. DOI: 10.1084/jem.20081370.
- Chambers, John B. (2009): Aortic stenosis. In: *European journal of echocardiography : the journal of the Working Group on Echocardiography of the European Society of Cardiology* 10 (1), i11-9. DOI: 10.1093/ejechocard/jen240.
- Cheng, Kui; Wang, Xiaohui; Yin, Hang (2011): Small-molecule inhibitors of the TLR3/dsRNA complex. In: *Journal of the American Chemical Society* 133 (11), S. 3764–3767. DOI: 10.1021/ja111312h.
- Cho, Jin Gu; Lee, Aram; Chang, Woochul; Lee, Myeong-Sok; Kim, Jongmin (2018): Endothelial to Mesenchymal Transition Represents a Key Link in the Interaction between Inflammation and Endothelial Dysfunction. In: *Frontiers in immunology* 9, S. 294. DOI: 10.3389/fimmu.2018.00294.
- Cho, Won Gil; Albuquerque, Romulo J. C.; Kleinman, Mark E.; Tarallo, Valeria; Greco, Adelaide; Nozaki, Miho et al. (2009): Small interfering RNA-induced TLR3 activation inhibits blood and lymphatic vessel growth. In: *Proceedings of the National Academy of Sciences of the United States of America* 106 (17), S. 7137–7142. DOI: 10.1073/pnas.0812317106.

- Chomczynski, P.; Sacchi, N. (1987): Single-step method of RNA isolation by acid guanidinium thiocyanate-phenol-chloroform extraction. In: *Analytical biochemistry* 162 (1), S. 156–159. DOI: 10.1006/abio.1987.9999.
- Chomczynski, Piotr; Sacchi, Nicoletta (2006): The single-step method of RNA isolation by acid guanidinium thiocyanate-phenol-chloroform extraction: twenty-something years on. In: *Nature protocols* 1 (2), S. 581–585. DOI: 10.1038/nprot.2006.83
- Clark, Mary Ann; Arnold, Suzanne V.; Duhay, Francis G.; Thompson, Ann K.; Keyes, Michelle J.; Svensson, Lars G. et al. (2012): Five-year clinical and economic outcomes among patients with medically managed severe aortic stenosis: results from a Medicare claims analysis. In: *Circulation. Cardiovascular quality and outcomes* 5 (5), S. 697–704. DOI: 10.1161/CIRCOUTCOMES.112.966002.
- Cowell, S. Joanna; Newby, David E.; Prescott, Robin J.; Bloomfield, Peter; Reid, John; Northridge, David B.; Boon, Nicholas A. (2005): A randomized trial of intensive lipid-lowering therapy in calcific aortic stenosis. In: *The New England journal of medicine* 352 (23), S. 2389–2397. DOI: 10.1056/NEJMoa043876.
- Crini, Grégorio (2020): The contribution of Franz Schardinger to cyclodextrins: a tribute on the occasion of the centenary of his death. In: J Incl Phenom Macrocycl Chem 97 (1-2), S. 19–28. DOI: 10.1007/s10847-020-00990-3.
- Danielsen, Ragnar; Aspelund, Thor; Harris, Tamara B.; Gudnason, Vilmundur (2014): The prevalence of aortic stenosis in the elderly in Iceland and predictions for the coming decades: the AGES-Reykjavík study. In: *International journal of cardiology* 176 (3), S. 916–922. DOI: 10.1016/j.ijcard.2014.08.053.
- Dass, C. R. (2000): Apolipoprotein A-I, phospholipid vesicles, and cyclodextrins as potential anti-atherosclerotic drugs: delivery, pharmacokinetics, and efficacy. In: *Drug delivery* 7 (3), S. 161–182. DOI: 10.1080/10717540050120205.
- Davis, Mark E.; Brewster, Marcus E. (2004): Cyclodextrin-based pharmaceutics: past, present and future. In: *Nature reviews. Drug discovery* 3 (12), S. 1023–1035. DOI: 10.1038/nrd1576.
- Deretic, Vojo (2021): Autophagy in inflammation, infection, and immunometabolism. In: *Immunity* 54 (3), S. 437–453. DOI: 10.1016/j.immuni.2021.01.018.

- Duewell P, Kono H, Rayner KJ et al. (2010) NLRP3 inflammasomes are required for atherogenesis and activated by cholesterol crystals. Nature 464:1357–1361. https://doi.org/10.1038/nature08938.
- Dweck, Marc R.; Boon, Nicholas A.; Newby, David E. (2012): Calcific aortic stenosis: a disease of the valve and the myocardium. In: *Journal of the American College of Cardiology* 60 (19), S. 1854–1863. DOI: 10.1016/j.jacc.2012.02.093.
- Dweck, Marc R.; Khaw, H. J.; Sng, G. K. Z.; Luo, E. L. C.; Baird, A.; Williams, M. C. et al. (2013): Aortic stenosis, atherosclerosis, and skeletal bone: is there a common link with calcification and inflammation? In: *European heart journal* 34 (21), S. 1567–1574. DOI: 10.1093/eurheartj/eht034.
- El-Khatib, Layan A.; Feijter-Rupp, Heather de; Janoudi, Abed; Fry, Levi; Kehdi, Michael; Abela, George S. (2020): Cholesterol induced heart valve inflammation and injury: efficacy of cholesterol lowering treatment. In: *Open heart* 7 (2). DOI: 10.1136/openhrt-2020-001274.
- Elshourbagy, Nabil A.; Meyers, Harold V.; Abdel-Meguid, Sherin S. (2014): Cholesterol: the good, the bad, and the ugly - therapeutic targets for the treatment of dyslipidemia. In: *Medical principles and practice : international journal of the Kuwait University, Health Science Centre* 23 (2), S. 99–111. DOI: 10.1159/000356856.
- Fedacko, Jan (2012): Association of High w-6/w-3 Fatty Acid Ratio Diet with Causes of Death Due to Noncommunicable Diseases Among Urban Decedents in north India. In: *TONUTRAJ* 5 (1), S. 113–123. DOI: 10.2174/1876396001205010113.
- Feingold, Kenneth R. (2000): Endotext. Introduction to Lipids and Lipoproteins. Hg. v. Kenneth R. Feingold, Bradley Anawalt, Marc R. Blackman, Alison Boyce, George Chrousos, Emiliano Corpas, et al. South Dartmouth (MA).
- Franczyk, Beata; Rysz, Jacek; Ławiński, Janusz; Rysz-Górzyńska, Magdalena; Gluba-Brzózka, Anna (2021): Is a High HDL-Cholesterol Level Always Beneficial? In: *Biomedicines* 9 (9). DOI: 10.3390/biomedicines9091083.
- Freeman, Rosario V.; Otto, Catherine M. (2005): Spectrum of calcific aortic valve disease: pathogenesis, disease progression, and treatment strategies. In: *Circulation* 111 (24), S. 3316–3326. DOI: 10.1161/CIRCULATIONAHA.104.486738.

- García-Rodríguez, Carmen; Parra-Izquierdo, Iván; Castaños-Mollor, Irene; López, Javier; San Román, J. Alberto; Sánchez Crespo, Mariano (2018): Toll-Like Receptors, Inflammation, and Calcific Aortic Valve Disease. In: *Frontiers in physiology* 9, S. 201. DOI: 10.3389/fphys.2018.00201.
- Gielen, Stephan; Landmesser, Ulf (2011): A new look at HDL in coronary disease: can we escape natural history? In: *Heart (British Cardiac Society)* 97 (23), S. 1899–1901. DOI: 10.1136/heartjnl-2011-300612.
- Hammad, Hamida; Lambrecht, Bart N. (2021): The basic immunology of asthma. In: *Cell* 184 (6), S. 1469–1485. DOI: 10.1016/j.cell.2021.02.016.
- Hastings, Nicole E.; Feaver, Ryan E.; Lee, Monica Y.; Wamhoff, Brian R.; Blackman, Brett R. (2009): Human IL-8 regulates smooth muscle cell VCAM-1 expression in response to endothelial cells exposed to atheroprone flow. In: *Arteriosclerosis, thrombosis, and vascular biology* 29 (5), S. 725–731. DOI: 10.1161/ATVBAHA.109.184382.
- Hewing, Bernd; Moore, Kathryn J.; Fisher, Edward A. (2012): HDL and cardiovascular risk: time to call the plumber? In: *Circulation research* 111 (9), S. 1117–1120. DOI: 10.1161/CIRCRESAHA.112.280958.
- Hinton, Robert B.; Alfieri, Christina M.; Witt, Sandra A.; Glascock, Betty J.; Khoury, Philip R.; Benson, D. Woodrow; Yutzey, Katherine E. (2008): Mouse heart valve structure and function: echocardiographic and morphometric analyzes from the fetus through the aged adult. In: *American journal of physiology. Heart and circulatory physiology* 294 (6), H2480-8. DOI: 10.1152/ajpheart.91431.2007.
- Honda, Shintaro; Miyamoto, Takuya; Watanabe, Tetsu; Narumi, Taro; Kadowaki, Shinpei; Honda, Yuki et al. (2014): A novel mouse model of aortic valve stenosis induced by direct wire injury. In: Arteriosclerosis, thrombosis, and vascular biology 34 (2), S. 270–278. DOI: 10.1161/ATVBAHA.113.302610.
- Hsu, Chia-Pei Denise; Hutcheson, Joshua D.; Ramaswamy, Sharan (2020): Oscillatory fluid-induced mechanobiology in heart valves with parallels to the vasculature. In: *Vascular biology (Bristol, England)* 2 (1), R59-R71. DOI: 10.1530/VB-19-0031.
- Hsu, Jeffrey J.; Tintut, Yin; Demer, Linda L. (2022): Regulation of cardiovascular calcification by lipids and lipoproteins. In: *Current opinion in lipidology* 33 (5), S. 289–294. DOI: 10.1097/MOL.0000000000000844.

- Jabłońska, Agnieszka; Neumayer, Christoph; Bolliger, Michael; Gollackner, Bernd; Klinger, Markus; Paradowska, Edyta et al. (2018): Analysis of host Toll-like receptor 3 and RIG-I-like receptor gene expression in patients with abdominal aortic aneurysm. In: *Journal of vascular surgery* 68 (6S), 39S-46S. DOI: 10.1016/j.jvs.2017.10.087.
- Janeway, Charles A.; Medzhitov, Ruslan (2002): Innate immune recognition. In: *Annual review of immunology* 20, S. 197–216. DOI: 10.1146/annurev.immunol.20.083001.084359.
- Jebari-Benslaiman, Shifa; Galicia-García, Unai; Larrea-Sebal, Asier; Olaetxea, Javier Rekondo; Alloza, Iraide; Vandenbroeck, Koen et al. (2022): Pathophysiology of Atherosclerosis. In: International journal of molecular sciences 23 (6). DOI: 10.3390/ijms23063346.
- Jiao, Kailin; Zhen, Jing; Wu, Maoxuan; Teng, Mengying; Yang, Keke; Zhou, Qian et al. (2020): 27-Hydroxycholesterol-induced EndMT acts via STAT3 signaling to promote breast cancer cell migration by altering the tumor microenvironment. In: *Cancer biology & medicine* 17 (1), S. 88–100. DOI: 10.20892/j.issn.2095-3941.2019.0262.
- Jin, S.; Mutvei, A. P.; Chivukula, I. V.; Andersson, E. R.; Ramsköld, D.; Sandberg, R. et al. (2013): Non-canonical Notch signaling activates IL-6/JAK/STAT signaling in breast tumor cells and is controlled by p53 and IKKα/IKKβ. In: *Oncogene* 32 (41), S. 4892–4902. DOI: 10.1038/onc.2012.517.
- Joseph, Jessica; Naqvi, Syed Yaseen; Giri, Jay; Goldberg, Sheldon (2017): Aortic Stenosis: Pathophysiology, Diagnosis, and Therapy. In: *The American journal of medicine* 130 (3), S. 253–263. DOI: 10.1016/j.amjmed.2016.10.005.
- Kaiser, William J.; Sridharan, Haripriya; Huang, Chunzi; Mandal, Pratyusha; Upton, Jason W.; Gough, Peter J. et al. (2013): Toll-like receptor 3-mediated necrosis via TRIF, RIP3, and MLKL. In: *The Journal of biological chemistry* 288 (43), S. 31268–31279. DOI: 10.1074/jbc.M113.462341.
- Kaisho, Tsuneyasu; Akira, Shizuo (2006): Toll-like receptor function and signaling. In: *The Journal of allergy and clinical immunology* 117 (5), 979-87; quiz 988. DOI: 10.1016/j.jaci.2006.02.023.
- Karikó, Katalin; Ni, Houping; Capodici, John; Lamphier, Marc; Weissman, Drew (2004): mRNA is an endogenous ligand for Toll-like receptor 3. In: *The Journal of biological chemistry* 279 (13), S. 12542–12550. DOI: 10.1074/jbc.M310175200.

- Kaur, Bani Preet; Secord, Elizabeth (2019): Innate Immunity. In: *Pediatric clinics of North America* 66 (5), S. 905–911. DOI: 10.1016/j.pcl.2019.06.011.
- Kavey, Rae-Ellen W.; Daniels, Stephen R.; Lauer, Ronald M.; Atkins, Dianne L.; Hayman, Laura L.; Taubert, Kathryn (2003): American Heart Association guidelines for primary prevention of atherosclerotic cardiovascular disease beginning in childhood. In: *Circulation* 107 (11), S. 1562–1566. DOI: 10.1161/01.CIR.0000061521.15730.6E.
- Kawata, Mikiko; Koinuma, Daizo; Ogami, Tomohiro; Umezawa, Kazuo; Iwata, Caname; Watabe, Tetsuro; Miyazono, Kohei (2012): TGF-β-induced epithelial-mesenchymal transition of A549 lung adenocarcinoma cells is enhanced by pro-inflammatory cytokines derived from RAW 264.7 macrophage cells. In: *Journal of biochemistry* 151 (2), S. 205–216. DOI: 10.1093/jb/mvr136.
- Kim, Young Keun; Shin, Jeon Soo; Nahm, Moon H. (2016): NOD-Like Receptors in Infection, Immunity, and Diseases. In: *Yonsei medical journal* 57 (1), S. 5–14. DOI: 10.3349/ymj.2016.57.1.5.
- Kleinman, Mark E.; Yamada, Kiyoshi; Takeda, Atsunobu; Chandrasekaran, Vasu; Nozaki, Miho; Baffi, Judit Z. et al. (2008): Sequence- and target-independent angiogenesis suppression by siRNA via TLR3. In: *Nature* 452 (7187), S. 591–597. DOI: 10.1038/nature06765.
- Komutrattananont, Pornhatai; Mahakkanukrauh, Pasuk; Das, Srijit (2019): Morphology of the human aorta and age-related changes: anatomical facts. In: *Anatomy & cell biology* 52 (2), S. 109–114. DOI: 10.5115/acb.2019.52.2.109.
- Kourkoveli, Panagiota; Spargias, Konstantinos; Hahalis, George (2018): TAVR in 2017-What we know? What to expect? In: *Journal of geriatric cardiology : JGC* 15 (1), S. 55–60. DOI: 10.11909/j.issn.1671-5411.2018.01.005.
- Kouro, Taku; Takatsu, Kiyoshi (2009): IL-5- and eosinophil-mediated inflammation: from discovery to therapy. In: *International immunology* 21 (12), S. 1303–1309. DOI: 10.1093/intimm/dxp102.
- Kovacic, Jason C.; Dimmeler, Stefanie; Harvey, Richard P.; Finkel, Toren; Aikawa, Elena; Krenning, Guido; Baker, Andrew H. (2019): Endothelial to Mesenchymal Transition in Cardiovascular Disease: JACC State-of-the-Art Review. In: *Journal of the American College of Cardiology* 73 (2), S. 190–209. DOI: 10.1016/j.jacc.2018.09.089.

- Kurtz, Christopher E.; Otto, Catherine M. (2010): Aortic stenosis: clinical aspects of diagnosis and management, with 10 illustrative case reports from a 25-year experience. In: *Medicine* 89 (6), S. 349–379. DOI: 10.1097/MD.0b013e3181fe5648.
- Lancaster, Madeline A.; Knoblich, Juergen A. (2014): Organogenesis in a dish: modeling development and disease using organoid technologies. In: *Science (New York, N.Y.)* 345 (6194), S. 1247125. DOI: 10.1126/science.1247125.
- Lee, Seung Hyun; Choi, Jae-Hoon (2016): Involvement of Immune Cell Ne2rk in Aortic Valve Stenosis: Communication between Valvular Interstitial Cells and Immune Cells. In: *Immune ne2rk* 16 (1), S. 26–32. DOI: 10.4110/in.2016.16.1.26.
- Li, Yingrui; Deng, Songbai; Liu, Bin; Yan, Yulin; Du, Jianlin; Li, Yu et al. (2021): The effects of lipid-lowering therapy on coronary plaque regression: a systematic review and meta-analysis. In: *Scientific reports* 11 (1), S. 7999. DOI: 10.1038/s41598-021-87528-w.
- Lindroos, M.; Kupari, M.; Heikkilä, J.; Tilvis, R. (1993): Prevalence of aortic valve abnormalities in the elderly: an echocardiographic study of a random population sample. In: *Journal of the American College of Cardiology* 21 (5), S. 1220–1225. DOI: 10.1016/0735-1097(93)90249-Z.
- Liu, Qiang; Imaizumi, Tadaatsu; Kawaguchi, Shogo; Aizawa, Tomomi; Matsumiya, Tomoh; Watanabe, Shojiro et al. (2018): Toll-Like Receptor 3 Signaling Contributes to Regional Neutrophil Recruitment in Cultured Human Glomerular Endothelial Cells. In: Nephron 139 (4), S. 349–358. DOI: 10.1159/000489507.
- Liu, Sue M.; Cogny, Anne; Kockx, Maaike; Dean, Roger T.; Gaus, Katharina; Jessup, Wendy; Kritharides, Leonard (2003): Cyclodextrins differentially mobilize free and esterified cholesterol from primary human foam cell macrophages. In: *Journal of lipid research* 44 (6), S. 1156–1166. DOI: 10.1194/jlr.M200464-JLR200.
- Loftsson, Thorsteinn; Brewster, Marcus E. (2010): Pharmaceutical applications of cyclodextrins: basic science and product development. In: *The Journal of pharmacy and pharmacology* 62 (11), S. 1607–1621. DOI: 10.1111/j.2042-7158.2010.01030.x.
- Loo, Yueh-Ming; Gale, Michael (2011): Immune signaling by RIG-I-like receptors. In: *Immunity* 34 (5), S. 680–692. DOI: 10.1016/j.immuni.2011.05.003.

- Lu, Changming; MacDougall, Mary (2017): RIG-I-Like Receptor Signaling in Singleton-Merten Syndrome. In: *Frontiers in genetics* 8, S. 118. DOI: 10.3389/fgene.2017.00118.
- M Maheriya, Pankaj (2017): Cyclodextrin: A Promising Candidate in Enhancing Oral Bioavailability of poorly Water Soluble Drugs. In: *MOJBB* 3 (3). DOI: 10.15406/mojbb.2017.03.00034.
- Ma, Jin; Sanchez-Duffhues, Gonzalo; Goumans, Marie-José; Dijke, Peter ten (2020a): TGF-β-Induced Endothelial to Mesenchymal Transition in Disease and Tissue Engineering. In: *Frontiers in cell and developmental biology* 8, S. 260. DOI: 10.3389/fcell.2020.00260.
- Ma, Xiaochun; Zhao, Diming; Yuan, Peidong; Li, Jinzhang; Yun, Yan; Cui, Yuqi et al. (2020b): Endothelial-to-Mesenchymal Transition in Calcific Aortic Valve Disease. In: *Acta Cardiologica Sinica* 36 (3), S. 183–194. DOI: 10.6515/ACS.202005_36(3).20200213A.
- Mach, François; Baigent, Colin; Catapano, Alberico L.; Koskinas, Konstantinos C.; Casula, Manuela; Badimon, Lina et al. (2020): 2019 ESC/EAS Guidelines for the management of dyslipidaemias: lipid modification to reduce cardiovascular risk. In: *European heart journal* 41 (1), S. 111–188. DOI: 10.1093/eurheartj/ehz455.
- Mahdy Ali, K.; Wonnerth, A.; Huber, K.; Wojta, J. (2012): Cardiovascular disease risk reduction by raising HDL cholesterol--current therapies and future opportunities. In: *British journal of pharmacology* 167 (6), S. 1177–1194. DOI: 10.1111/j.1476-5381.2012.02081.x.
- Mahjoubin-Tehran, Maryam; Kovanen, Petri T.; Xu, Suowen; Jamialahmadi, Tannaz; Sahebkar, Amirhossein (2020): Cyclodextrins: Potential therapeutics against atherosclerosis. In: *Pharmacology & therapeutics* 214, S. 107620. DOI: 10.1016/j.pharmthera.2020.107620.
- Makieła, Damian; Janus-Zygmunt, Iwona; Górny, Krzysztof; Gburski, Zygmunt (2018): Investigation of the influence of β-cyclodextrin on cholesterol lodgement — A molecular dynamics simulation study. In: *Journal of Molecular Liquids* 262, S. 451–459. DOI: 10.1016/j.molliq.2018.04.098.
- Makkar, Raj R.; Fontana, Gregory P.; Jilaihawi, Hasan; Kapadia, Samir; Pichard, Augusto D.; Douglas, Pamela S. et al. (2012): Transcatheter aortic-valve replacement

for inoperable severe aortic stenosis. In: *The New England journal of medicine* 366 (18), S. 1696–1704. DOI: 10.1056/NEJMoa1202277.

- Maleszewska, Monika; Gjaltema, Rutger A. F.; Krenning, Guido; Harmsen, Martin C. (2015): Enhancer of zeste homolog-2 (EZH2) methyltransferase regulates transgelin/smooth muscle-22α expression in endothelial cells in response to interleukin-1β and transforming growth factor-β2. In: *Cellular signalling* 27 (8), S. 1589–1596. DOI: 10.1016/j.cellsig.2015.04.008.
- Martínez-García, Erika Aurora; Zavala-Cerna, Maria Guadalupe; Lujano-Benítez, Andrea Verónica; Sánchez-Hernández, Pedro Ernesto; Martín-Márquez, Beatriz Teresita; Sandoval-García, Flavio; Vázquez-Del Mercado, Mónica (2018): Potential Chronotherapeutic Optimization of Antimalarials in Systemic Lupus Erythematosus: Is Toll-Like Receptor 9 Expression Dependent on the Circadian Cycle in Humans? In: *Frontiers in immunology* 9, S. 1497. DOI: 10.3389/fimmu.2018.01497.
- Medici, Damian; Shore, Eileen M.; Lounev, Vitali Y.; Kaplan, Frederick S.; Kalluri, Raghu; Olsen, Bjorn R. (2010): Conversion of vascular endothelial cells into multipotent stem-like cells. In: Nature medicine 16 (12), S. 1400–1406. DOI: 10.1038/nm.2252.
- Medzhitov, Ruslan (2008): Origin and physiological roles of inflammation. In: *Nature* 454 (7203), S. 428–435. DOI: 10.1038/nature07201.
- Mendis, Shanthi (Hg.) (2011): Global atlas on cardiovascular disease Prevention and control. Weltgesundheitsorganisation; World Heart Federation. Geneva: World Health Organization.
- Meng, Xiao-Ming; Nikolic-Paterson, David J.; Lan, Hui Yao (2016): TGF-β: the master regulator of fibrosis. In: *Nature reviews. Nephrology* 12 (6), S. 325–338. DOI: 10.1038/nrneph.2016.48.
- Merryman, W. David; Schoen, Frederick J. (2013): Mechanisms of calcification in aortic valve disease: role of mechanokinetics and mechanodynamics. In: *Current cardiology reports* 15 (5), S. 355. DOI: 10.1007/s11886-013-0355-5.
- Mesas, Arthur Eumann; Garrido-Miguel, Miriam; Fernández-Rodríguez, Rubén; Fernández Franco, Sofía; Lugones-Sánchez, Cristina; García-Ortiz, Luis; Martínez-Vizcaíno, Vicente (2022): Egg Consumption and Blood Lipid Parameters According to the Presence of Chronic Metabolic Disorders: The EVIDENT II Study. In: The Journal

of clinical endocrinology and metabolism 107 (3), e963-e972. DOI: 10.1210/clinem/dgab802

- Miller, Carolyn A.; Corbin, Karen D.; Da Costa, Kerry-Ann; Zhang, Shucha; Zhao, Xueqing; Galanko, Joseph A. et al. (2014): Effect of egg ingestion on trimethylamine-N-oxide production in humans: a randomized, controlled, dose-response study. In: *The American journal of clinical nutrition* 100 (3), S. 778–786. DOI: 10.3945/ajcn.114.087692.
- Mjaatvedt, Corey H.; Kern, Christine B.; Norris, Russel A.; Fairey, Sarah; Cave, Courtney L. (2005): Normal distribution of melanocytes in the mouse heart. In: *The anatomical record. Part A, Discoveries in molecular, cellular, and evolutionary biology* 285 (2), S. 748–757. DOI: 10.1002/ar.a.20210.
- Montalescot, Gilles; Sechtem, Udo; Achenbach, Stephan; Andreotti, Felicita; Arden, Chris; Budaj, Andrzej et al. (2013): 2013 ESC guidelines on the management of stable coronary artery disease: the Task Force on the management of stable coronary artery disease of the European Society of Cardiology. In: *European heart journal* 34 (38), S. 2949–3003. DOI: 10.1093/eurheartj/eht296.
- Moore, Kathryn J.; Sheedy, Frederick J.; Fisher, Edward A. (2013): Macrophages in atherosclerosis: a dynamic balance. In: *Nature reviews. Immunology* 13 (10), S. 709–721. DOI: 10.1038/nri3520.
- Moura, Luis M.; Ramos, Sandra F.; Zamorano, José L.; Barros, Isabel M.; Azevedo, Luis F.; Rocha-Gonçalves, Francisco; Rajamannan, Nalini M. (2007): Rosuvastatin affecting aortic valve endothelium to slow the progression of aortic stenosis. In: *Journal of the American College of Cardiology* 49 (5), S. 554–561. DOI: 10.1016/j.jacc.2006.07.072.
- Moustakas, Aristidis; Heldin, Carl-Henrik (2007): Signaling ne2rks guiding epithelial-mesenchymal transitions during embryogenesis and cancer progression. In: *Cancer science* 98 (10), S. 1512–1520. DOI: 10.1111/j.1349-7006.2007.00550.x.
- New, Sophie E. P.; Aikawa, Elena (2011): Molecular imaging insights into early inflammatory stages of arterial and aortic valve calcification. In: *Circulation research* 108 (11), S. 1381–1391. DOI: 10.1161/CIRCRESAHA.110.234146.
- Niepmann, Sven Thomas; Steffen, Eva; Zietzer, Andreas; Adam, Matti; Nordsiek, Julia; Gyamfi-Poku, Isabella et al. (2019): Graded murine wire-induced aortic valve stenosis

model mimics human functional and morphological disease phenotype. In: *Clinical research in cardiology : official journal of the German Cardiac Society* 108 (8), S. 847–856. DOI: 10.1007/s00392-019-01413-1.

- Niepmann, Sven Thomas; Willemsen, Nicola; Boucher, Ann Sophie; Stei, Marta; Goody, Philip; Zietzer, Andreas et al. (2023): Toll-like receptor-3 contributes to the development of aortic valve stenosis. In: *Basic Res Cardiol* 118 (1). DOI: 10.1007/s00395-023-00980-9.
- Oduro, Patrick Kwabena; Zheng, Xianxian; Wei, Jinna; Yang, Yanze; Wang, Yuefei; Zhang, Han et al. (2022): The cGAS-STING signaling in cardiovascular and metabolic diseases: Future novel target option for pharmacotherapy. In: *Acta pharmaceutica Sinica. B* 12 (1), S. 50–75. DOI: 10.1016/j.apsb.2021.05.011.
- Osnabrugge, Ruben L. J.; Mylotte, Darren; Head, Stuart J.; van Mieghem, Nicolas M.; Nkomo, Vuyisile T.; LeReun, Corinne M. et al. (2013): Aortic stenosis in the elderly: disease prevalence and number of candidates for transcatheter aortic valve replacement: a meta-analysis and modeling study. In: *Journal of the American College of Cardiology* 62 (11), S. 1002–1012. DOI: 10.1016/j.jacc.2013.05.015.
- Otto, Catherine M.; Nishimura, Rick A.; Bonow, Robert O.; Carabello, Blase A.; Erwin, John P.; Gentile, Federico et al. (2021): 2020 ACC/AHA Guideline for the Management of Patients With Valvular Heart Disease: A Report of the American College of Cardiology/American Heart Association Joint Committee on Clinical Practice Guidelines. In: *Journal of the American College of Cardiology* 77 (4), e25-e197. DOI: 10.1016/j.jacc.2020.11.018.
- Otto, Catherine M.; Prendergast, Bernard (2014): Aortic-valve stenosis--from patients at risk to severe valve obstruction. In: *The New England journal of medicine* 371 (8), S. 744–756. DOI: 10.1056/NEJMra1313875.
- Parkin, J.; Cohen, B. (2001): An overview of the immune system. In: *Lancet (London, England)* 357 (9270), S. 1777–1789. DOI: 10.1016/S0140-6736(00)04904-7.
- Pawade, Tania A.; Newby, David E.; Dweck, Marc R. (2015): Calcification in Aortic Stenosis: The Skeleton Key. In: *Journal of the American College of Cardiology* 66 (5), S. 561–577. DOI: 10.1016/j.jacc.2015.05.066.
- Pfaffl, M. W. (2001): A new mathematical model for relative quantification in real-time RT-PCR. In: *Nucleic acids research* 29 (9), e45. DOI: 10.1093/nar/29.9.e45.

- Piper, Wolfgang (2013): Krankheiten des Herz-Kreislauf-Systems. In: Wolfgang Piper (Hg.): Innere Medizin. Berlin, Heidelberg: Springer Berlin Heidelberg (Springer-Lehrbuch), S. 1–180.
- Pirher, Nina; Pohar, Jelka; Manček-Keber, Mateja; Benčina, Mojca; Jerala, Roman (2017): Activation of cell membrane-localized Toll-like receptor 3 by siRNA. In: *Immunology letters* 189, S. 55–63. DOI: 10.1016/j.imlet.2017.03.019.
- Puchtler, H.; Meloan, S. N.; Terry, M. S. (1969): On the history and mechanism of alizarin and alizarin red S stains for calcium. In: The journal of histochemistry and cytochemistry : official journal of the Histochemistry Society 17 (2), S. 110–124. DOI: 10.1177/17.2.110.
- Rafieian-Kopaei, Mahmoud; Setorki, Mahbubeh; Doudi, Monir; Baradaran, Azar; Nasri, Hamid (2014): Atherosclerosis: Process, Indicators, Risk Factors and New Hopes. In: *International Journal of Preventive Medicine* 5 (8), S. 927–946.
- Ramasamy, Indra (2014): Recent advances in physiological lipoprotein metabolism. In: *Clinical chemistry and laboratory medicine* 52 (12), S. 1695–1727. DOI: 10.1515/cclm-2013-0358.
- Riera Romo, Mario; Pérez-Martínez, Dayana; Castillo Ferrer, Camila (2016): Innate immunity in vertebrates: an overview. In: *Immunology* 148 (2), S. 125–139. DOI: 10.1111/imm.12597.
- Rosenhek, Raphael; Klaar, Ursula; Schemper, Michael; Scholten, Christine; Heger, Maria; Gabriel, Harald et al. (2004): Mild and moderate aortic stenosis. Natural history and risk stratification by echocardiography. In: *European heart journal* 25 (3), S. 199–205. DOI: 10.1016/j.ehj.2003.12.002.
- ROSS, D. N. (1962): Homograft replacement of the aortic valve. In: *Lancet (London, England)* 2 (7254), S. 487. DOI: 10.1016/S0140-6736(62)90345-8.
- Rossebø, Anne B.; Pedersen, Terje R.; Boman, Kurt; Brudi, Philippe; Chambers, John B.; Egstrup, Kenneth et al. (2008): Intensive lipid lowering with simvastatin and ezetimibe in aortic stenosis. In: *The New England journal of medicine* 359 (13), S. 1343–1356. DOI: 10.1056/NEJMoa0804602.
- Saeed, Sahrai; Dweck, Marc R.; Chambers, John (2020): Sex differences in aortic stenosis: from pathophysiology to treatment. In: *Expert review of cardiovascular therapy* 18 (2), S. 65–76. DOI: 10.1080/14779072.2020.1732209.

- Schardinger, Franz (1903): Über thermophile Bakterien aus verschiedenen Speisen und Milch. In: Zeitschr. f. Untersuchung d. Nahr.-u. Genußmittel 6 (19), S. 865–880. DOI: 10.1007/BF02067497.
- Schneider, William M.; Chevillotte, Meike Dittmann; Rice, Charles M. (2014): Interferon-stimulated genes: a complex web of host defenses. In: *Annual review of immunology* 32, S. 513–545. DOI: 10.1146/annurev-immunol-032713-120231.
- Serbina, Natalya V.; Shi, Chao; Pamer, Eric G. (2012): Monocyte-mediated immune defense against murine Listeria monocytogenes infection. In: *Advances in immunology* 113, S. 119–134. DOI: 10.1016/B978-0-12-394590-7.00003-8.
- Shinde, Arti V.; Humeres, Claudio; Frangogiannis, Nikolaos G. (2017): The role of α-smooth muscle actin in fibroblast-mediated matrix contraction and remodeling. In: *Biochimica et biophysica acta. Molecular basis of disease* 1863 (1), S. 298–309. DOI: 10.1016/j.bbadis.2016.11.006.
- Singh, R. B.; Watson, Ronald R.; Takahashi, Tōru (Hg.) (2019): The role of functional food security in global health. London: Academic Press an imprint of Elsevier. Online verfügbar unter http://www.sciencedirect.com/science/book/9780128131480.
- Soda, Nobumasa; Sakai, Nobuhiro; Kato, Hiroki; Takami, Masamichi; Fujita, Takashi (2019): Singleton-Merten Syndrome-like Skeletal Abnormalities in Mice with Constitutively Activated MDA5. In: *Journal of immunology (Baltimore, Md. : 1950)* 203 (5), S. 1356–1368. DOI: 10.4049/jimmunol.1900354.
- Spears, Jenna; Al-Saiegh, Yousif; Goldberg, David; Manthey, Sina; Goldberg, Sheldon (2020): TAVR: A Review of Current Practices and Considerations in Low-Risk Patients. In: *Journal of interventional cardiology* 2020, S. 2582938. DOI: 10.1155/2020/2582938.
- Spence, J. David; Srichaikul, Korbua Kristie; Jenkins, David J. A. (2021): Cardiovascular Harm From Egg Yolk and Meat: More Than Just Cholesterol and Saturated Fat. In: *Journal of the American Heart Association* 10 (7), e017066. DOI: 10.1161/JAHA.120.017066.
- Starr, Albert; Fessler, Cindy L.; Grunkemeier, Gary; He, Guo-Wei (2002): Heart valve replacement surgery: past, present and future. In: *Clinical and experimental pharmacology & physiology* 29 (8), S. 735–738. DOI: 10.1046/j.1440-1681.1999.03710.x.

- Starr, Albert; Herr, Rodney H.; Wood, James A. (1967): Mitral replacement. In: *The Journal of Thoracic and Cardiovascular Surgery* 54 (3), S. 333–358. DOI: 10.1016/S0022-5223(19)43077-8.
- STARR, A.; EDWARDS, M. L. (1961): Mitral replacement: clinical experience with a ball-valve prosthesis. In: *Annals of surgery* 154 (4), S. 726–740. DOI: 10.1097/00000658-196110000-00017.
- Stella, Valentino J.; He, Quanren (2008): Cyclodextrins. In: *Toxicologic pathology* 36 (1), S. 30–42. DOI: 10.1177/0192623307310945.
- Stevens, D. A. (1999): Itraconazole in cyclodextrin solution. In: *Pharmacotherapy* 19 (5), S. 603–611. DOI: 10.1592/phco.19.8.603.31529.
- Stewart, B.Fendley; Siscovick, David; Lind, Bonnie K.; Gardin, Julius M.; Gottdiener, John S.; Smith, Vivienne E. et al. (1997): Clinical Factors Associated With Calcific Aortic Valve Disease fn1fn1This study was supported in part by Contracts NO1-HC85079 through HC-850086 from the National Heart, Lung, and Blood Institute, National Institutes of Health, Bethesda, Maryland. In: *Journal of the American College of Cardiology* 29 (3), S. 630–634. DOI: 10.1016/S0735-1097(96)00563-3.
- Su, Qingfeng; Zhang, Linhu; Qi, Zhenhui; Huang, Bo (2022): The Mechanism of Inflammatory Factors and Soluble Vascular Cell Adhesion Molecule-1 Regulated by Nuclear Transcription Factor NF-κB in Unstable Angina Pectoris. In: *Journal of immunology research* 2022, S. 6137219. DOI: 10.1155/2022/6137219.
- Takeda, Kiyoshi; Akira, Shizuo (2015): Toll-like receptors. In: *Current protocols in immunology* 109, 14.12.1-14.12.10. DOI: 10.1002/0471142735.im1412s109.
- Takemura, Naoki; Kawasaki, Takumi; Kunisawa, Jun; Sato, Shintaro; Lamichhane, Aayam; Kobiyama, Kouji et al. (2014): Blockade of TLR3 protects mice from lethal radiation-induced gastrointestinal syndrome. In: *Nature communications* 5, S. 3492. DOI: 10.1038/ncomms4492.
- Takeuchi, Osamu; Akira, Shizuo (2010): Pattern recognition receptors and inflammation. In: *Cell* 140 (6), S. 805–820. DOI: 10.1016/j.cell.2010.01.022.
- Tasneem, S.; Adam, F.; Minullina, I.; Pawlikowska, M.; Hui, S. K.; Zheng, S. et al. (2009): Platelet adhesion to multimerin 1 in vitro: influences of platelet membrane

receptors, von Willebrand factor and shear. In: Journal of thrombosis and haemostasis : JTH 7 (4), S. 685–692. DOI: 10.1111/j.1538-7836.2009.03284.x.

- Thiriet, Marc (2018): Cardiovascular Disease: An Introduction. In: Marc Thiriet (Hg.): Vasculopathies, Bd. 8. Cham: Springer International Publishing (Biomathematical and Biomechanical Modeling of the Circulatory and Ventilatory Systems), S. 1–90
- Troncoso, Mayarling Francisca; Ortiz-Quintero, Jafet; Garrido-Moreno, Valeria; Sanhueza-Olivares, Fernanda; Guerrero-Moncayo, Alejandra; Chiong, Mario et al. (2021): VCAM-1 as a predictor biomarker in cardiovascular disease. In: *Biochimica et biophysica acta. Molecular basis of disease* 1867 (9), S. 166170. DOI: 10.1016/j.bbadis.2021.166170.
- Tsuji-Tamura, Kiyomi; Morino-Koga, Saori; Suzuki, Shingo; Ogawa, Minetaro (2021): The canonical smooth muscle cell marker TAGLN is present in endothelial cells and is involved in angiogenesis. In: *Journal of cell science* 134 (15). DOI: 10.1242/jcs.254920.
- Uekama, Kaneto (2004): Design and evaluation of cyclodextrin-based drug formulation. In: *Chemical & pharmaceutical bulletin* 52 (8), S. 900–915. DOI: 10.1248/cpb.52.900.
- V. Antoine: Sur la fermentation de la fécule par l'action du ferment butyrique Comptes Rendus de l'Académie Des Sciences, 112 (1891), pp. 536-538
- Vaslef, S. N.; Roberts, W. C. (1993): Early descriptions of aortic valve stenosis. In: *American heart journal* 125 (5 Pt 1), S. 1465–1474. DOI: 10.1016/0002-8703(93)91036-E.
- Xavier, Sandhya; Vasko, Radovan; Matsumoto, Kei; Zullo, Joseph A.; Chen, Robert; Maizel, Julien et al. (2015): Curtailing endothelial TGF-β signaling is sufficient to reduce endothelial-mesenchymal transition and fibrosis in CKD. In: Journal of the American Society of Nephrology: JASN 26 (4), S. 817–829. DOI: 10.1681/ASN.2013101137.
- Yang, Xiaoping; Fullerton, David A.; Su, Xin; Ao, Lihua; Cleveland, Joseph C.; Meng, Xianzhong (2009): Pro-osteogenic phenotype of human aortic valve interstitial cells is associated with higher levels of Toll-like receptors 2 and 4 and enhanced expression of bone morphogenetic protein 2. In: *Journal of the American College of Cardiology* 53 (6), S. 491–500. DOI: 10.1016/j.jacc.2008.09.052.

- Yao, Jiayi; Wu, Xiuju; Qiao, Xiaojing; Zhang, Daoqin; Zhang, Li; Ma, Jocelyn A. et al. (2021): Shifting osteogenesis in vascular calcification. In: *JCI insight* 6 (10). DOI: 10.1172/jci.insight.143023.
- Yao, Yucheng; Jumabay, Medet; Ly, Albert; Radparvar, Melina; Cubberly, Mark R.; Boström, Kristina I. (2013): A role for the endothelium in vascular calcification. In: *Circulation research* 113 (5), S. 495–504. DOI: 10.1161/CIRCRESAHA.113.301792.
- Yasuda, Koubun; Nakanishi, Kenji; Tsutsui, Hiroko (2019): Interleukin-18 in Health and Disease. In: *International journal of molecular sciences* 20 (3). DOI: 10.3390/ijms20030649.
- Yip, Cindy Ying Yin; Chen, Jan-Hung; Zhao, Ruogang; Simmons, Craig A. (2009): Calcification by valve interstitial cells is regulated by the stiffness of the extracellular matrix. In: *Arteriosclerosis, thrombosis, and vascular biology* 29 (6), S. 936–942. DOI: 10.1161/ATVBAHA.108.182394.
- Yoneyama, Mitsutoshi; Kikuchi, Mika; Natsukawa, Takashi; Shinobu, Noriaki; Imaizumi, Tadaatsu; Miyagishi, Makoto et al. (2004): The RNA helicase RIG-I has an essential function in double-stranded RNA-induced innate antiviral responses. In: *Nature immunology* 5 (7), S. 730–737. DOI: 10.1038/ni1087.
- Zhan, Qiong; Song, Rui; Li, Fei; Ao, Lihua; Zeng, Qingchun; Xu, Dingli et al. (2017): Double-stranded RNA upregulates the expression of inflammatory mediators in human aortic valve cells through the TLR3-TRIF-noncanonical NF-κB pathway. In: *American journal of physiology. Cell physiology* 312 (4), C407-C417. DOI: 10.1152/ajpcell.00230.2016.
- Zhan, Qiong; Song, Rui; Zeng, Qingchun; Yao, Qingzhou; Ao, Lihua; Xu, Dingli et al. (2015): Activation of TLR3 induces osteogenic responses in human aortic valve interstitial cells through the NF-κB and ERK1/2 pathways. In: *International journal of biological sciences* 11 (4), S. 482–493. DOI: 10.7150/ijbs.10905.
- Zhou, Qian; Cao, Hong; Hang, Xiaoyi; Liang, Huamin; Zhu, Miaomiao; Fan, Yixian et al. (2021): Midkine Prevents Calcification of Aortic Valve Interstitial Cells via Intercellular Crosstalk. In: *Frontiers in cell and developmental biology* 9, S. 794058. DOI: 10.3389/fcell.2021.794058.
- Zimmer, Sebastian; Grebe, Alena; Bakke, Siril S.; Bode, Niklas; Halvorsen, Bente; Ulas, Thomas et al. (2016): Cyclodextrin promotes atherosclerosis regression via macrophage

reprogramming. In: *Science translational medicine* 8 (333), 333ra50. DOI: 10.1126/scitranslmed.aad6100.

5.1 Websites

- [1]https://www.who.int/news/item/09-12-2020-who-reveals-leading-causes-of-death-and-disability-worldwide-2000-2019 (29thDecember, 2022)
- [2]https://www.who.int/news-room/fact-sheets/detail/cardiovascular-diseases-(cvds) (12thMay, 2023)
- [3]https://www.statista.com/outlook/cmo/food/worldwide#key-market-indicators (24thDecember, 2022)
- [4]https://www.okheart.com/about-us/ohh-news/plaque-in-the-arteries-causes-symptoms-and-treatments#:~:text=When%20preventative%20measures%20are%20not%20enough%2C%20plaque%20in,blood%20flow%20to%20resume%20and%20prevents%20further%20narrowing (24thDecember,2022)

6. Supplements

6.1. Establishing a protocol to induce endothelial to mesenchymal transition

For establishing a protocol for EndMT induction, cells were stimulated for 7 days every other day with the underlying stimuli shown in the table below. The potential of BMPs, including BMP2, BMP4, and BMP9, to induce EndMT *in vitro* has been recognized in addition to the established role of TGFβ1. These BMPs have shown the ability to initiate EndMT in VECs (Shapero et al. 2015, Zhong et al. 2018, Hjortnaes et al. 2015, Yang et al. 2008, Wylie-Sears et al. 2014, Kovacic et al. 2019, Ma et al. 2020).

Table 10 Protocol
To establish an EndMT protocol, selected stimuli were used at the beginning based on other publications.

Stimulus	**Concentration**	**Catalog Number, Company**
BMP2	100ng/ml	355-BM-010, R&D Systems
BMP4	100ng/ml	314-BP-010, R&D Systems
BMP6	50ng/ml	507-BP-020, R&D Systems
BMP9	10ng/ml	3209-BP-010, R&D Systems
TGFβ1	10ng/ml	240-B-002, R&D Systems
TGFβ1	2ng/ml	240-B-002, R&D Systems
IL1β	1ng/ml	201-LB-010, R&D Systems
TNFα	30ng/ml	300-01A-250; PeproTech

BMP= Bone morphogenetic proteins, TGFβ1= Transforming growth factor-beta 1; TNFα= Tumor necrosis factor-alpha, IL1β= Interleukin 1 beta

Figure 55 shows various BMP stimuli as well as TGFβ1, IL1β and TNFα. VECs stimulated with BMPs, or TGFβ1 single stimulation did not show an effect of EndMT measured with endothelial (*VWF* and *NOS3)* and mesenchymal markers (*ACTA2* and *VCAM1)*, while TGFβ1 in combination with IL1β and TNFα only, showed increased *ACTA2* and *VCAM1* gene expression in comparison to only TGFβ1 stimulation. *Vimentin* as a mesenchymal marker did not show a crucial effect. *VWF* and *NOS3* gene expression decreased after TNFα, or TGFβ1+IL1β stimulation, whereas *VWF* gene expression did not change after stimulation with TGFβ1 only

(Figure 55). Surprisingly, *PECAM1*, which is known to be an endothelial marker, showed a rather higher gene expression compared to neg control.

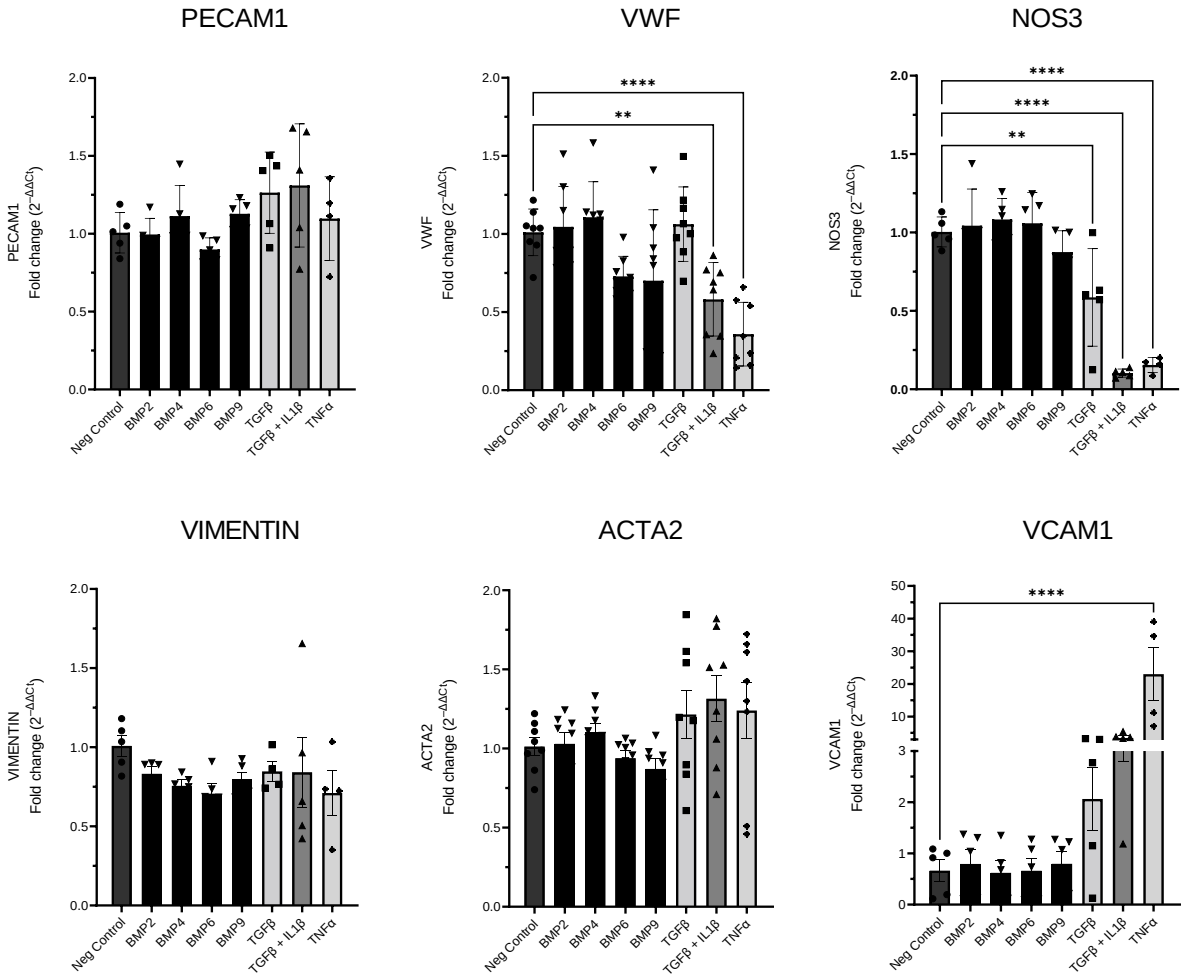

Figure 55 Establishing endothelial to mesenchymal transition

*Various stimuli for EndMT were investigated in VECs. RNA was isolated after 7 days. The relative levels of target gene expression were calculated by the Comparative Ct Method (ΔΔCt Method). One-way ANOVA test with Dunnett's post test for multiple comparisons was used to test the statistical significance of qPCR data. Bars displayed the fold change of gene expression normalized by neg control ± SEM. n=2; ** p< 0.005, ****p< 0.00005*

ACTA2= Smooth muscle alph-2 actin; EndMT= Endothelial to mesenchymal transition; NOS3= Nitric oxide synthase 3; PECAM1= Platelet endothelial cell adhesion molecule-1; TAGLN= Transgelin; TGFβ1= Transforming growth factor-beta 1; TNFα= Tumor necrosis factor-alpha; VCAM1= Vascular cell adhesion molecule 1; VEC= Valvular endothelial cell; VWF= Von Willebrand factor

Moreover, cell culture media ingredients such as hydrocortisone and VEGF are two factors that have an intricate role in this process. Hydrocortisone is a steroid hormone that has anti-

inflammatory properties and is commonly used to maintain the phenotype of endothelial cells in culture. On the other hand, VEGF is a pro-angiogenic growth factor that promotes endothelial cell proliferation and migration. VEGF for example inhibits TGFβ induced EndMT.

Two media formulations were examined in the study. Media 1 (Med1) contained all the necessary supplements for culturing VECs. Media 2 (Med2), on the other hand, included all supplements except for Hydrocortisone and VEGF, as these factors promote the endothelial phenotype and are intended to prevent the occurrence of EndMT.

Both media formulations were investigated, and VECs were subjected to stimulation with TGFβ1, TGFβ1+IL1β, TNFα, or left unstimulated. After a 7-day period, RNA isolation was performed, followed by qPCR to assess gene expression levels. Both endothelial and mesenchymal markers exhibited a similar expression pattern, although Med1 appeared to have a more favorable impact on endothelial marker expression. In contrast, the mesenchymal marker demonstrated slightly higher expression levels when treated with TGFβ1+IL1β and TNFα in Med2 (Figure 56).

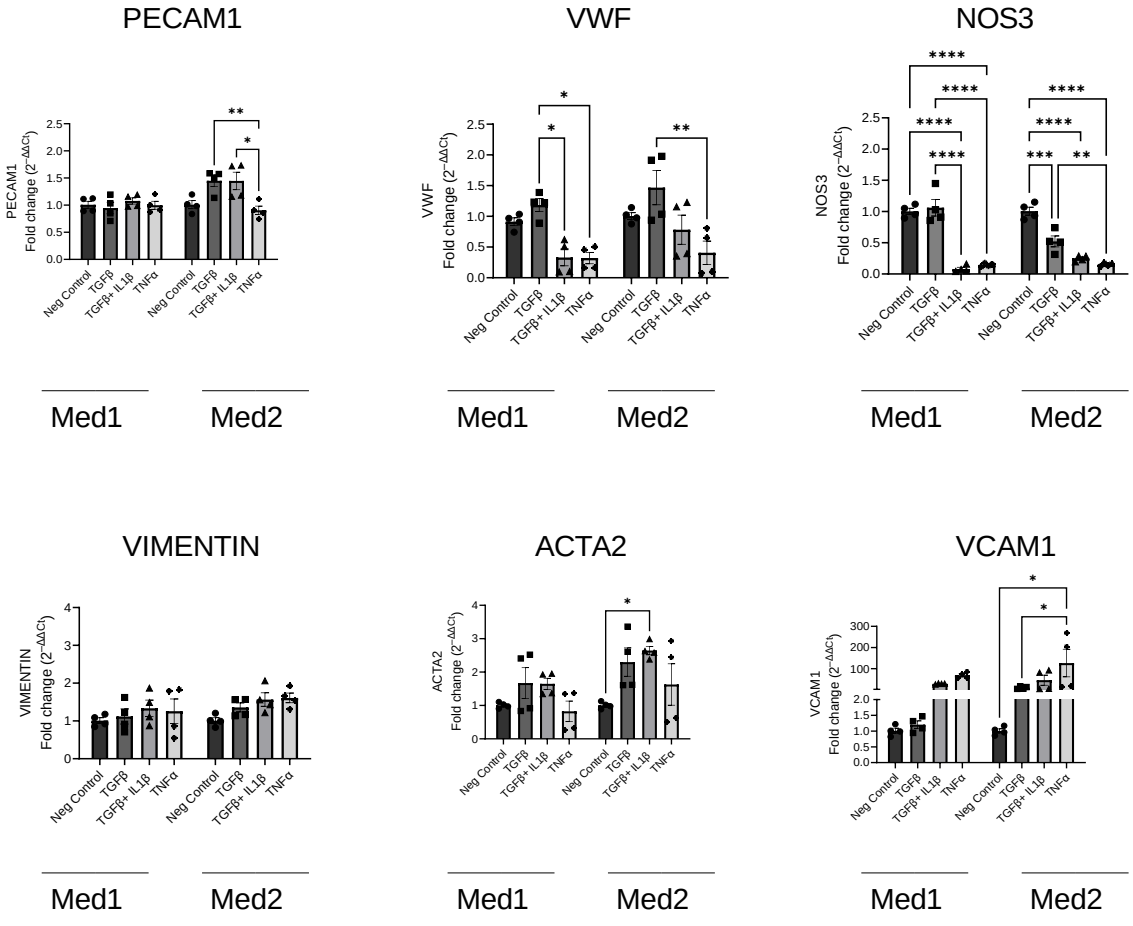

Figure 56 Different media for endothelial to mesenchymal transition protocol

*Two media were investigated for EndMT in VECs. Med1 contained all supplements while Med2 contained all supplements except of Hydrocortisone and VEGF. Both media were investigated and cells were treated with TGFβ1, TGFβ1+IL1β, TNFα, or non-treated. RNA was isolated after 7 days. The relative levels of target gene expression were calculated by the Comparative Ct Method (ΔΔCt Method). 2-way ANOVA test with Tukey's post test for multiple comparisons was used to test the statistical significance of qPCR data. Bars displayed the fold change of gene expression normalized by neg control in each medium ± SEM. n=2 *p < 0.05, ** p< 0.005, *** p< 0.0005, ****p< 0.00005*

ACTA2= Smooth muscle alpha-2 actin; EndMT= Endothelial to mesenchymal transition; Med= Medium; NOS3= Nitric oxide synthase 3; PECAM1= Platelet endothelial cell adhesion molecule-1; TAGLN= Transgelin; TGFβ1= Transforming Growth Factor-beta 1; TNFα= Tumor necrosis factor-alpha; VCAM1= Vascular cell adhesion molecule 1; VEC= Valvular endothelial cell; VWF= Von Willebrand factor

Further, two concentrations of TGFβ1 were tested. Cells were stimulated with TGFβ1 (2ng/10ng) and TGFβ1 (2ng/10ng) +IL1β and kept unstimulated. RNA was isolated after 7 days and qPCR was performed to measure the gene expression.

Regarding the endothelial marker, a similar pattern was shown. Moreover, *VWF* as well as *NOS3* were higher expressed in 10ng compared to 2ng TGFβ1. All in all, both concentrations showed a similar pattern, so experiments were performed with the lower concentration of 2ng TGFβ1 in combination with IL1β.

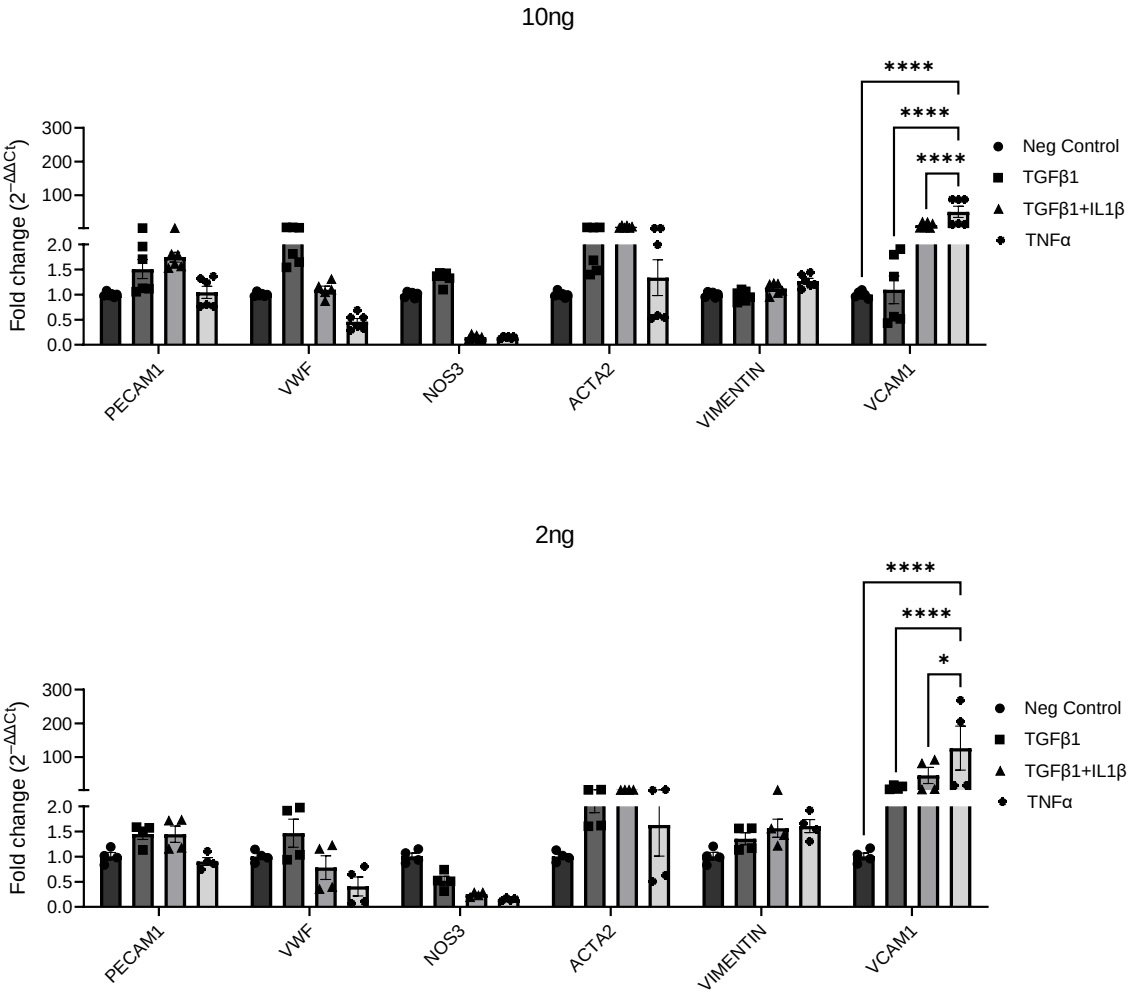

Figure 57 Different concentrations for endothelial to mesenchymal transition protocol

*Two concentrations of TGFβ1 were investigated for EndMT in VECs. Cells were treated with TGFβ1 (2ng/ 10ng), TGFβ1 (2ng/10ng) +IL1β, TNFα, or non-treated. RNA was isolated after 7 days. The relative levels of target gene expression were calculated by the Comparative Ct Method (ΔΔCt Method). 2-way ANOVA test with Tukey's post test for multiple comparisons was used to test the statistical significance of qPCR data. Bars displayed the fold change of gene expression normalized by neg control in each medium ± SEM. n=2; *p < 0.05, ** p< 0.005, *** p< 0.0005, ****p< 0.00005*

ACTA2= Smooth muscle alpha-2 actin; EndMT= Endothelial to mesenchymal transition; NOS3= Nitric oxide synthase 3; PECAM1= Platelet endothelial cell adhesion molecule-1; TAGLN= Transgelin; EndMT= Endothelial to mesenchymal cells; TGFβ1= Transforming growth factor - beta 1; TNFα= Tumor necrosis factor-alpha; VCAM1= Vascular cell adhesion molecule 1; VEC= Valvular endothelial cell; VWF= Von Willebrand factor

6.1.2 Proteomic data

The analysis of TGFβ1 compared to the corresponding control (neg control) did not reveal any significant differences within the protein expression of the 4 donors. Nevertheless, Vimentin

was upregulated after TGFβ1 stimulation. Regarding the experiment of the single donor, VWF was significantly higher expressed after TGFβ1 stimulation compared to neg control. In conclusion, this result confirmed the approach of the here presented EndMT induction using TNFα as well as TGFβ1+IL1β for stimulation.

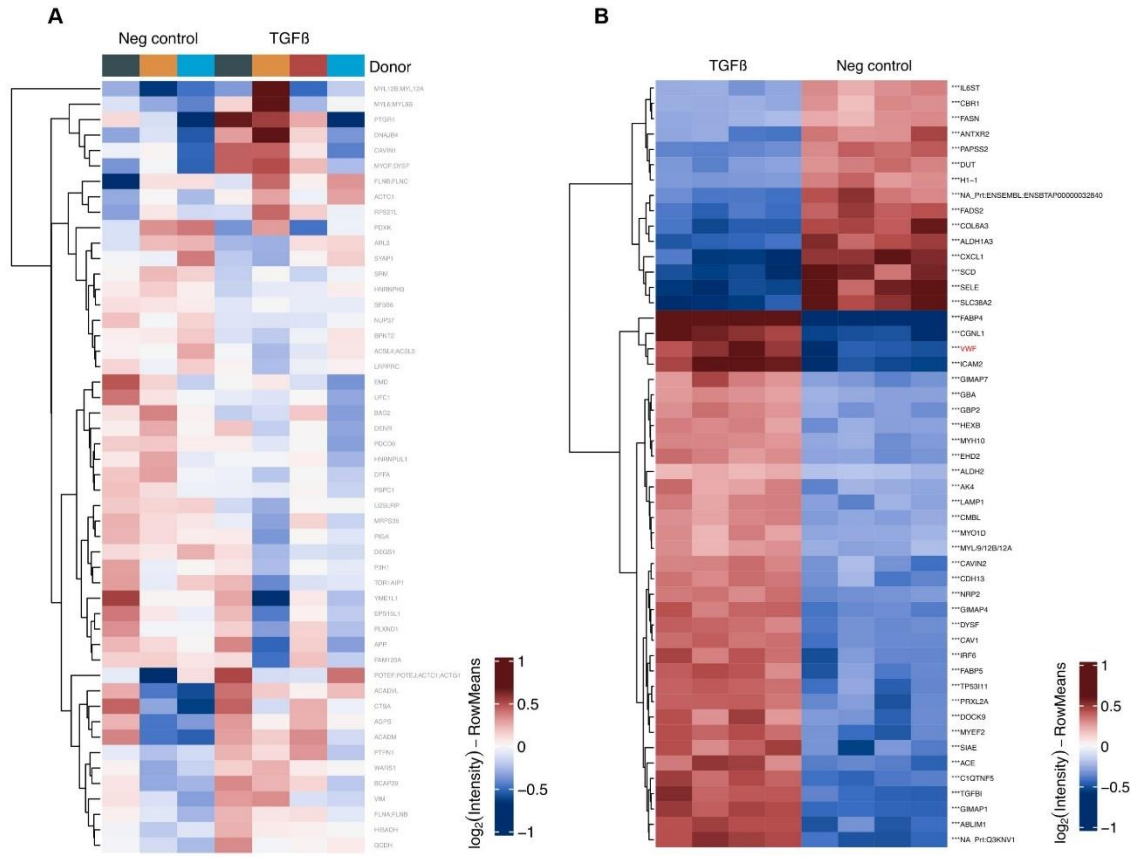

Figure 58 Proteomic analysis of negative control compare to TGFβ1 stimulated valvular endothelial cells

*VECs from **A**: 4 different donors, or **B**: one donor with 4replicates, were stimulated with TGFβ1 or left unstimulated (neg control) for 7 days. Proteomic analysis was performed in the core facility for mass spectrometry. The results showed high aberrations within the 4donors and no significant results whereas one donor revealed repetitious accuracy within the technical replicates. TGFβ1 stimulation resulted to a higher VWF expression compared to control.*

VECs= Valvular endothelial cells; TGFβ1 = Transforming growth factor-beta 1

When comparing TGFβ1+IL1β with the control condition, Transgelin was found to be upregulated in the stimulated cells within the 4 different donors. NOS3 expression was upregulated in the control cells within the single donor analysis.

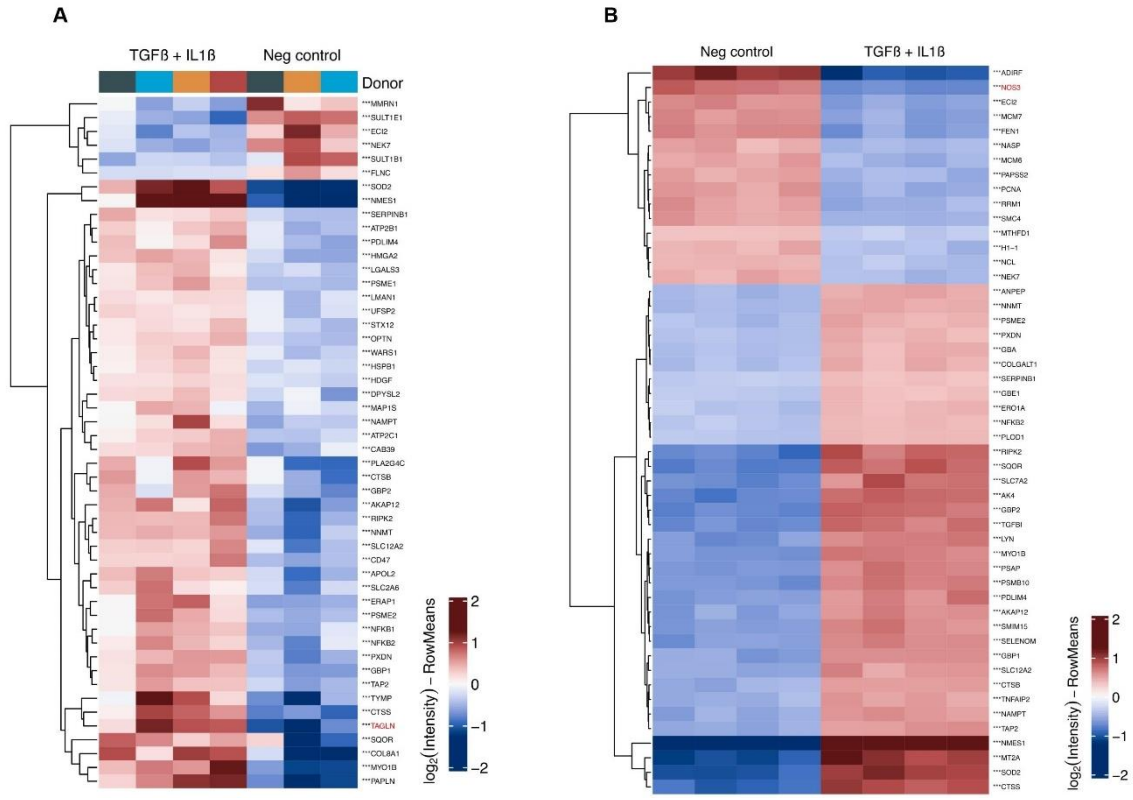

Figure 59 Proteomic analysis of negative control compared to TGFβ1+IL1β stimulated valvular endothelial cells

*VECs from **A**: 4 different donors, or **B**: one donor with 4replicates, were stimulated with TGFβ1+ IL1β or left unstimulated (neg control) for 7 days. Proteomic analysis was performed in the core facility for mass spectrometry. The results showed high aberrations within the 4donors and no significant results whereas one donor revealed repetitious accuracy within the technical replicates*

VECs= Valvular endothelial cells; TGFβ1= Transforming growth factor -beta 1; IL1β = Interleukin 1 beta

TNFα stimulation resulted in an upregulated expression of RIG-I (*DDX58*) as well as VCAM1 in comparison to the control condition within both analysis such as for the 4 donors and the single one.

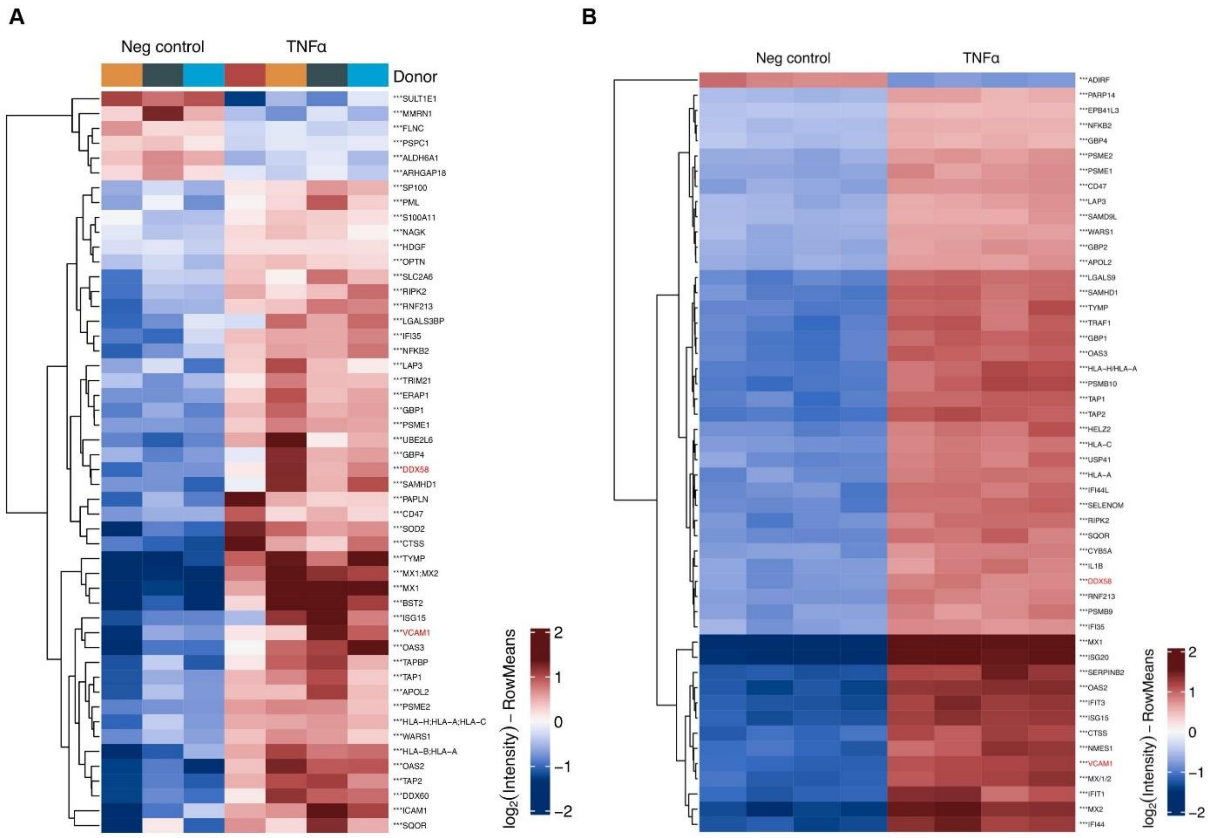

Figure 60 Comparison of negative control versus TNFα stimulation in valvular endothelial cells

*VECs from **A**: 4 different donors, or **B**: one donor with 4replicates, were stimulated with TNFα or left unstimulated (neg control) for 7 days. Proteomic analysis was performed in the core facility for mass spectrometry. The results showed high aberrations within the 4 donors whereas one donor revealed repetitious accuracy within the technical replicates.*

VECs= Valvular endothelial cells; TNFα= Tumor necrosis factor-alpha

6.2 TLR3 in the process of endothelial to mesenchymal transition

6.2.1 Unstimulated cells

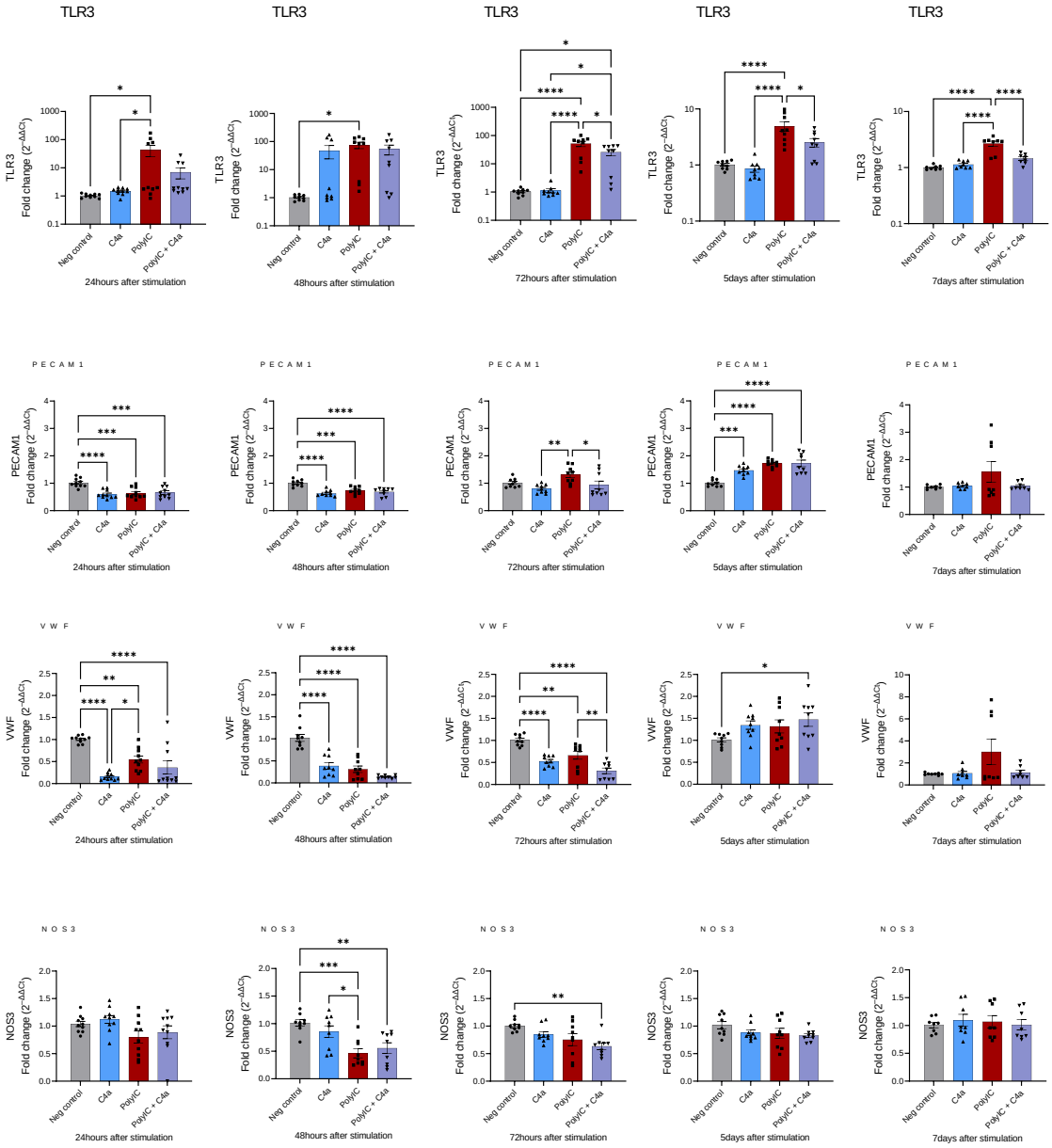

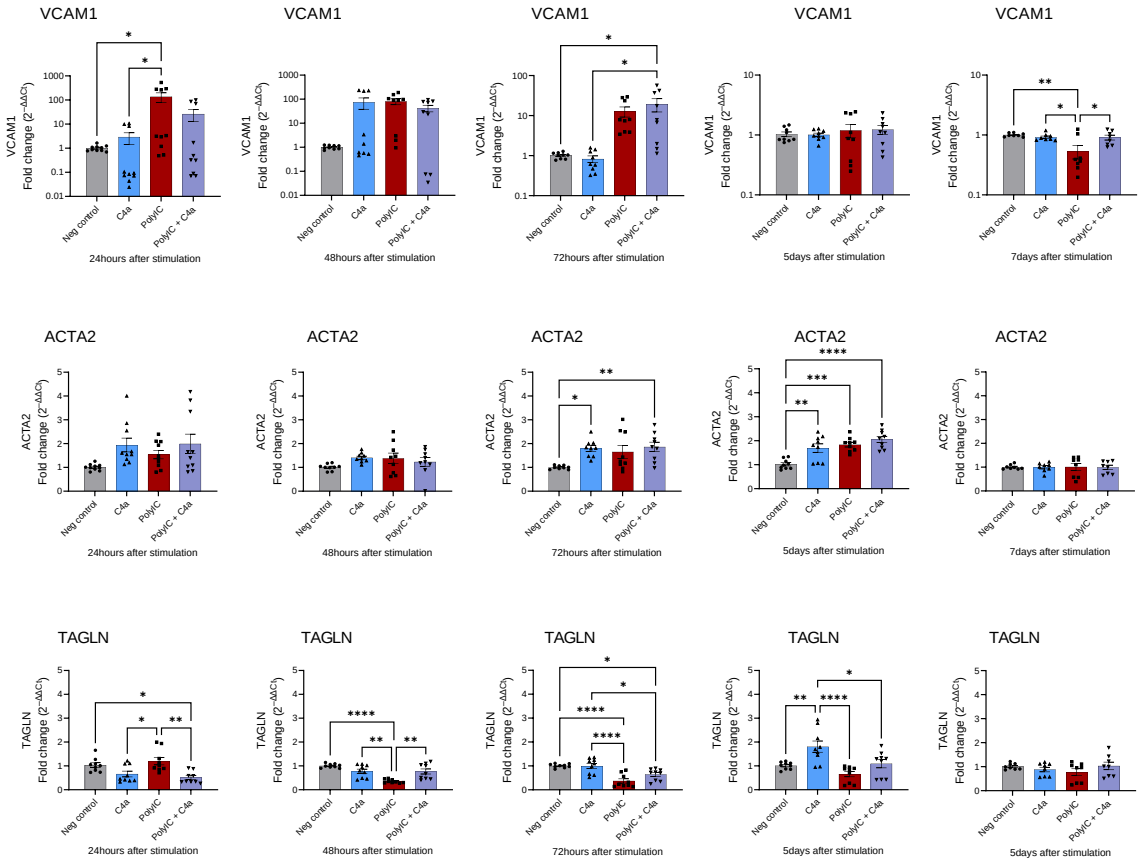

Figure 61 Gene expression in treated valvular endothelial cells

*VECs were treated with PolyIC, C4a, or both for 24 hours. Afterwards, medium was changed to EndMT media. RNA was isolated after 24 hours, 48 hours, 72 hours, 5 days, and 7 days after treatment. The relative levels of target gene expression were calculated by the Comparative Ct Method (ΔΔCt Method). One-way ANOVA test with Tukey's post test for multiple comparisons was used to test the statistical significance of qPCR data. Bars displayed the fold change of gene expression normalized by neg control ± SEM. n=3 *p < 0.05, ** p< 0.005, *** p< 0.0005, **** p< 0.00005*

ACTA2= Smooth muscle alpha-2 actin; C4a= Compound 4a; EndMT= Endothelial to mesenchymal transition; NOS3= Nitric oxide synthase 3; PECAM1= Platelet endothelial cell adhesion molecule-1; PolyIC= Polyinosinic:Polycytidylic acid; TAGLN= Transgelin;

TLR3=Toll-like recpetor3; VCAM1= Vascular cell adhesion molecule 1; VEC= Valvular endothelial cell; VWF= Von Willebrand factor

6.2.2 TGFβ1+IL1β stimulation

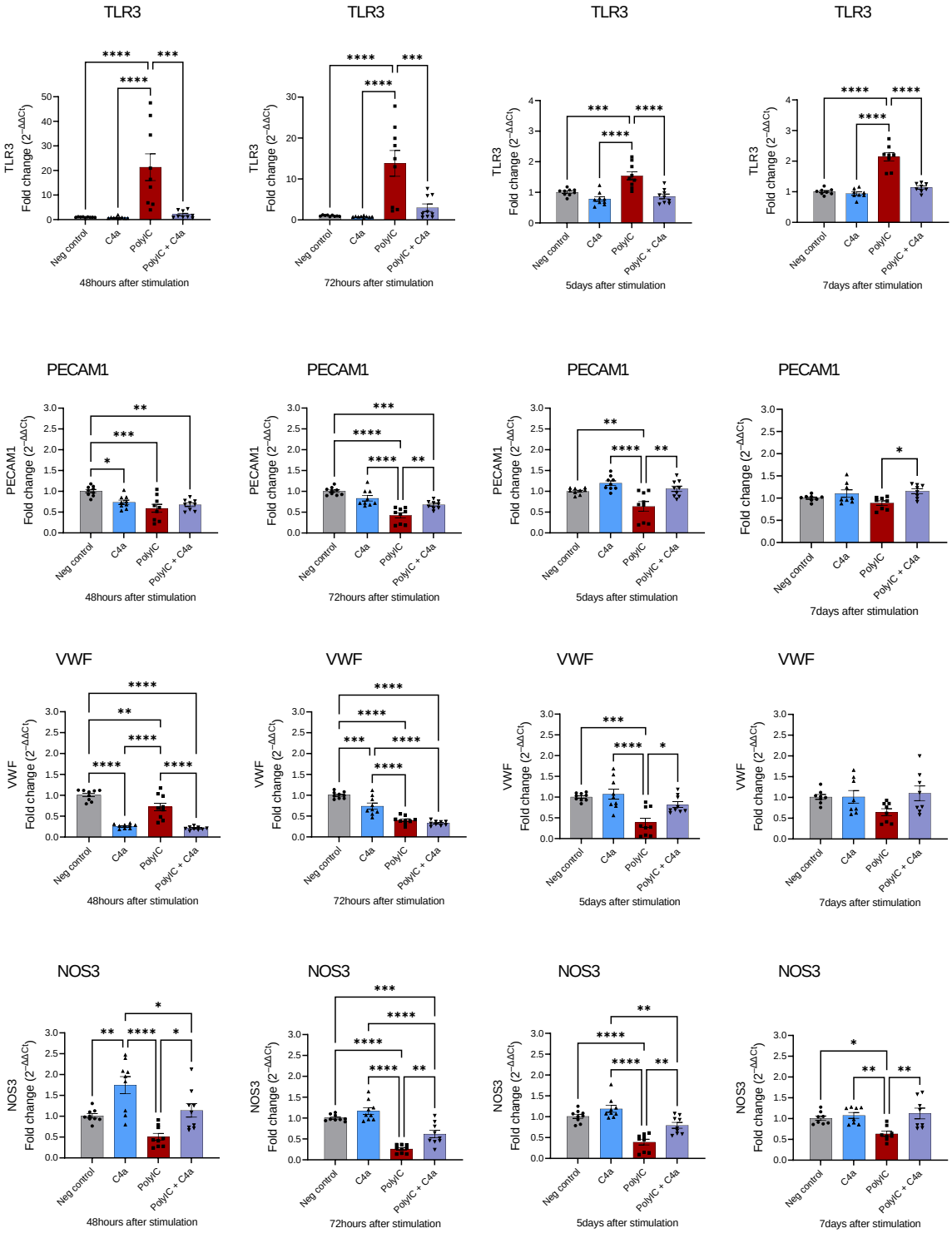

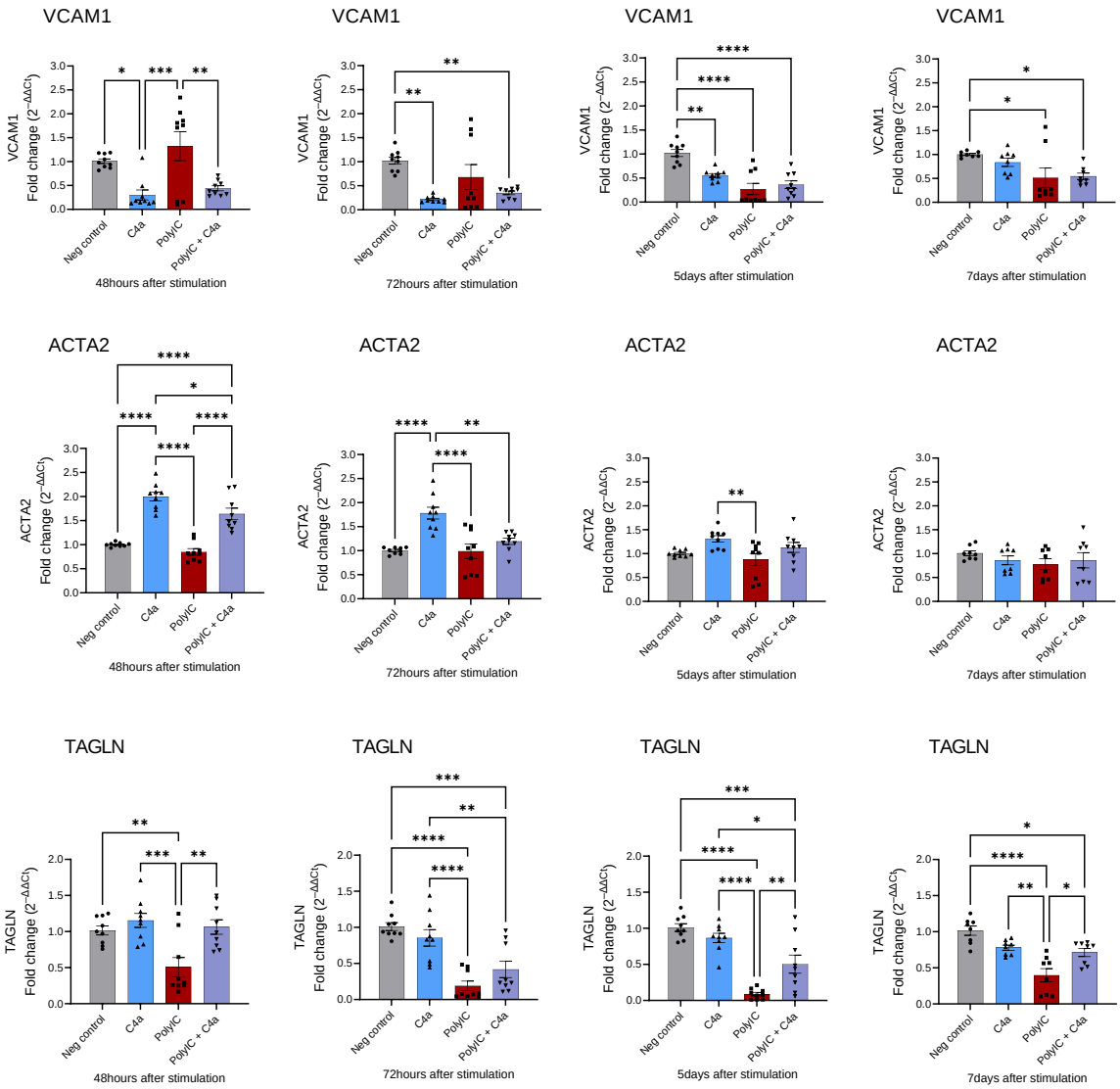

Figure 62 Gene expression in treated valvular endothelial cells after TGFβ1+Ilβ stimulation

*VECs were treated with PolyIC, C4a, or both for 24 hours. Afterwards, medium was changed to EndMT medium and TGFβ1+IL1β was added to induce EndMT. RNA was isolated after 48 hours, 72 hours, 5 days, and 7 days after treatment. The relative levels of target gene expression were calculated by the Comparative Ct Method (ΔΔCt Method). One-way ANOVA test with Tukey's post test for multiple comparisons was used to test the statistical significance of qPCR data. Bars displayed the fold change of gene expression normalized by neg control ± SEM. n=3 *p < 0.05, ** p< 0.005, *** p< 0.0005, **** p< 0.00005*

ACTA2= Smooth muscle alpha-2 actin; C4a= Compound 4a; EndMT= Endothelial to mesenchymal transition; NOS3= Nitric oxide synthase 3; PECAM1= Platelet endothelial cell adhesion molecule-1; PolyIC= Polyinosinic:Polycytidylic acid; TAGLN= Transgelin; TGFβ1= Transforming growth factor-beta 1; TLR3= Toll-like receptor3; VCAM1= Vascular cell adhesion molecule 1; VEC= Valvular endothelial cell; VWF= Von Willebrand factor

6.2.3 TNFα Stimulation

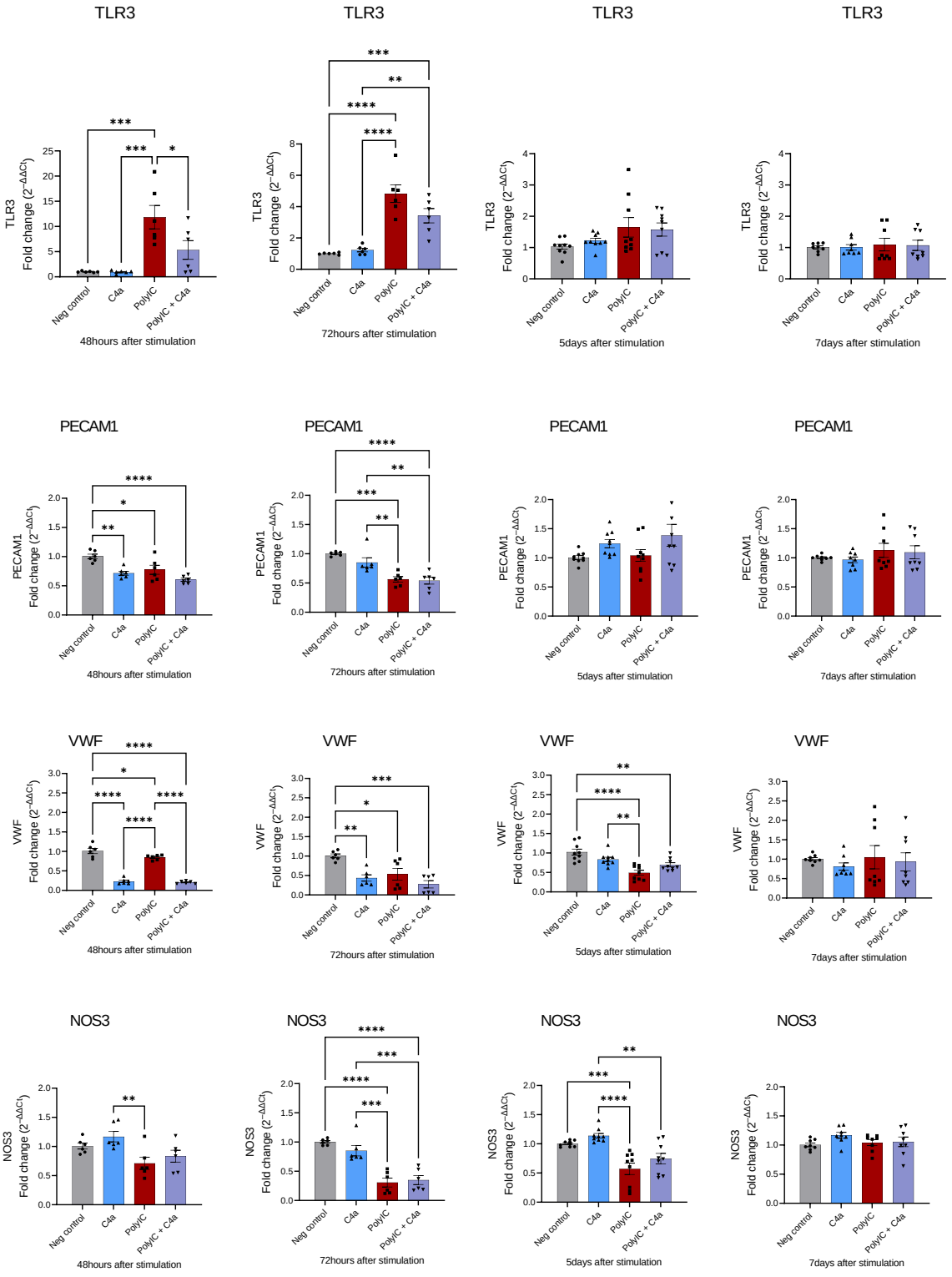

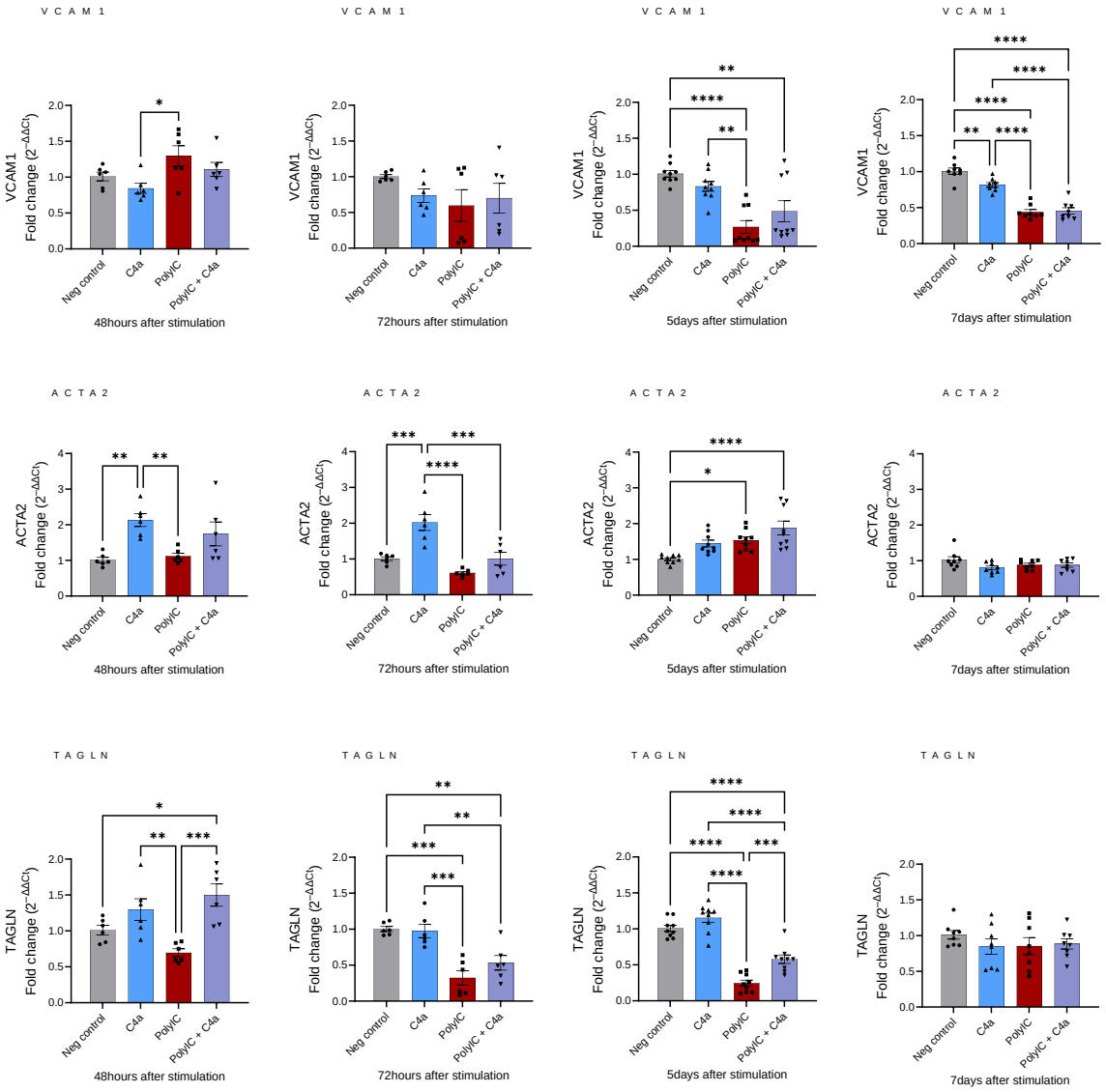

Figure 63 Gene expression in treated valvular endothelial cells stimulated with TNFα

*VECs were treated with PolyIC, C4a, or both for 24 hours. Afterwards, medium was changed to EndMT medium and TNFα was added to induce EndMT. RNA was isolated after, 48 hours, 72 hours, 5 days, and 7 days after treatment. The relative levels of target gene expression were calculated by the Comparative Ct Method (ΔΔCt Method). One-way ANOVA test with Tukey's post test for multiple comparisons was used to test the statistical significance of qPCR data. Bars displayed the fold change of gene expression normalized by neg control ± SEM. n=3 *p < 0.05, ** p< 0.005, *** p< 0.0005, **** p< 0.00005*

ACTA2= Smooth muscle alpha-2 actin; C4a= Compound 4a; EndMT= Endothelial to mesenchymal transition; NOS3= Nitric oxide synthase 3; PECAM1= Platelet endothelial cell adhesion molecule-1; PolyIC= Polyinosinic:Polycytidylic acid; TAGLN= Transgelin; TLR3= Toll-like receptor 3; TNFα= Tumor necrosis factor-alpha; VCAM1= Vascular cell adhesion molecule 1; VEC= Valvular endothelial cell; VWF= Von Willebrand factor

7. List of Figures and Tables

8. Acknowledgements

Danksagung

„Und wenn du denkst es geht nicht mehr, dann löffle das Nutella leer“. Über die Jahre hat sich dieser Spruch durchgezogen, nicht nur, weil er auf meiner Kaffeetasse stand, sondern wurden auch hier und da einige Gläser Nutella leer gelöffelt. „Mach auf keinen Fall einen PhD“, war das, was mir geraten wurde hinsichtlich meiner Karriere. Dennoch hat es sich richtig angefühlt den Vertrag für eine Doktorarbeit mit dem Titel „Danger signaling pathways in aortic disease“ zu unterschreiben. Und so begann eine unvergessliche Zeit, mit viel Arbeit, Fleiß und Kaffee, aber auch mit viel Freude und wunderbaren Momenten, die ich nicht missen möchte. Während meiner Zeit hier am UKB habe ich ganz tolle Menschen kennen gelernt, die mich in allen Lebenslagen unterstützt und mir Freude und Kraft geschenkt haben. Ohne euch würde ich diesen Text jetzt nicht schreiben und dafür bin ich sehr dankbar.

Ich bin dankbar, überhaupt die Chance bekommen zu haben hier zu starten. Danke an mein Thesis Komitee, für Ihre Zeit und Feedback. Ein großes Dankeschön an meinen Doktorvater, Prof. Dr. Sebastian Zimmer, der dies alles möglich gemacht hat. Sebastian, ich danke dir für die Betreuung und deine positive Einstellung. Ich weiß nicht, wie du es schaffst, aber einen Chef wie dich bräuchte jeder. Weiterhin bedanke ich mich für die Betreuung bei Sven, der mich hier eingearbeitet hat und für Tipps immer zu haben war. Damit geht auch ein großes Dankeschön für all die Unterstützung, die Zusammenarbeit und schöne Atmosphäre der gesamten AG Zimmer und kooperierenden AGs, besonders an Marko, Hannah, Sandra und Marta, Madeleine und Peter.

Aus Kollegen wurden Freunde und ich bin jeden Tag mit einem Lächeln zur Arbeit gefahren, weil ich wusste, dass wir über irgendwas zusammen lachen und wir über jeglichen Unsinn reden werden. Bei Bedarf kann man immer Anna fragen. Zusammen mit Paula rockt ihr beide das Labor. Danke für eure Hilfe, eure Unterstützung und all die unvergesslichen Momente, Ohrwürmer und Lachanfälle, “ihr seid wertvoll“! Zusammen mit Henning, Gloria, Pia und Annika werden wir noch den Euro-Jackpot knacken und unsere 90 Millionen Euro gewinnen. Danke auch euch für eure Hilfe und die Zusammenarbeit.

Nicht nur die MedII war eine Bereicherung meiner Zeit, sondern auch das Nachbarlabor mit Daniel, Melanie, Michi und Mona. Ohne euch hätte ich niemals so unterhaltsame Kaffeepausen

gehabt, oder auch private Mädels Abende, Unternehmungen, oder 10km Läufe. Danke, dass ihr immer ein Ohr für mich hattet und mich so unterstützt habt!
Aber wie wäre die Zeit ohne meine beiden Mädels, Denise und Kathi, gewesen? Gar nicht auszumalen! Wir haben es gerockt und das PhD-Leben zusammen gemeistert, sind durch Höhen und Tiefen gegangen. Höhen und Tiefen auch bei unseren all-you-can-eat Sushi Abenden, nach denen wir uns kaum bewegen konnten. Ihr beide habt mir nicht nur gezeigt, wie man viel Geld in der Black Week ausgeben kann, sondern mich auch der Ordnung und des Zeitmanagements belehrt. Ihr seid mir in der kurzen Zeit unendlich ans Herz gewachsen und ohne euch wären diese Jahre unvorstellbar gewesen.
Anna, du hast mich schon im Bachelor unterstützt. Unser gemeinsames Lernen und Studentenleben und alles was dazu gehört war die perfekte Basis und ich bin froh, dass sich unsere Wege in Bonn wieder gekreuzt haben.
Für meine Masterarbeit durfte ich nach England reisen, wo ich mit drei ganz tollen Jungs zusammengelebt und mit ihnen drei Freunde fürs Leben gefunden habe, die mich seitdem in allem unterstützen. Tim, Andi und Mario, danke.
Ich möchte mich auch bei meiner Familie bedanken. Ohne euch wäre ich nicht da, wo ich jetzt bin. Durch die Liebe und Zusammenhalt schaffen wir alles und ich hätte meinen bisherigen Weg niemals ohne euch so gemeistert. Zu meiner Familie gehören auch meine Mädels aus der Heimat, ihr seid die besten Freunde, die es gibt. Hier brauche ich gar nicht erst anzufangen, was ihr mir bedeutet und was ihr mir alle gebt. Danke für eure Unterstützung!